ISSN 2079-1372 *DOI: 10.31891/2079-1372*

THE INTERNATIONAL SCIENTIFIC JOURNAL

PROBLEMS OF TRIBOLOGY

Volume 30 ***No 4/118-2025***

МІЖНАРОДНИЙ НАУКОВИЙ ЖУРНАЛ

ПРОБЛЕМИ ТРИБОЛОГІЇ

PROBLEMS OF TRIBOLOGY

INTERNATIONAL SCIENTIFIC JOURNAL

Published since 1996, four time a year

Volume 30 No 4/118-2025

Establishers:
Khmelnytskyi National University (Ukraine)
Lublin University of Technology (Poland)

Associated establisher:
Vytautas Magnus University (Lithuania)

Editorial board address:
International scientific journal "Problems of Tribology",
Khmelnytskyi National University,
Instytutska str. 11, Khmelnytskyi, 29016, Ukraine
phone +380975546925

Indexed: CrossRef, DOAJ, Ulrichsweb, ASCI, Google Scholar, Index Copernicus

E-mail: tribology@khmnu.edu.ua

Internet: http://tribology.khnu.km.ua

ПРОБЛЕМИ ТРИБОЛОГІЇ

МІЖНАРОДНИЙ НАУКОВИЙ ЖУРНАЛ

Видається з 1996 р. ***Виходить 4 рази на рік***

Том 30 **№ 4/118-2025**

Адреса редакції:
Україна, 29016, м. Хмельницький, вул. Інститутська 11, к. 4-401
Хмельницький національний університет, редакція журналу "Проблеми трибології"
тел. +380975546925, **E-mail**: tribology@khmnu.edu.ua

Internet: http://tribology.khnu.km.ua

Зареєстровано Міністерством юстиції України
Свідоцтво про держреєстрацію друкованого ЗМІ: Серія КВ № 1917 від 14.03. 1996 р.
(перереєстрація № 24271-14111ПР від 22.10.2019 року)

Входить до переліку наукових фахових видань України
(Наказ Міністерства освіти і науки України № 612/07.05.19. Категорія Б.)

Індексується в МНБ: CrossRef, DOAJ, Ulrichsweb, ASCI, Google Scholar, Index Copernicus

Рекомендовано до друку рішенням вченої ради ХНУ, протокол № 8 від 11.12.2025 р.

ISSN 2079-1372 Problems of Tribology, V. 30, No 4/118-2025

Problems of Tribology
Website: http://tribology.khnu.km.ua/index.php/ProbTrib
E-mail: tribosenator@gmail.com

CONTENTS

***ISSN 2079-1372 Problems of Tribology**, V. 30, No 4/118-2025*

Problems of Tribology
Website: http://tribology.khnu.km.ua/index.php/ProbTrib
E-mail: tribosenator@gmail.com

ЗМІСТ

ISSN 2079-1372 Problems of Tribology, V. 30, No 4/118-2025, 6-13

Problems of Tribology
Website: http://tribology.khnu.km.ua/index.php/ProbTrib
E-mail: tribosenator@gmail.com

DOI: https://doi.org/10.31891/2079-1372-2025-118-4-6-13

Development of Plasma-Sprayed Copper Alloy–Nickel-Clad Graphite Composite Coatings with Enhanced Tribological Properties

O. Terentjev* 0000-0002-4723-9305 , **O. Umanskyi** 0000-0003-3629-7224 , **O. Kushchev** 0009-0003-9056-0123 , **V. Varchenko** 0009-0007-6133-6711 , **V. Konoval** 0000-0003-2780-9064, **O. Bondarenko** 0009-0008-4492-3719, **V. Kurilovych** 0009-0005-3737-1862

Frantsevich Institute for Problems of Materials Sciences National Academy of Sciences of Ukraine, Ukraine

**E-mail: aleks.tmu@gmail.com*

Received: 30 July 2025: Revised 10 September 2025: Accept: 1 October 2025

Abstract

This study is focused on the development of composite plasma-sprayed coatings with a low coefficient of friction based on copper alloys with additions of nickel-clad graphite and on the investigation of their physicomechanical and tribological properties. Composite coatings were produced by atmospheric plasma spraying (APS) from agglomerated powders of copper alloys with the following compositions: BrONG-30 (70 wt.% BrOF10-1 + 30 wt.% nickel-clad graphite), BrOSNG-30 (70 wt.% BrOCTS5-5-5 + 30 wt.% nickel-clad graphite), and LNG-30 (70 wt.% L63 + 30 wt.% nickel-clad graphite). The application of graphite in a nickel shell improves its wettability by the metallic matrix and enhances adhesion. The obtained coatings exhibit high adhesion strength to the substrate (33–38 MPa) and density (94–97%). Tribological tests demonstrated that the LNG-30 – steel 45 friction pair showed the best performance. The inclusion of nickel-clad graphite reduced the friction coefficient by up to 1.5 times and increased wear resistance by up to 3.8 times. Using EDS and Auger spectroscopy, it was established that during friction in the LNG-30 – steel 45 pair, a film consisting of graphite (16–17 nm thick) and oxides of copper, zinc, nickel, and iron is formed on the counterbody wear track. The presence of such oxide films indicates a predominantly oxidative mechanism of friction, with minor adhesive interaction. The proposed coatings are promising for application in friction units, particularly under conditions where the use of liquid lubricants is limited or impossible.

Keywords: nickel-clad graphite, copper alloy, composite coatings, thermal spray coatings, friction and wear

Introduction

In modern mechanical engineering, friction units made of composite materials produced by powder metallurgy and containing solid lubricants are widely used. Such materials include iron–graphite and bronze–graphite composites. The areas of application and fabrication technologies of these materials are described in detail in a number of studies [1–3]. Bronze–graphite components are generally produced from tin bronze containing 88–92 wt.% copper and 8–11 wt.% tin with an addition of 1–4 wt.% graphite. These types of materials are used in friction units operating under low loads (3–4 MPa), sliding speeds (1–2 m/s), and temperatures (60–80 °C) in the presence of lubrication. They are widely used for the production of parts in instrument making, mechanical engineering, automotive engineering, as well as in equipment for light industry [4]. Impregnation of porous bronze–graphite products with lubricating oils (up to 2 %) allows the friction coefficient to be reduced to 0.03–0.06. Research is underway on the possibility of increasing the graphite content in such composites up to 25 % by powder metallurgy methods without decreasing their strength [5,6]. However, there are a number of engineering tasks that require components to operate under dry sliding conditions, where the use of conventional bronze–graphite materials is not feasible due to their low strength and inability to operate at elevated temperatures, loads, and sliding velocities.

It is known that for certain high-load and high-speed special friction units, virtually pure copper or tompac (a copper–zinc alloy containing 10 or 20 % zinc) has been used [7,8]. Tompac is characterized by high corrosion resistance and increased plasticity, and it can be readily processed by hot and cold deformation. However, it also has a tendency to adhere to steel, which may lead to an undesirable adhesive wear mechanism and consequently to rapid wear of the tribocouple. Adhesion during sliding friction can be prevented by forming a composite that exhibits a low friction coefficient due to the presence of a solid lubricating phase. In the present work, an innovative approach for extending the service life of friction units is proposed through the use of composite coatings with a low coefficient of friction based on copper alloys containing nickel-clad graphite. The proposed coatings are characterized by high run-in ability in friction against steel and by a self-lubricating effect. The use of nickel-clad graphite as a solid lubricant is justified by the fact that graphite in its pure form is not wetted by copper and its alloys (wetting angle $\Theta \approx 140°$) [9]. Poor adhesion of graphite to the metallic matrix in a composite coating results in its pull-out during operation and a deterioration of the functional properties of the coating. Moreover, during thermal spraying, unprotected graphite undergoes high-temperature oxidation and burns out in the plasma jet [10]. This leads to uncontrolled changes in the phase composition of the coating and poor stability and repeatability of results [11]. The wettability of graphite by nickel ensures the adhesion of the nickel film during cladding, while nickel, in turn, is well wetted by copper and its alloys [12]. As a result, graphite protected by a nickel shell does not burn out during spraying and remains well retained in the coating, ensuring a stable and controlled phase composition.

The aim of this work is to obtain composite plasma anti-friction coatings based on copper alloys with additions of nickel-clad graphite and to investigate their physico-mechanical and tribological properties.

Materials and equipment

For the purposes of this study, experimental batches of composite agglomerated powders were produced at the Institute for Problems of Materials Science of the NAS of Ukraine using industrial powders of the following copper-based alloys:

- tin bronze BrOF10-1 (with composition 89 mas. % Cu; 10 mas % Sn; 1 mas.% P) – agglomerated powder BrONG-30;
- tin–lead bronze BrOZS5-5-5 (with composition 85 mas. % Cu; 5 mas % Sn; 5 mas.% Zn; 5 mas. % Pb) – agglomerated powder BrOSNG-30;
- brass L63 (with composition 63 mas. % Cu; 37 mas.% Zn) – agglomerated powder LNG-30.

Each agglomerated composite powder composition contained 30 wt.% nickel-clad graphite powder (NPG-50). The particle size of the developed composite agglomerated powder materials for plasma spraying was in the range of –100 +80 μm.

The composite clad powder NPG-50 (produced by “Composite Systems Ltd.”, Zaporizhzhia, Ukraine) consisted of graphite coated with a nickel shell, the amount of nickel in the powder being 50 wt.%.

To increase adhesion, all coatings were deposited onto samples made of steel 45 (equivalents – AISI 1045, JIS S45C, DIN C45) through a bond coat formed from the thermoreactive powder material PTU5N containing 95 wt.% Ni and 5 wt.% Al (analogue – Metco 450NS).

Prior to deposition, the surface of the samples was subjected to grit blasting with electrocorundum powder grade 14A with particle size F22–F24 (ISO 8486-86) in order to clean, activate, and roughen the surface (Rz 63–Rz 80). The treatment was carried out at a distance of 90–150 mm and an angle of 60°–90°, using compressed air at a pressure of 0.5–0.7 MPa. The composite coatings of the above compositions were applied by atmospheric plasma spraying (APS) using an UPU-3D unit in a protective chamber equipped with a 15VB manipulator and an F4-MB plasma gun (Metco, USA). A mixture of argon and hydrogen was used as the plasma-forming gas. For comparative assessment of the influence of graphite on the tribological characteristics of the composite coatings, control test samples of plasma-sprayed L63 brass coatings were also prepared. The microstructure of the obtained plasma coatings and metallographic analysis were carried out using a REM-106 scanning electron microscope. Micro-X-ray spectral analysis (EDS) was performed on a JEOL JAMP-9500 microanalyzer.

The porosity of the coatings was determined using the intercept method (Rozival’s linear method). The principle of this method is that the volume fraction of phases comprising the structure of the material under examination can be determined from the relative area of the phases in the obtained microstructural images [13]. The adhesion strength of the coatings to the substrate was determined by a pin-test method as the arithmetic mean of five measurements. Tribological tests were carried out using an M-22M friction machine (designed at the I.M. Frantsevich Institute for Problems of Materials Science of the NAS of Ukraine) according to the “shaft – partial bearing” scheme, at a sliding speed of 4 m/s and a specific load of 2.5 kg/cm² (0.25 MPa); the sliding distance was 3 km. The counterbody was a steel 45 roller with a diameter of 40 mm and hardness of HRC 45–48.

The tests were performed at room temperature in open air under dry sliding conditions.

Results and their discussion

To optimize the technological parameters of plasma spraying for the composite powder materials BrONG-30, BrOSNG-30, LNG-30, as well as the reference coating from L63 brass powder, the argon flow rate, arc voltage

(U, V) and current (I, A) were used as variable parameters, and the spraying distance was adjusted accordingly. The powder materials employed in the study exhibit similar physico-mechanical properties, comparable morphology, granulometric distribution and close melting temperatures; therefore, the optimum spraying parameters obtained for each powder were found to be similar (Table 1).

Table 1

Modes of sputtering of plasma coatings

№	Coating material	Arc current, A	Arc voltage, V	Argon flow rate, l/min.	Hydrogen consum-ption, l/min.	Spraying distance, mm	Coating thickness, mm	Adhe-sion, MPa	Poro-sity, %
1	BrONG -30	450	60	45	7	150	0,4	35	3-5
2	BrOSNG -30	450	60	45	7	150	0,6	33	4-6
3	LNG -30	450	65	45	9	160	0,6	38	3-5
4	L63	450	65	45	9	160	0,6	40	3-4

The optimum spraying regimes were determined based on the following criteria: microstructure, density, and adhesion to the substrate. All coatings exhibited a density of 94–97 %, and the adhesion strength to the substrate was in the range of 33–38 MPa.

The obtained composite coatings possess a multiphase lamellar microstructure typical of plasma-sprayed coatings. In order to increase adhesion to the substrate, the coatings were deposited through an intermediate layer of Ni + 5 wt.% Al thermoreactive powder. All coatings adhere tightly to the substrate, and no delamination was observed in any case (Fig. 1).

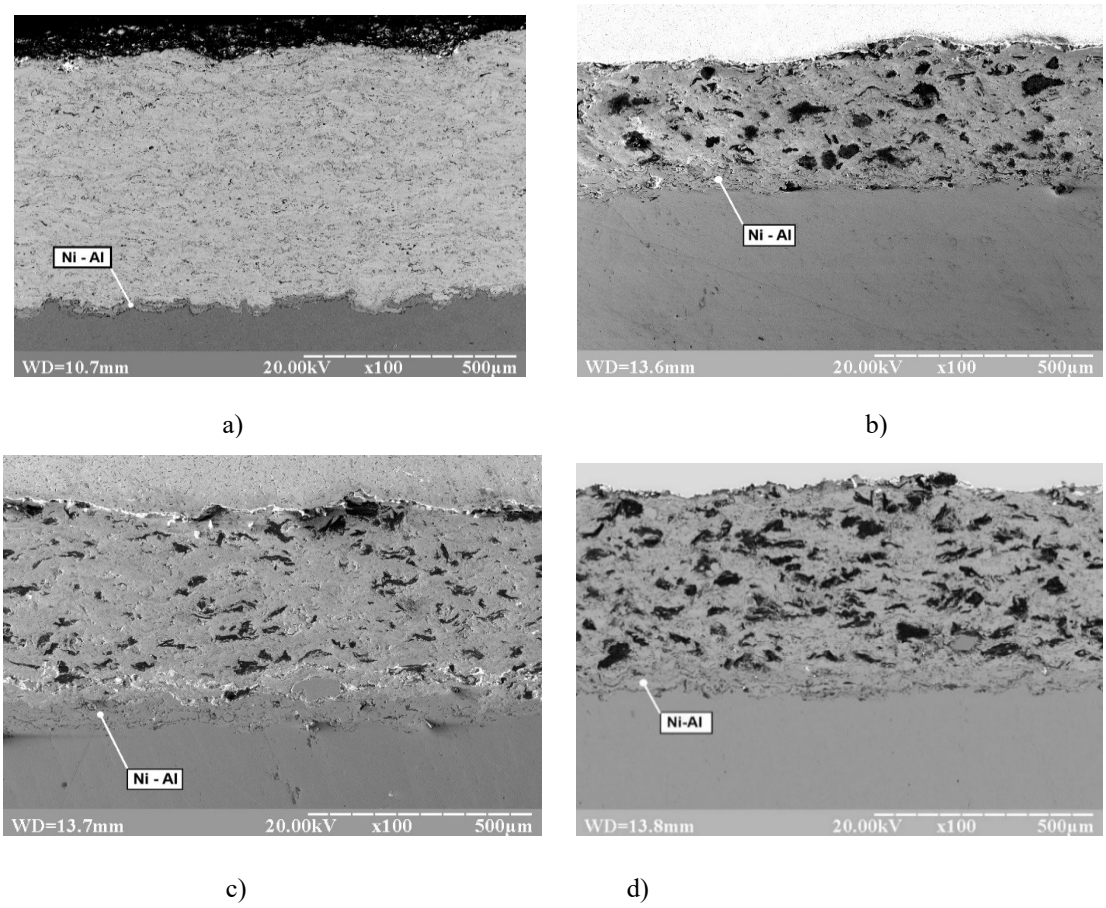

Fig.1. Microstructure of plasma composite coatings at 100x magnification: a – L63; b – BrONG -30; c – BrOSNG-30; d – LNG-30

The metallic matrix in all composite coatings is homogeneous and consists of Cu–Sn–P alloys (Fig. 2a, point 2), Cu–Sn–Zn–Pb alloys (Fig. 2b, point 3), and Cu–Zn alloys (Fig. 2c, point 4). Graphite grains are uniformly distributed within the metallic matrix (Fig. 2, point 1). During preparation of the transverse polished section of the coating, no pull-out of graphite particles was observed, indicating a high degree of cohesion, which is attributed to the use of nickel-clad graphite [14].

The results of the tribological tests of the composite plasma-sprayed coatings were determined as the arithmetic mean of five samples for each coating. Analysis of the obtained data showed that all composite coatings, when paired with steel 45, exhibit a coefficient of friction that is 1.6–1.8 times lower than that of the steel 45 – L63 coating friction pair (Table 2, Fig. 3).

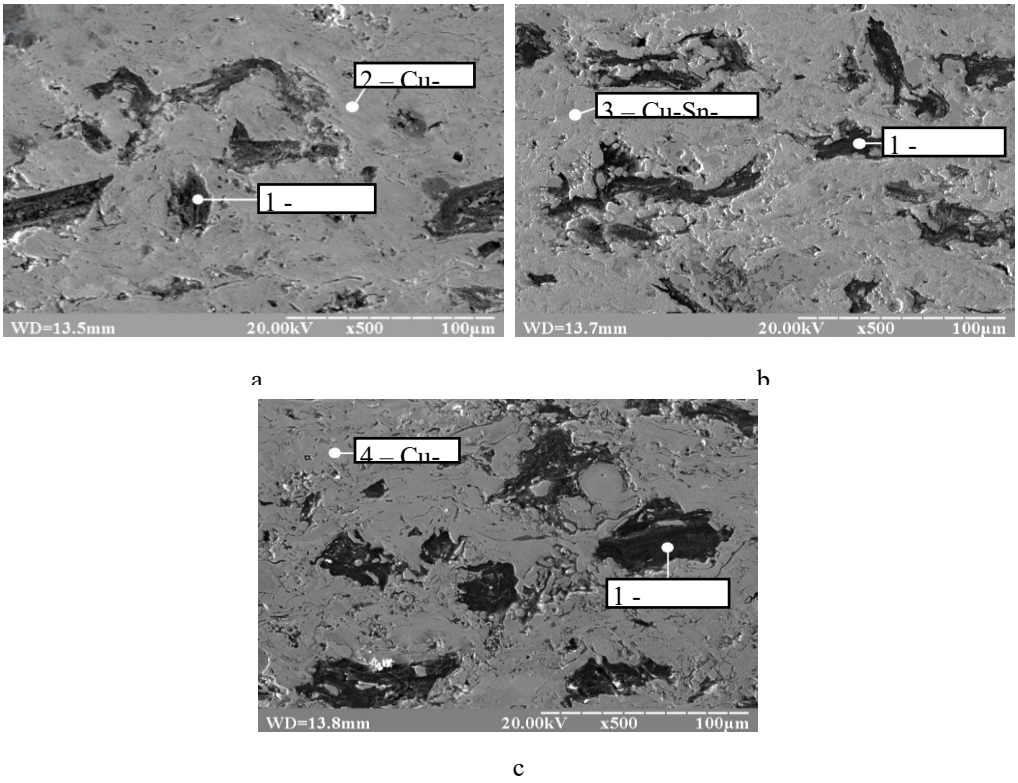

Fig. 2. Phase composition of composite plasma coatings: a – BrONG -30; b – BrOSNG -30; c – LNG-30

Table 2

Results of tribotechnical tests of plasma composite coatings.

№	Coating material	Friction path, L, km.	Coefficient of friction, f	Linear wear of friction pair, I, µm/km	Sample temperature, TºC
1	L63	3	0.3	18.9	100
2	LNG-30		0.20	4.9	86
3	BrONG -30		0.24	7.9	92
4	BrOSNG -30		0.27	12.8	120

As can be seen, the wear resistance of the samples with composite coatings is higher than that of the sample coated with L63. The lowest wear was observed for the LNG-30 coating, whereas the wear of the BrOSNG-30 coating was more than two times higher and the total linear wear of the friction pair reached 12.8 µm/km. Thus, it can be concluded that the BrOSNG-30 – steel 45 friction pair showed the poorest performance among all the composite coatings tested.

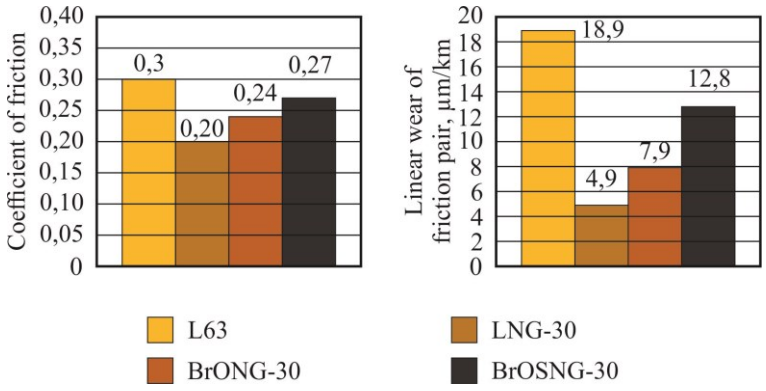

Fig. 3. Results of the study of tribotechnical properties of coating samples

The linear wear of the BrONG-30 – steel 45 friction pair amounted to 7.9 μm/km, while that of the LNG-30 coating was 4.9 μm/km. This is the best result among all the coatings tested. For comparison, the wear of the L63 – steel 45 pair was 18.9 μm/km, which is almost 4 times higher than that of the LNG-30 coating. The highest temperature in the contact zone was observed for the BrOSNG-30 coating (120 °C), whereas the lowest was recorded for the LNG-30 coating (86 °C), which correlates well with the friction coefficient values.

No delamination, microcracking or evidence of scuffing/adhesive seizure was observed on the working surfaces of the composite coatings. However, pores and pits are clearly visible, caused by the pull-out of graphite particles from the metallic matrix during friction (Fig. 4). Considering the obtained tribological results, it can be stated that under the given test conditions, the LNG-30 composite plasma coating showed the best functional performance when paired with steel 45. Therefore, this friction pair was selected for more detailed investigation.

In order to clarify the mechanisms of friction and determine the chemical composition of secondary structures formed on the working surfaces of the counterbody (Fig. 5), micro-X-ray spectral analysis was carried out on the wear tracks. The microstructure and composition of the wear track on the counterbody surface indicate minor transfer of coating material and formation of secondary structures consisting of complex oxides due to adhesive interaction, which is consistent with the results obtained during tribological tests (Table 2). The results of the chemical analysis of the wear track surface before ion etching (Table 3) show that the main element covering the entire surface is carbon. Its content at points 1 and 2 is the highest – 69.2 at.% and 53.2 at.%, respectively.

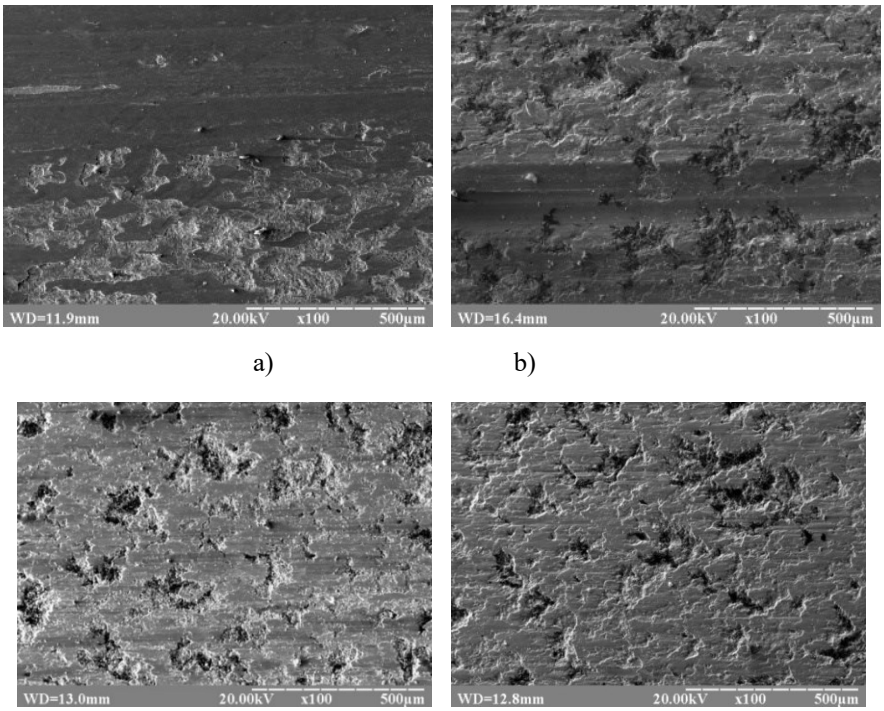

Fig.4. Microstructure of the friction surfaces of plasma coating samples: a – L63, b – LNG-30, c – BrONG-30, d – BrOSNG-30

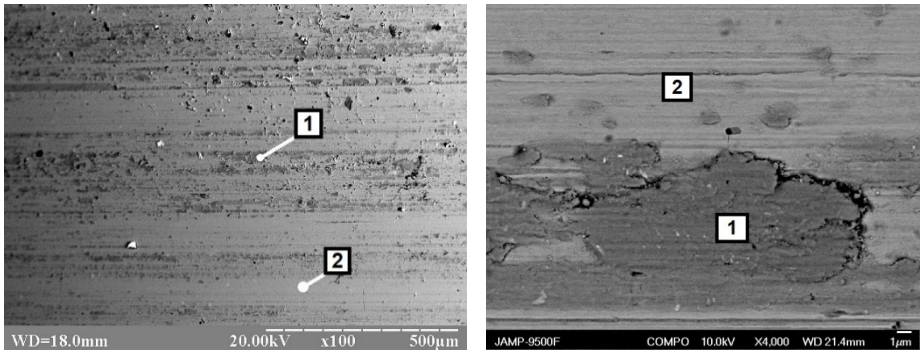

Fig. 5. Microstructure of the surface of the friction track of the counterbody (aand the places of analysis of the chemical composition of the transfer products from the composite coating sample LNG-30 (b)

This indicates that, during friction, graphite is transferred from the composite coating to the surface of the counterbody, which explains the significant reduction in the coefficient of friction (Table 2, Fig. 3). The small number of adhesive seizure areas and the presence on the surface of elements such as oxygen, copper, zinc, nickel, and iron suggest the formation of oxide films of complex chemical composition on the counterbody surface. This fact indicates that, in the steel 45 – LNG-30 coating friction pair, the oxidative wear mechanism prevails over the adhesive one.

Table 3

The content of friction track elements on the surface of the counter-body before ion etching

Analysis area	Chemical composition, at.%							
	C	N	O	Fe	Ni	Cu	Zn	S
1	69.3	1.6	13.8	2.8	1.3	9.6	1.2	0.4
2	53.4	2.1	25.3	12.9	1.1	4.0	0.8	0.4

After ion etching for two minutes at a rate of 8 nm/min, the carbon content on the surface of the wear track decreases to 2.4–3.4 at.% (zones 1 and 2, respectively) (Table 4). Thus, the thickness of the graphite film is 16–17 nm.

Table 4

The content of friction track elements on the surface of the counter-body after ion etching.

Analysis area	Chemical composition, at.%							
	C	N	O	Fe	Ni	Cu	Zn	S
1	2.4	1.5	45.8	22.5	8.7	13.8	5.3	0.0
2	3.4	0.9	1.8	93.3	0.2	0.2	0.2	0.0

The chemical composition of the secondary structure consists of complex oxides of copper, zinc, and nickel. The significant increase in iron (22.5 at.%) can be explained by the background from the substrate of the steel 45 counterbody. These oxides are absent on the surface of the counterbody (zone 2, Fig. 5a, Table 4).

Conclusions

The results of this study show that the introduction of a solid lubricant into copper-based antifriction alloys in the form of nickel-clad graphite makes it possible to obtain plasma-sprayed composite coatings with high functional performance. The microstructure of the composite coatings consists of a metallic copper-based matrix with uniformly distributed graphite grains. Graphite protected by a nickel shell does not oxidise or burn out in the high-temperature plasma jet during spraying and participates in the formation of the coating. Even with a nickel-clad graphite content of 30 wt.%, the coating exhibits a high adhesion strength to the substrate (33–38 MPa) and a high density (94–97 %).

All three composite coating compositions (BrONG-30, BrOSNG-30 and LNG-30) demonstrated better tribological properties in friction against steel 45 compared with the coating deposited from L63 brass powder. The best results were observed for the LNG-30 – steel 45 friction pair. The friction coefficient in this pair was 0.20, and the linear wear was 4.9 μm/km, which is 1.5 and 3.8 times lower, respectively, than in the L63 friction pair.

XPS and Auger spectroscopy confirmed that, during friction of the LNG-30 – steel 45 pair, a film consisting of graphite (16–17 nm thick) and oxides of copper, zinc, nickel and iron is formed on the wear track of the counterbody. The presence of solid lubricant in the form of graphite in the contact area promotes a reduction in the coefficient of friction and the linear wear of the friction pair. The presence of oxide films of metals originating from both the coating and the counterbody indicates the prevalence of an oxidative wear mechanism in this friction pair.

It was also established that there are local adhesion spots on the wear track surface of the counterbody, where secondary structures containing oxides of copper, zinc, nickel and iron are formed. The presence of such adhesion spots indicates that an adhesive wear mechanism is also present in this pair. However, the small number of these areas and the significant improvement in the tribological performance of the coating allow the conclusion that the dominant wear mechanism in the LNG-30 – steel 45 pair is oxidative.

Based on the results of the conducted research, the composite coatings BrONG-30, BrOSNG-30 and LNG-30 can be recommended for use in friction units of various mechanisms operating under extreme conditions. One of the possible applications of the LNG-30 composite coating is as an antifriction coating for the driving bands of artillery shells in order to extend the service life of gun barrels.

This work was carried out with the support of the National Research Foundation of Ukraine within the framework of project No. 2023.04/0066.

Author contributions

Terentjev O.: Conceptualization, Analysis, Investigation, Writing original draft; Umanskyi O.: Conceptualization, Analysis, Investigation, Methodology; Kushchev O.: Analysis, Investigation, Visualization, Writing original draft; Varchenko V.: analysis, Investigation; Konoval V.: Writing original draft, Review & editing, Bondarenko O.: Analysis, Investigation; Kurilovych V.: Review & editing.

References

1. Zhao X., Ma Z., Liu Y., Wang J., Zhang Q. Study on the friction and wear performance of graphene/porous bronze composites // *Journal of Tribology*. – 2025. – Vol. 147, No. 8. – P. 081402. – doi:10.1115/1.4059390.

2. Korol'kov D.V., Luk'yanov S.A. Phase formation and structure of bronze–iron–graphite composite powder material during hot forming // *Powder Metallurgy and Metal Ceramics*. – 2002. – Vol. 41, No. 3-4. – P. 160–165. https://10.1023/A:1021181413333

3. Wang L., Zhang Y., Liu Z. The study and application of bronze-graphite oil-containing self-lubricating composites // *Tribology*. – 1992. – Vol. 12, No. 1. – P. 23–28. http://dx.doi.org/10.1108/ILT-01-2016-0007

4. Yang Y., Zhou X., Li C., Zhang L., Chen J. Fabrication and properties of bronze–graphite composites by powder metallurgy // *Materials Today Communications*. – 2023. – Vol. 36. – P. 107666. – https://10.1016/j.mtcomm.2023.107666

5. Farouk M. Mahdi, Raed N. Razooqi, Saif S. Irhayyim. The Influence of Graphite Content and Milling Time on Hardness, Compressive Strength and Wear Volume of Copper - Graphite Composites Prepared Via Powder Metallurgy. Tikrit Journal of Engineering Sciences. 24 (3) (2017) c. 47 – 54 DOI: http://dx.doi.org/10.25130/tjes.24.2017.31

6. Shihong Ren, Xingchuan Xia, Kaihong Song, Jian Ding, Keping Geng, Guoxiong Song, Chenxu Huo, Yujie Wang, Weidan Liao, Nianxi Hua, Xueguang Chen. Effect of adding copper-plated graphite on the organization and wear reduction of Copper-Nickel alloy Composite Coatings. Surface and Coatings Technology, Volume 496, 15 January 2025, 131661. https://doi.org/10.1016/j.surfcoat.2024.131661

7. Kuanyshev, M., Nuralin, B., Salimov, B. et al. The improvement of friction bearing manufacturing technology by using copper alloy // *International Journal of Advanced Manufacturing Technology*. – 2017. – Vol. 88. – P. 317–324. https://10.1007/s00170-016-8758-2

8. Kuznetsov, I. S., Chernyshov, N. S., Logachev, V. N. et al. Combined anti-friction coatings based on nichrome and copper // Journal of Friction and Wear. – 2024. – Vol. 45, No. 3. – P. 172–178. – https://10.3103/S1068366624700260

9. Naydich Yu.V., Kolesnichenko G.A. Interaction of metal melts with the surface of diamond and graphite. Kyiv: Naukova Dumka, 1967. 89 p.

10. Kushchev O.V., Terentyev O.E., Brazhevsky V.P., Kostyunik R.E., Vedel D.V., Vasilyev O.O., Chernyshov O.O., Krasikova I.E., Martsenyuk I.S., Umansky O.P. Influence of high-temperature flow on the morphology and chemical composition of nickel-graphite composite powder during plasma coating. Powder Metallurgy – No. 7/8, 2024.

11. Kushchev O.V., Terentyev O.E., Brazhevsky V.P., Chernyshov O.O., Vasiliev O.O., Kostyunik R.E., Martsenyuk I.S., Umansky O.P. Influence of sputtering modes and manufacturing features of composite powders of the nickel-graphite system on the structure and chemical composition of plasma coatings Powder Metallurgy – No. 9/10, 2024.

12. Naidich Ju.V. The Wettability of Solids by Liquid Metals. Progress in Surface and Membrane Science. Volume 14, 1981, Pages 353-484.

13. Kharlamov V.F. Prediction of powder coating porosity // *Powder Metallurgy and Metal Ceramics*. – 1990. – Vol. 29, No. 6. – P. 493–498. https://10.1007/BF00793381

14. Durov, O., Umanskyi, O., Kushchev, A., & Krasovskyy, V. The use of nickel interlayer to improve the wetting of graphite with bronze in the development of composite materials for gas-thermal coatings // *The Journal of Adhesion*, 2025. https://10.1080/00218464.2025.2526480

Терентьєв О.Є., Уманський О.П., Кущев А.В., Варченко В.Т., Коновал В.П., Бондаренко О.А., Костюнік Р.Є., Курілович В.Д. Розробка плазмових композиційних покриттів системи мідний сплав-плакований графіт з підвищенним рівнем триботехнічних властивостей

Данна робота присвячена розробці композиційних плазмових покриттів з низьким коефіцієнтом тертя на основі сплавів міді з добавками графіту, плакованого нікелем і дослідження їх фізико-механічних та трибологічних властивостей. Відпрацьовано технологію нанесення композиційних покритий методом плазмового напилення (APS) з конгломерованих порошків на основі мідних сплавів наступних складів: БрОНГ-30 (70 мас.% БрОФ10-1 + 30 мас.% графіту, плакованого нікелем); БрОСНГ-30 (70 мас.% БрОЦС5-5-5 + 30 мас.% графіту, плакованого нікелем); ЛНГ-30 (70 мас.% Л63 + 30 мас.% графіту, плакованого нікелем). Застосування графіту у нікелевій оболонці вирішує проблему підвищуення змочуваність графітової фази металевою матрицею, а також покращує адгезію. Отримані покриття мають високий адгезійний зв'язок з основою (33 - 38 МПа) і високу щільність (94 - 97%).

В результаті проведених трибологичних випробувань встановлено, що Найкращі результати спостерігалися в парі тертя ЛНГ-30 - сталь 45 покриття. Включення до складу композиційних покриттів на основі мідних сплавів плакованого нікелем графіту, забезпечує зниження коефіцієнта тертя у трибопарі до 1,5 разів та підвищує її зносостійкість – до 3,8 разів.

Методами МРСА та Оже-спектроскопії встановлено, що на поверхні доріжки тертя контртіла пари ЛНГ-30 – сталь 45 у процесі тертя формується плівка з графіту (завтовшки 16 – 17 нм) та оксидів міді, цинку, нікелю та заліза. Присутність окисних плівок металів зі складу покриття та контртіла свідчить про переважно окисний механізм тертя у цій парі тертя.

Отже, запропоновані покриття можуть бути перспективними для застосування у вузлах тертя особливо в умовах, де використання рідких змащувальних матеріалів є обмеженим або неможливим.

Ключові слова: плакований нікелем графіт, мідний сплав, композитні покриття, газотермічні покриття, тертя та зношування

ISSN 2079-1372 Problems of Tribology, V. 30, No 4/118-2025, 14-20

Problems of Tribology
Website: http://tribology.khnu.km.ua/index.php/ProbTrib
E-mail: tribosenator@gmail.com

DOI: https://doi.org/10.31891/2079-1372-2025-118-4-14-20

Initiation of a data bank of activation energy values for tribo-reaction wear and modification of Shkh 15 and Steel 45 steels in the environment of hydrocarbon liquids

O. I. Bogdanovych[0000-0002-3358-3324], **S. O. Puzik**[0000-0001-6151-1240], **V. V. Tokaruk**[0000-0002-1965-1765], **A. M. Khimko**[0009-0009-8059-880X]

State University "Kyiv Aviation Institute", Ukraine

**E-mail: vetalion1980@gmail.com*

Received: 05 August 2025: Revised 20 September 2025: Accept: 05 October 2025

Abstract

The kinetic technique, which is developed on the basis of the kinetic three-stage model of normal mechano-chemical wear, is considered. The values of the activation energy of wear of secondary structures of structural steels in the medium of hydrocarbon liquids are obtained by the experimental-calculation method. The obtained results of the assessment of the energy of activation of wear and chemical modification of structural steels in the media of hydrocarbon liquids allow us to establish a data bank of anti-wear and modification properties of secondary structures, which can serve as reference data on the anti-wear and modification properties of secondary structures on structural steels in the media of hydrocarbon liquids.

Keywords: tribokinetic experiment, triboconjugation, activation energy, kinetic model, wear resistance criterion

Introduction

Numerous units of fuel and hydraulic systems of modern technology (pumps, valves, regulators, distributors, etc.) operate in the environment of low molecular weight hydrocarbon liquids, which are at the same time a lubricating medium for the listed units.

Among the tribocoupals of fuel units operating under frictional conditions, the most loaded are the units of high-performance high-pressure fuel pumps, which pump fuel to the consumable tanks of aircraft and storage tanks of low molecular weight hydrocarbon liquids, as well as supply this fuel to the combustion chambers of turbojet and turboprop engines. It is the wear resistance of these components that largely determines the resource and reliability of fuel pumps. The most common are plunger and centrifugal pumps. In plunger pumps, there is a linear contact between the parts of the components that are subjected to friction, namely, the spherical end of the plunger and the inclined washer form a friction pair [1].

The development of scientific and technological progress is impossible without the development of new structural and fuel-lubricants (PMM). To do this, it is necessary to conduct modeling and full-scale (industrial) tests of such materials. These tests require the use of unified, universal, energy, i.e. invariant in known ranges of load values, criteria for assessing the wear resistance of structural materials and anti-wear properties of fuel and lubricants [2].

Analysis of research and publications

Recently, the number of scientific and experimental works on the use of fracture activation energy, including surface (i.e. wear) to explain the destructive processes of structural materials, mainly steels, in the fuel and lubricants environment has increased [3]. The use of activation energy is also present in the dissertation [4], where its value is determined by the cohesive properties of matter.

In the structural-energetic theory of friction and wear and the theory of structural adaptability of tricoupling materials, the following characteristics are used: specific fracture work – A_D, energy intensity of the friction system by thermal index – "ECTq", critical value of friction work – A_{cv}, critical (limiting) density of internal energy – U^*, (for abrasive wear), surface energy or surface tension – γ, the work of the *WOE* electron output, exo-electron emission – *EEE*, contact potential difference – U_{CPD} [5, 6, 7]. At the same time, the energy characteristics of wear resistance characterize the processes of surface failure, reasonably assess the friction conditions, the choice of tricoupling materials, their coupling within normal wear (without damage) determine the boundaries of the transition to damage.

Thus, the most common, best studied and experimentally tested criterion is the specific work of surface fracture (the ratio of the work of friction force to the amount of wear) is an imaginary characteristic of wear resistance and depends not only on the surface strength of the material, but also on the ability of the tribosystem to dissipate energy. Use of surface energy γ complicated by the lack of reliable data on the value γ of pure metals, not to mention alloys in real conditions.

The energy criterion for assessing compatibility – surface energy or surface tension γ, electron output work, etc., as well as wear resistance criteria, are not direct compatibility characteristics. In addition, there are no reliable data γ even for pure metals, the values γ and electron yield are different for different faces of the crystal.

The most direct, quantitative, structural-energetic (materials science), kinetic (physicochemical) characteristic useful for assessing the wear resistance of triboconjugation materials is the activation energy of surface destruction (wear) E^D, which characterizes a potential barrier to the implementation of elementary acts of destruction. At the same time, in the range of structural adaptability of triboconjugation materials, E^D must be invariant, which can be used as a criterion assessment of anti-wear properties of lubricants. This, in contrast to the existing variety of criteria for assessing wear resistance, regulated by GOST 9490-75 and GOST 23.002-78, allows the use of E^D as a universal, the only criterion for assessing the tribological properties of triboconjugation materials [8].

The universality of E^D is confirmed by its use as a criterion for evaluating various physical processes. For example, the use of activation energy U as a function of resistance to deformation of a plastically deformable metal sample is known. In this case, U, which describes the processes of rearrangement of atoms in the crystal lattice, is determined by the degree of violation of the order caused by the deformation. Despite the good singing of the fall in U values with the activation energy of diffusion and self-diffusion, as well as the confirmation of the equality of $U \cong 20RT_{mp}$. (T_{mp} is the melting point), this conclusion does not inspire much confidence due to the low accuracy of estimating the degree of violation of the order of the crystal lattice [8].

However, even the correct choice of the criterion for evaluating the wear resistance and compatibility of triboconjugation materials does not guarantee the correct determination of the wear resistance and compatibility of these materials. The correct choice of the criterion for assessing wear resistance and compatibility is a necessary condition, but not sufficient. A sufficient condition for the correct assessment of wear resistance and compatibility of triconjugation materials is the correct methodology for assessing the wear resistance and compatibility of these materials.

To date, there are three methods for estimating the activation energy: 1) graphical; 2) extrapolation; 3) kinetic. In the first methodology, the value of E^D depends on the scale of the coordinate system. Therefore, E^D can only be used in comparative tests. In the second methodology, the value of E^D depends on the subjective qualities of the researcher (tester), since extrapolation is an approximate determination of the values of $f(x)$ at points x that lie outside the segment (x_0, x_n) by their values at points x_o<x<... <x_n. However, the best, i.e. the most accurate, technique is the third, kinetic, where the value *of* E^D is determined by the laws and equations of chemical kinetics, when the order of a chemical reaction is first determined, then the rate constant of this reaction is at least two temperatures, and according to the Arrhenius equation, E^D is calculated [8].

Research methodology

Next, we will consider the kinetic technique, which is developed on the basis of a kinetic, three-stage model of normal mechano-chemical wear, for the description of which the following scheme of the tribological reaction (TR) is used:

$$RB \overset{A}{\leftrightarrow} Me_{x_1}(RB)^*_{y_1} \overset{M}{\rightarrow} Me_{x_2}(RB)^*_{y_2} \overset{D}{\rightarrow} Me_{x_3}(RB)^*_{y_3} \overset{D}{\rightarrow} Me^0, \quad (1)$$

where *RB* is the lubricant involved in triborecia: in the simpler case, only the effect of the active component of the lubricant – the additive, *R* – the hydrocarbon radical of the additive, *B* – the active component of the additive, Me^o – the juvenile areas of the surfaces of the contacting materials of triboconjugation; x_i, y_i is the fractional coefficient of components that are analogues of stoichiometric coefficients in a true chemical reaction.

An asterisk indicates active triboreaction complexes:

$Me_{x_1}(RB)^*_{y_1}$ – adsorption complex formed as a result of adsorption of lubricant (*RB*) on juvenile areas of surfaces of structural materials triboconjugations (Me^o). This complex is active in relation to the next stage – chemical modification (M);

$Me_{x_2}(RB)^*_{y_2}$ – modified (dissipative secondary) structures active in relation to the stage of surface destruction (D);

$Me_{x_3}(RB)^*_{y_3}$ is a complex of surface destruction (wear products), in fact, a product of a tribological reaction.

As can be seen from equation (1), only the first stage - adsorption (A) is accepted as reverse, i.e. bilateral. The rest of the stages are considered to be significantly reversed, i.e. unilateral. Juvenile sections of contacting structural materials are both the initial reaction component and the catalyst of triborereaction, which accelerates the course of the first stage A. At the same time, the total area of juvenile areas, i.e. the concentration of Me^o at normal (stationary) wear remains constant, while the amount of starting materials is constantly decreasing due to wear. The amount of lubricants and structural materials is assumed to be large enough and their concentration does not depend on the duration of triboreaction. Otherwise, it is necessary to use absolute values, not concentrations.

According to the given kinetic three-stage model of normal mechano-chemical wear, an experimental and computational method for assessing the kinetic characteristics and activation energies of all three stages of triboreaction was developed. According to which, we first determine the kinetic characteristics and activation energy - the E^D of the third, last stage of triboreaction, that is, in fact, wear, since as a result of tribokinetic tests of triboconjugation materials.

We measure the diameters of the wear spots of the three balls and calculate the wear volumes, i.e. the volumes of the ball segments V_w. After conducting similar tribokinetic tests at 4-5 values of the duration of such tests (t), we plot the dependence of $\lg V_w$ on the duration of the tests t. Straight lines of such graphs indicate the first order of the stage under study (in this case, the third stage of the triboreaction), i.e. $N^D \cong 1$, and the tangent of the angle of inclination of the lines to the abscissa axis graphically determines the velocity constants of the stage under study, in this case K^D. But the graphical assessment and value of the order and rate constants of the studied stages of triborereaction is approximate. Therefore, more accurate values of these kinetic characteristics must be established analytically, that is, determined by the appropriate formulas.

$$N^D = \frac{\lg W_2/W_1}{\lg V_w t_{i+1}/V_w t_i},$$

where W_1 and W_2 are the rates of stage III, i.e. wear, which are determined for the intervals of duration of tribokinetic tests:

$$\Delta t = t_{i+1} - t_i.$$

That is,

$$W_1 = \frac{V_w t_{i+1} - V_w t_i}{\Delta t},$$

where $V_w t_{i+1}$ and $V_w t_i$ are the wear volumes of the three balls during the duration of tribokinetic tests at the duration t_{i+1} and t_i, respectively.

In this case, the order of the third stage can be calculated in two ways: 1) for each interval Δt, and then calculate the arithmetic mean of N_i; 2) for the initial and final intervals Δt, that is, N^D is calculated during the entire duration of tribokinetic tests.

The rate constant of the III stage, i.e. wear, was calculated using the difference V_w in the interval Δt, according to the equation:

$$K^D = \frac{\Delta V_w}{\Delta t V_{w.m}} = \frac{W}{V_{w.m}}$$

where $V_{w.m}$ is the arithmetic mean of V at the beginning and end of the interval Δt.

Having established at least 4 values *of* K^D, it is possible to carry out statistical processing of the results obtained, i.e. to calculate the average values *of* K^D, the confidence interval of the estimate *of* $K^D - \Delta K^D$, and the coefficient of variation of the assessment of the specified estimate – Z_c.

Repeating the tribokinetic tests according to the above method at a temperature other than T_1, according to the Arrhenius equation, we calculate the activation energy of the III stage of TR - the actual wear of triboconjugation materials.

In addition, the formula proposed by the author for calculating the area of secondary structures participating in the TR (S_{ss}.) [8] and, as a result, the calculation of the relative area of secondary structures:

$$\delta = \frac{S_{ss}}{S_к}$$

where S_k is the contact area, i.e. the area of three contact spots, made it possible to calculate the kinetic (N^m, K^m) characteristics and activation energy of the second stage of TR-chemical modification (E^m):

$$S_{вс} = S_к - \frac{\Delta V_{w.m}}{\Delta t h_{ss} K^D}$$

where $\Delta V_{w.m} = V_{wti+1} - V_{wti}$ is the wear volume of three bullets in the interval $\Delta t = t_{i+1} - t_i$, respectively; h_{ss} is the thickness of secondary structures or the thickness of chemical modification, the value is variable: with an increase in the duration of tribokinetic tests, h_{ss} decreases.

The kinetic characteristics of the first stage of TR (N^a, K^a) and the activation energy can be determined by conducting tribokinetic tests according to the specified algorithm with a lubricant with a chemically active substance, i.e. an additive, for example, oleic acid [2], which allows determining the specified kinetic parameters and activation energy of tribosorption for the operation of a chemically active substance.

These tribokinetic tests were performed at one fixed temperature T_1. If we conduct similar tribokinetic tests at a temperature other than T_1 T_2, we get the values of similar kinetic criteria N and K of the three stages of TR. And knowing K at two temperatures (T_1 and T_2) we calculate the activation energies of these stages according to the Arrhenius equation:

$$E = \frac{RT_1T_2}{T_1 - T_2} \ln\frac{K_2}{K_1} = \frac{1{,}9144T_1T_2}{T_2 - T_2} \lg\frac{K_2}{K_1} \cdot 10^2$$

where K_1 and K_2 are the rate constants at temperatures T_1 and T_2, respectively; 1.9144 is the product of the gas constant $R=(8.3143 \pm 0.0012)\cdot 10^3$ J/K·mol times the modulus of conversion of natural logarithms into decimals, which is equal to 2.3056.

The proposed method for conducting tribokinetic tests of triboconjugation materials was tested experimentally. On the friction machine "UPS-01" (Fig. 1, 2 and 3), which is a modernized, i.e. improved, analogue of the friction machine “КИИГА-2”, Steel 45 was studied, in the environments of aviation fuel RT, aviation oil hydraulic oil AMG-10, aviation oil MK-8 with the addition of oleic acid [2]. The “КИИГА-2” friction machine was used to determine the wear resistance of ShKh 15 in the long-term storage environments of TS-1 and TS-1* aviation fuels [8-11]. In addition, tribological tests of Steel 45 steel were carried out in the environment of inactive vaseline oil on the ATKD friction machine (modernized MT-1 friction machine) in the reciprocating mode [12].

Fig.1. Appearance of the device UPS -01

Research results.

The conducted tribokinetic tests established kinetic (N^D, K^D, N^m, K^m) and energy-activation (E^D, E^m) criteria for assessing the wear resistance of ShKh 15 and anti-wear properties of RT and AMG-10, as well as kinetic (N^a, K^a, N^m, K^m, N^D, K^D) criteria for assessing the wear resistance of Steel 45 and the anti-wear properties of MK-8 with

the addition of oleic acid [2]. Later, using the developed method of tribokinetic tests, kinetic (N^D, K^D) and activation energies of wear ShKh 15 (E^D) were established in the aviation fuel media "TS-1" and "TS-1*" of long-term storage [8, 9], kinetic (N^m, K^m) and activation energy of the II stage of TR - chemical modification (E^m) SHX-15 in the medium "TS-1" [10, 11], as well as the kinetic (N^D, K^D) and activation energy of TR - surface destruction, i.e., actually wear (E^D) [12] Steel 45 during reciprocating motion.

The values of the activation energy of the wear of secondary structures on the ShKh 15 in the aviation fuel environment for RT turbojet engines and in the aviation lubricant environment for AMG-10 hydraulic systems with the reproducibility of the results characterized by a coefficient of variation of not more than 2.5 % were established [2].

All results are shown in Table 1. E^D, E^m. According to the results of tribological tests of Steel 45 steel in the medium of inactive vaseline oil on the ATKD friction machine in the reciprocating motion mode, kinetic characteristics (reaction rates, order and velocity constants) and shear activation energy E^D =8.96 kJ/mol were determined, which is significantly less than in unidirectional motion [12].

Table 1.

Research results

	Name of the PMM	Meaning E^D kJ/mol	Meaning E^m kJ/mol
1	AMG-10 oil	51,76	1,14
2	Fuel RT	21,28	9,39
3	Fuel TS-1	20,31	0,296
4	Fuel TS-1* for long-term storage	19,58	1,98

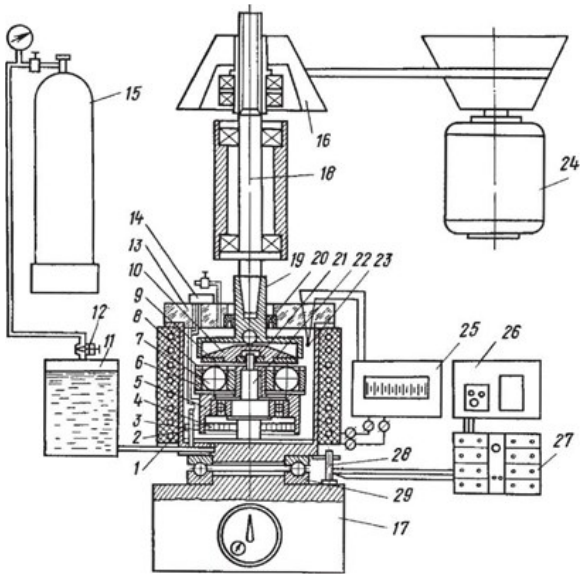

Fig. 2.- Scheme of the UPS -01 device: 1 - electric spiral; 2 - fuel chamber; 3 - limiter; 4 - spiral spring; 5 - movable block; 6 - separator; 7 - sample ball; 8 - pressure washer; 9 - sample disk; 10 - sample disk holder; 11 - fuel tank; 12-throttle valve; 13-fuel chamber cover; 14-limit switch; 15-nitrogen cylinder; 16 - flat disk drive pulley; 17 - arrow indicator; 18 - drive shaft; 19-adapter; 20 - sealing collar; 21-spherical bearing; 22 - central axis; 23-thermocouple; 24-electric motor; 25-thermoregulator KMP1-502; 26-automatic unit; 27-amplifier; 28-tension beam; 29-bearing

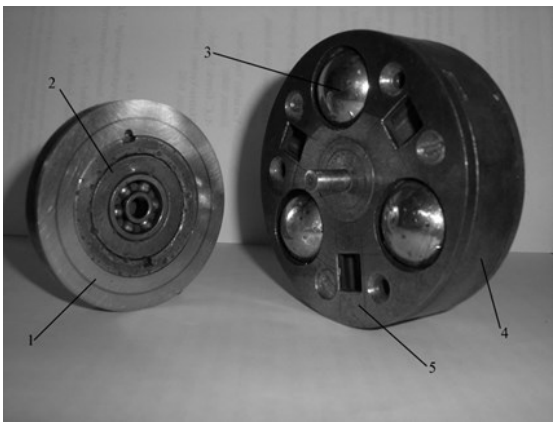

Fig. 3. Friction pair of friction machines UPS -01 and "КИИГА-2": 1-disk-sample; 2-disk-sample holder;

3-ball; 4-separator; 5-thrust washer

Conclusions

1. The obtained results of the assessment of the energy of activation of wear E^D and chemical modification of ShKh 15 steel in the oil (Table 1) allow us to establish a data bank of anti-wear and modification properties of ShKh 15 steel, which can serve as reference data on anti-wear and modification properties of ShKh 15 steel in the environments above the specified hydrocarbon liquids E^m.

2. To obtain secondary structures steel ShKh 15 with better anti-wear properties, it is necessary to spend more energy for the activation of chemical modification, with the exception of TS-1* fuel for long-term storage E^m

3. An exception to this rule can be preliminarily explained by changes in the physicochemical composition of TS- 1 fuel* in comparison with the similar composition of TS-1 according to ДСТУ 320.001249943.011-99, which indicates the influence of the physicochemical composition of fuel and lubricants on energy costs when modifying the aircraft on ShKh 15 steel in the environments above the specified fuel and lubricants.

4. For a more accurate explanation of this phenomenon, it is necessary to conduct additional studies to establish the reasons for the increase for less wear-resistant aircraft on ShKh 15 steel in the TS-1 fuel environment* E^m

References

1.Chebotarev L. I., Puzik S. O., Borsuk P. S. Technical Operation of Means of Fuel Supply of Airports: Textbook. Kyiv: NAU, 2018. 264 p. http://ufd.lib.nau.edu.ua:8080/library/DocumentView?doc_id=486138

2. Bogdanovich A. I. Kinetic and energetic-activation characteristics of wear resistance and compatibility of materials of tribospjuzheniy. Dis.... Tech. Sci.: 05.02.04 Kiev, 1987. 23 p

3. Mikosyanchyk O.O. Structural-energy and rheological indicators of the lubricating layer in the friction contact in the conditions of unstable modes of operation: Author. Dis. … Dr. Techn. Sci.: 05.02.04 Kyiv, 2017. 40 p. https://uacademic.info/ua/document/0517U000492

4. Dukhota O.I. Scientific and Technical Foundations of Improving the Durability of Parts of Aviation Tribomechanical Systems under the Conditions of Their Freting-Contact Interaction: Author. Dis. … Dr. Techn. Sci.: 05.02.04 Kyiv, 2019. 44 p. https://nau.edu.ua/site/variables/news/2019/2/avtoreferatDuhota.pdf

5. Spikes, H. Stress-augmented thermal activation: Tribology feels the force. Friction, 2018 vol 6, pp. 1–31. https://doi.org/10.1007/s40544-018-0201-2

6. Kajdas C. K., Kulczycki I. A., Kurzydłowski K. J., Molina G. J. Activation energy of tribochemical and heterogeneous catalytic reactions Materials Science-Poland, 2010, Vol. 28, No. 2, pp. 523-533. https://www.materialsscience.pwr.wroc.pl/bi/vol28no2/articles/ms_15_2009-373kajdas.pdf

7. Li Y. S., Bhuiyan F. H., Lee J., Martini A., Kim S. H. Elucidating Tribochemical Reaction Mechanisms: Insights into Tribofilm Formation from Hydrocarbon Adsorbates Coupled with Tribochemical Substrate Wear. RSC Mechanochem., 2024, 32 p. https://doi.org/10.1039/D3MR00036B

8. Bogdanovych O. I., Al-Quraan T. M. A., Tokaruk V. V., Haddad J. S. Algorithm for Tribokinetic Modeling Tests of Triboconjuction Materials for Industrial Products. Tribology in Industry. 2021. Vol. 43, № 1. P. 159–166. https://doi.org/10.24874/ti.977.10.20.02

9. Bogdanovych O. I., A., Tokaruk V. V., Comparison of activation energy of surface fracture of ShKh15 steel in the environment of aviation fuels media "TS-1" and "TS-1*" of long-term storage. "AVIA-2017": materials of the XIII International. Scientific and Technical Conference, Kyiv, April 19-21. 2017, pp. 19.78-19.82. https://avia.nau.edu.ua/doc/avia-2017/AVIA_2017.pdf

10. Bogdanovych A. I., Tokaruk V. V., Statnikov Y. I. determination of the energy activation of mechanicalchemical modification of ShKh 15 steel in aviation fuel “TS -1” long-term storage. Problems of friction and wear, 2020, 1 (86) P. 93-97. https://doi.org/10.18372/0370-2197.1(86).14492

11. Bogdanovych A.I. Estimation of kinetic characteristics and modification activation energy ShKh 15 in aviation fuel "TS-1". – Proceedings the fifth world congress “Aviation in the XXI-st century”, September 25-27, 2012, vol.1, Kyiv, Ukrain, p. 1.1.1.-1.1.4. https://congress.nau.edu.ua/doc/congress-2012/Congress_2012_V1.pd

12. Bogdanovich A.I., Tkachenko I.V., Grinkevich K.E. Assessment of kinetic characteristics and energy of activation of wear in reciprocating movement. "AVIA-2009": materials of the IX International. Scientific and Technical Conf., Kyiv, September 21-23, 2009, pp. 14.5-14.8. https://avia.nau.edu.ua/doc/avia-2009/AVIA_2009_v2.pdf

Богданович О. І., Пузік С. О., Токарук В. В., Хімко А.М. Започаткування банка даних значень енергії активації трибореакції зносу та модифікування сталей ШХ15 та Ст 45 в середовищі вуглеводневих рідин

Розглянуто кінетичну методику, яка розроблена на основі кінетичної трьох стадійної моделі нормального механо-хімічного зносу. Представлені значення енергії активації зносу вторинних структур конструкційних сталей в середовищі вуглеводневих рідин отримані експериментально-розрахунковим методом. Отримані результати оцінки енергії активації зносу та хімічного модифікування конструкційних сталей в середовищах вуглеводневих рідин дозволяють започаткувати банк даних протизносних та модифікаційних властивостей вторинних структур, що може слугувати довідковими даними по протизносним та модифікаційним властивостям вторинних структур на конструкційних сталях в середовищах вуглеводневих рідин.

Ключові слова: трибокінетичний експеримент, трибоспряження, енергія активації, кінетична модель, критерій зносостійкості

ISSN 2079-1372 Problems of Tribology, V. 30, No 4/118-2025, 21-30

Problems of Tribology
Website: http://tribology.khnu.km.ua/index.php/ProbTrib
E-mail: tribosenator@gmail.com

DOI: https://doi.org/10.31891/2079-1372-2025-118-4-21-30

Modifying NiAl intermetallic powder by phosphorus cladding for plasma-sprayed coatings and studying their structure and tribological properties

T. Levchuk[1] 0009-0008-5818-6684, **O. Poliarus**[1,2] 0000-0003-3181-419X, **V. Konoval**[1] 0000-0003-2780-9064, **O. Makarenko**[1] 0000-0002-8500-1365

[1]*Frantsevich Institute for Problems of Materials Sciences National Academy of Sciences of Ukraine*
[2]*Institute of Metallurgy and Materials Science, Polish Academy of Sciences, Krakow, Poland*
**E-mail: t.levchuk@ipms.kyiv.ua*

Received: 07 August 2025: Revised 25 September 2025: Accept: 10 October 2025

Abstract

This article examines the impact of adding phosphorus to NiAl intermetallic powder on the structure, microhardness, and tribological properties of plasma-sprayed coatings, which are suitable for use under dry friction conditions. A composite powder designated NiAl+P was obtained by cladding NiAl powder with phosphorus-containing compounds. It was found that the addition of phosphorus promotes the formation of phosphate phases in the coatings, which reduces microhardness but significantly increases wear resistance. In the NiAl+P coating, a protective phosphate film forms on the friction surface during tribological tests, acting as a solid lubricant that reduces the wear rate by almost 2.5 times. The results demonstrate the effectiveness of phosphorus as an alloying element for enhancing the service life of NiAl-based coatings in tribological assemblies.

Keywords: NiAl intermetallic, phosphorus cladding, plasma spraying, phosphate film, tribological properties, wear resistance, solid lubricant, microstructure.

Introduction

Nickel–aluminum intermetallic alloy (NiAl) is widely used to produce thermal spray coatings for high-temperature service [1–6]. Owing to the formation of a dense protective aluminum oxide (Al_2O_3) film on the NiAl surface upon heating, such coatings exhibit excellent heat resistance and serve as an effective barrier against oxidation of the base material [3, 7–8]. NiAl-based coatings have been successfully used as heat-resistant and thermal barrier coatings under high-temperature conditions [1–5, 7]. However, expanding NiAl coatings to friction conditions (tribological units) is promising, but another problem arises in such applications. Under frictional loads, the protective Al_2O_3 oxide film breaks down, allowing direct contact with the counterface material, resulting in surface seizure (galling) and, consequently, catastrophic adhesive wear [3, 9–11]. According to the phenomenological model of fatigue tribological damage accumulation in the surface layer under friction [12], the durability of friction units is primarily governed by the kinetics of surface damage accumulation and the possibility of forming protective secondary structures on the contact surfaces. It is known that to improve wear resistance and provide a low friction coefficient in a contact pair of materials, it is advisable to introduce specific components into the coatings that can form films during friction, acting as solid lubricants [3, 5, 9, 10, 13–18]. This approach enables the coatings to perform effectively at both room and elevated temperatures without experiencing severe wear. In this work, phosphorus oxide-based compounds are introduced by cladding the initial NiAl powder, proposed for forming solid lubricant films within the coating material. This research aims to study the structural features of NiAl intermetallic powder after cladding with phosphorus-containing compounds and to determine the effect of phosphorus addition on the microstructure and tribological properties of composite plasma-sprayed coatings based on the NiAl intermetallic.

Materials and methods

For obtaining the plasma-sprayed coatings, NiAl intermetallic powder grade PN70Yu30 (composition Ni–Al with ~30.5% Al, Fe < 0.2%, C < 0.07%, Ni – balance) with a particle size up to 63 μm (ISO 7530-7:1992) was

used as the base material without additives. A NiAl+P powder, containing phosphorus, was used as the composite material, manufactured by the "Composite Systems" company in Zaporizhzhia. The NiAl+P powder was obtained by phosphorus cladding of the original NiAl powder: the NiAl intermetallic particles were uniformly coated with a layer of phosphorus-containing compounds by mixing the powder with a solution of orthophosphoric acid (H_3PO_4), followed by heating, drying of the resulting agglomerate, and crushing. As a result of this process, a composite powder was obtained whose particle surfaces contain phosphorus compounds (phosphorus oxides and other derivatives of phosphoric acid). The resulting NiAl and NiAl+P powders were then used for spraying the coatings. Coatings were deposited by plasma spraying using a UPU-3D plasma unit. Steel cylindrical specimens made of St3 steel (10 mm diameter, 17 mm height) were used as substrates. Spraying was carried out in an argon atmosphere at a plasma arc current of 425–450 A and an arc voltage of 65 V. The spray distance was 160 mm. To increase coating adhesion to the substrate and to clean and roughen the substrate surface, the samples were pre-treated by abrasive blasting with electrocorundum to achieve a surface roughness of $Rz \leq 80$. The porosity of the resulting coatings did not exceed 5%. The microstructure of the obtained powders and coatings was examined by metallography and by scanning electron microscopy (Philips XL30 ESEM). The chemical composition and elemental distribution were determined by energy-dispersive X-ray spectroscopy (EDS) on powder samples and polished cross-sections of the coatings. Coating microhardness was measured with a PMT-3 microhardness tester (Vickers indenter, load P = 50 g). Tribological tests were performed on an M22-P friction machine in a "shaft (counterbody) – segment insert (specimen)" configuration. Tests were conducted under dry sliding conditions at room temperature. The counterbody (shaft) was made of 45 steel (HRC 48–50), and the specimen was a steel cylinder with the NiAl-based coating deposited on its end face. The normal load on the specimen during testing was 10 kg, corresponding to a contact pressure of 1.27 Mpa (contact area 0.785 cm^2). The sliding speed was 4 m/s. The wear intensity was evaluated by the mass loss of the specimen and counterbody, normalized per sliding distance (mg/km). After the tribological tests, the wear track surfaces were analyzed by optical microscopy using a Keyence VHX-7000 digital microscope and by scanning electron microscopy with EDS of the worn surfaces to determine the phase composition of wear products. Additionally, using the digital microscope software, profilograms of the wear tracks were obtained, which allowed measurement of the geometric parameters of the worn layer (depth and width of the wear tracks) to identify the wear patterns of the developed thermal spray coatings.

Results and discussion

Microstructure and composition of the initial powders. NiAl powder consists predominantly of equiaxed particles of various sizes (up to 63 μm) with smooth surfaces (Fig. 1a). Metallographic examination of a cross-section of the particles revealed a single-phase, uniform structure of the NiAl intermetallic (Fig. 1b).

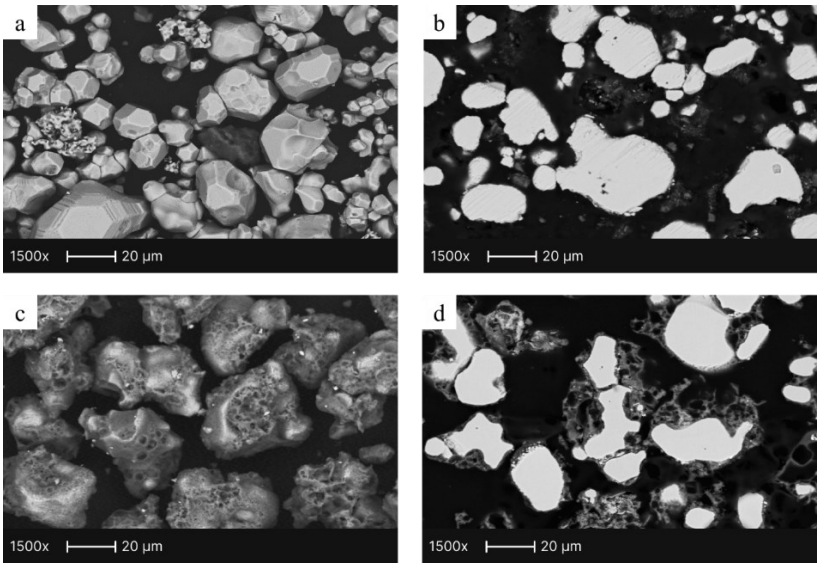

Fig. 1. Morphology of the initial powders: NiAl (a, b) and NiAl+P (c, d).

After cladding with phosphorus-containing compounds (NiAl+P, Fig. 1c, d), the powder particles retain their overall shape. Still, a layer of reaction products from the interaction with orthophosphoric acid is observed on their surface. This surface layer imparts increased roughness to the particles and can cause several particles to agglomerate, coalescing together during the heat treatment. Chemical analysis of the powders (Table 1) confirms the presence of phosphorus in the composite NiAl+P powder.

A significant oxygen content in the NiAl+P powder indicates that phosphorus is present in the form of oxide compounds (likely nickel phosphide Ni_3P and aluminum phosphate $AlPO_4$) coating the particles. Figure 2

shows the elemental distribution map for the NiAl+P powder: phosphorus and oxygen uniformly cover the particle surfaces, forming a shell, whereas nickel and aluminum are concentrated primarily on the particle cores.

Table 1

Chemical composition of the initial powders (EDS, wt.%)

Powder	Ni (wt.%)	Al (wt.%)	P (wt.%)	O (wt.%)
NiAl	69,50	30,50	–	–
NiAl+P	48,67	7,40	24,83	19,03

This confirms that, as a result of the cladding process, a NiAl core coated with a layer of phosphorus-containing compounds was obtained.

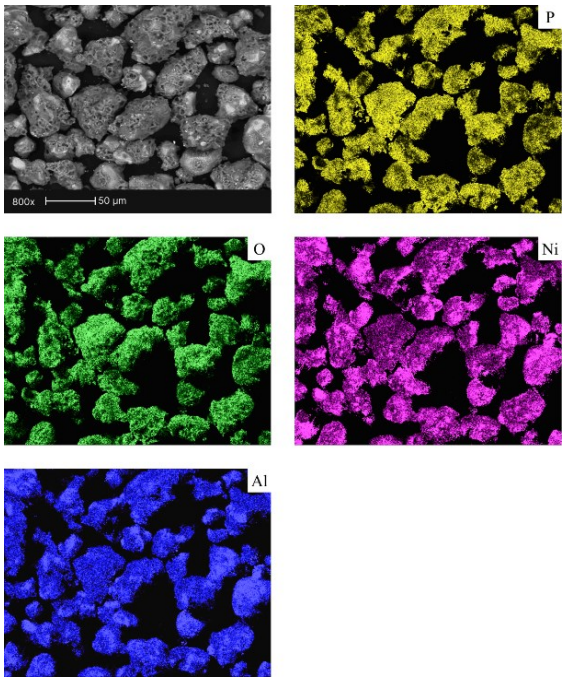

Fig. 2. Elemental distribution map in NiAl+P powder

Structure of the plasma-sprayed coatings. Plasma-sprayed coatings were obtained from both the original intermetallic powder and the phosphorus-clad powder. The cross-section of the coating from the original NiAl (Fig. 3a, b) shows a typical lamellar structure characteristic of thermally sprayed materials. The melted NiAl particles are bonded together and separated by thin oxide boundaries that formed during spraying. Pores and minor defects are uniformly distributed throughout the coating's thickness, and their number is low. The average thickness of this NiAl coating is about 360 µm.

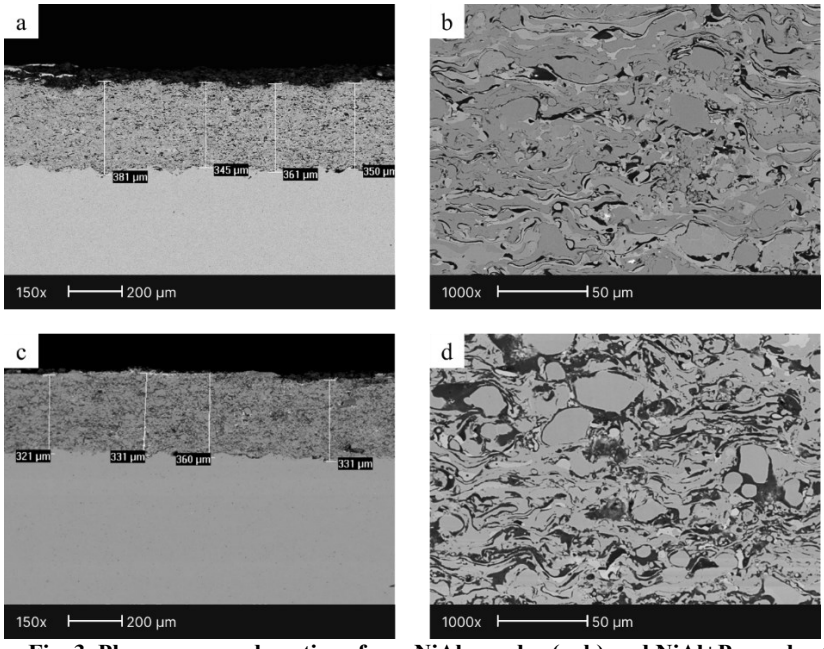

Fig. 3. Plasma-sprayed coatings from NiAl powder (a, b) and NiAl+P powder (c, d)

The NiAl+P coating, with an average thickness of 330 μm (Fig. 3c, d), also exhibits the general lamellar structure. Still, some differences are observed: the material contains inclusions and interlayers of light and dark contrast, indicating the presence of new phases. These inclusions are likely oxide-phosphate phases introduced from the clad powder. The increased fraction of dark oxide layers in the NiAl+P coating is consistent with the EDS chemical composition data (Table 2).

Table 2

Chemical composition of the plasma-sprayed coatings (EDS, wt.%)

Coating	Ni (wt.%)	Al (wt.%)	P (wt.%)	O (wt.%)
NiAl	66.57	26,51	0	3,93
NiAl + P	60,6	24,02	6,87	8,5

In particular, the NiAl+P coating was found to contain ~6.9 wt.% phosphorus and an elevated oxygen content (8.5 wt.% compared to 3.9 wt.% in the pure NiAl coating). Accordingly, the nickel and aluminum contents in the composite coating are slightly lower (approximately 60.6% Ni and 24.0% Al, versus 66.6% Ni and 26.5% Al in NiAl). This means that during spraying, the phosphorus-containing components from the powder were transferred into the coating, forming a separate phase and enriching the coating with phosphorus and oxygen. The elemental distribution in the coatings (Figs. 4 and 5) confirms the absence of phosphorus in the pure NiAl coating and its homogeneous presence throughout the NiAl+P coating. On the elemental map of the NiAl coating (Fig. 4), only Ni and Al are observed, along with a few isolated oxide areas containing O (plus minor Fe impurities near the interface with the steel substrate).

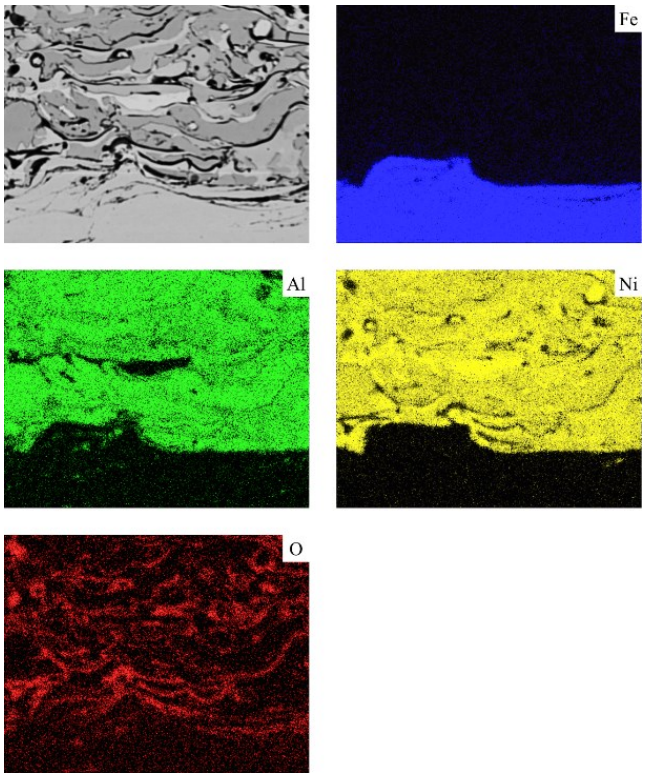

Fig. 4. Microstructure and elemental distribution maps of the NiAl coating

By contrast, the elemental maps of the NiAl+P coating (Fig. 5) clearly record the presence of phosphorus throughout the structure together with increased oxygen content, indicating the uniform incorporation of a phosphate phase between the intermetallic lamellae.

Microhardness of the coatings. The introduction of phosphorus slightly changes the hardness of the coating material. According to the measurements, the microhardness of the plasma-sprayed coating from pure NiAl is 3.68 ± 0.25 GPa, whereas for the composite NiAl+P coating, it decreases to 3.10 ± 0.17 GPa. Thus, the addition of phosphorus results in a decrease in microhardness of approximately 15%. This reduction in microhardness may be related to the formation of relatively soft oxide-phosphate phases or to a slightly higher level of porosity in the NiAl+P coating.

Tribological properties. The tribological test results showed that the NiAl+P coatings perform significantly better under dry friction conditions than the coatings from the original NiAl powder. The quantitative indicators of wear resistance are given in Table 3.

Table 3

Tribological characteristics of the coatings (dry friction, 20 °C)

Parameter	NiAl	NiAl+P
Mass wear of the sample (mg/km)	186,6 ± 5,3	97,0 ± 3,9
Counterbody mass change (mg/km)	+0,85 ± 0,04	+3,6 ± 0,18
Linear wear of pair (μm/km)	222 ± 13	93,8 ± 9,4

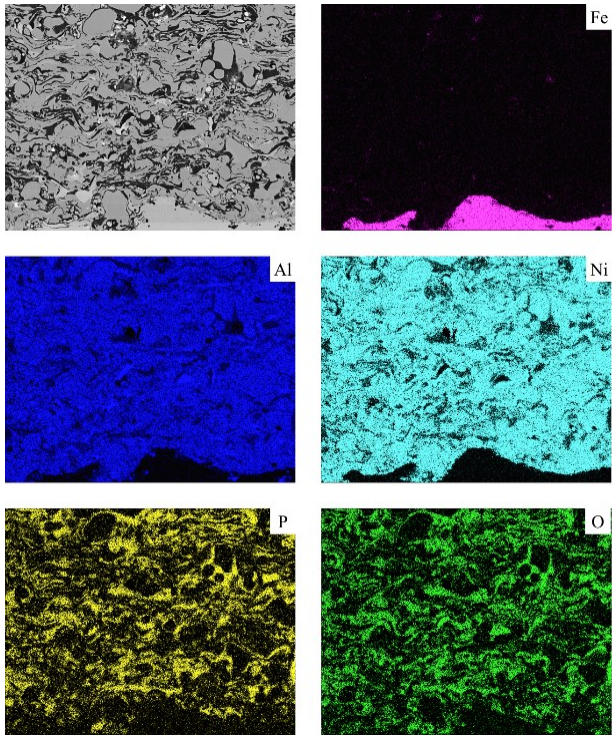

Fig. 5. Microstructure of the NiAl+P coating and its elemental distribution maps.

The mass loss of the NiAl-coated sample (without phosphorus) was 186.6 mg per 1 km of sliding, whereas for the sample with the NiAl+P coating, it did not exceed 97 mg/km, i.e., almost half as much. The total wear of the friction pair (specimen + counterbody) with the NiAl coating was 222 μm/km, while for NiAl+P it was only 93.8 μm/km, which is 2.4 times lower. Thus, the addition of phosphorus significantly reduced the wear rate of the plasma-sprayed coating (by more than a factor of 2), representing a substantial improvement in tribological performance.

The wear profiles of the coatings obtained from the original and clad powders were studied using profilometry. In the case of the pure NiAl coating (Fig. 6), the wear track is relatively deep and wide, with clearly pronounced irregularities in the profile. Significant variations in depth, reaching about 12–15 μm, were observed, indicating an intense adhesive wear mechanism. The surface is characterized by deep, ragged grooves and pronounced peaks and valleys, pointing to a non-uniform wear process.

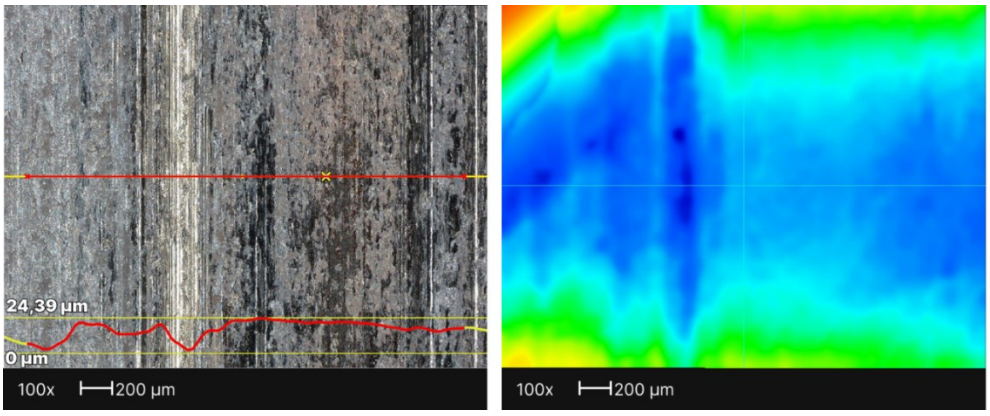

Fig. 6. Profilogram of the NiAl coating after tribological testing.

For the NiAl+P coating (Fig. 7), the wear track profile exhibits significantly more minor depth variations, not exceeding 5–7 μm. The worn surface exhibits a much more uniform character, lacking sharp depth differences, which indicates a significant reduction in the intensity of the wear process compared to pure NiAl.

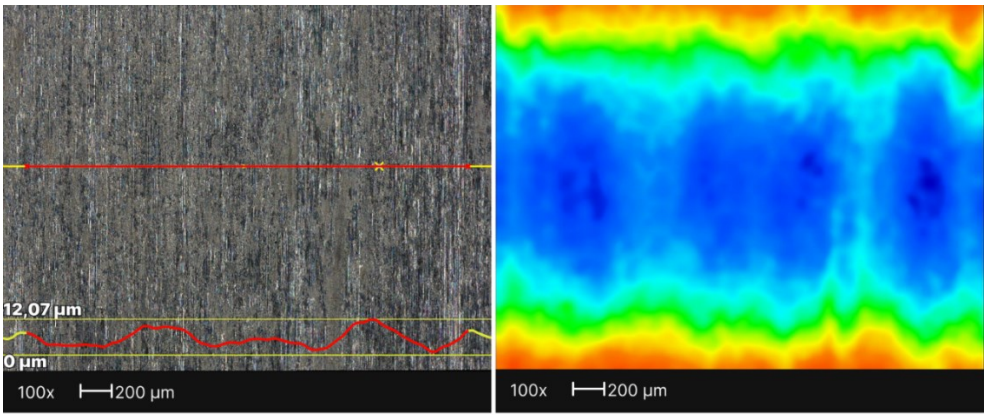

Fig. 7. Profilogram of the NiAl+P coating after tribological testing.

Visual analysis of the wear tracks further confirms the changes in wear mechanisms. On the surface of the original NiAl coating (Fig. 8), characteristic signs of severe adhesive wear are observed, in particular, deep, torn grooves. This is associated with a galling (seizure) process between the contact surfaces, which significantly increases wear and leads to highly non-uniform material removal.

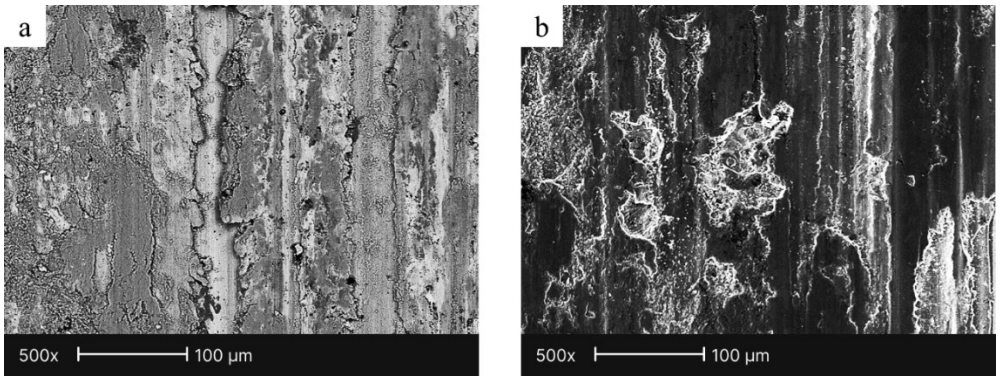

Fig. 8. Wear tracks of the NiAl coating after tribological testing: (a) microstructure (SEM/BSE) and (b) topography (SEM/SE).

In the case of the NiAl+P coating (Fig. 9), the dominant wear mechanism is altered compared to the pure NiAl coating. While the NiAl coating exhibited intense adhesive wear, the addition of phosphorus altered the wear mechanism: the intensity of adhesive interaction decreased, indicating a change in the friction conditions. Thin phosphate or oxide-phosphate films are likely formed on the wear surface, acting as a protective layer and partially serving as a solid lubricant. As a result, the tendency toward adhesion (surface seizure) is diminished, and hence the overall wear intensity is reduced.

Thus, adding phosphorus to the coating effectively prevents surface seizure during friction. Consequently, a significant improvement in tribological characteristics is achieved in both mass and geometric terms: the mass wear is reduced by more than twofold, and the geometric characteristics of the worn surfaces become much more uniform.

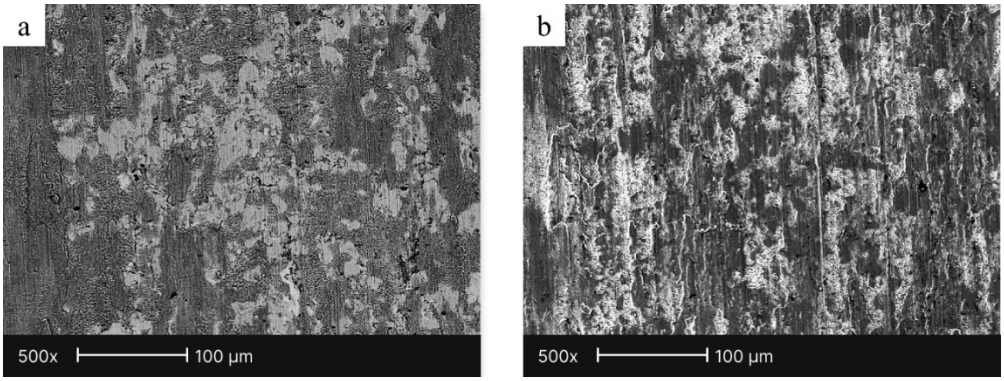

Fig. 9. Wear tracks of the NiAl+P coating after tribological testing: (a) microstructure (SEM/BSE) and (b) topography (SEM/SE).

The EDS analysis of the worn surfaces (Figs. 10 and 11) provides further evidence of the change in wear mechanism. On the worn surface of the NiAl coating (Fig. 10), in addition to the base elements Ni and Al, a considerable amount of iron was detected. This indicates the transfer of iron (as iron oxides) from the steel counterbody onto the coating's wear surface due to intense adhesive contact.

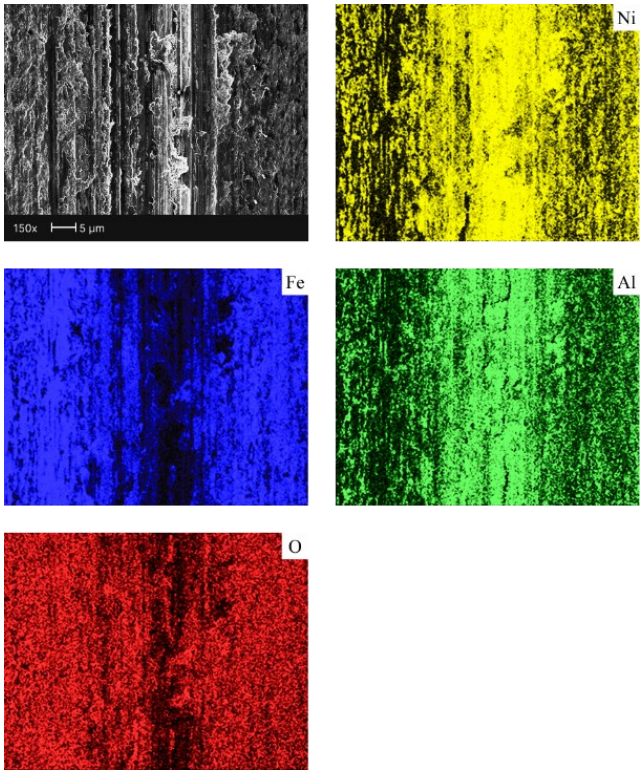

Fig. 10. Elemental distribution map of the NiAl coating after tribological testing.

By contrast, on the worn surface of the NiAl+P coating (Fig. 11), virtually no iron is detected. Instead, an increased concentration of phosphorus and oxygen is present.

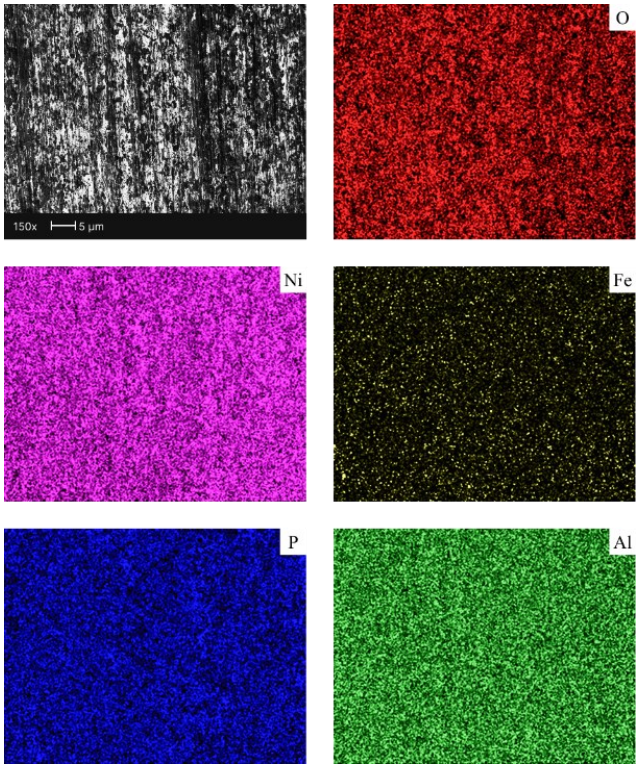

Fig. 11. Elemental distribution map of the NiAl+P coating after tribological testing.

The presence of phosphorus on the NiAl+P friction surface indicates the likely formation of a protective phosphate film during sliding. Notably, the mass of the counterbody (steel shaft) in tests with the NiAl coating increased slightly (+0.85 mg/km, see Table 3), implying the transfer of a small amount of coating material onto the counterbody. In the pair with the NiAl+P coating, the counterbody's mass gain was higher (+3.6 mg/km), meaning a larger quantity of material from the composite coating was transferred to it. This suggests that the formed phosphate film effectively bears the load and protects the main coating from further wear — a portion of the coating material is sacrificed and transferred to the counterbody, creating a transfer film. Although this transferred film slightly increases the mass of the shaft, it serves as a solid lubricant, thereby reducing the overall wear of the tribosystem.

The results of these studies confirm that the presence of phosphorus significantly improves the wear resistance of the coating under friction due to the formation of protective phases on the surface that act as a solid lubricant.

Conclusions

1. Phosphorus cladding of NiAl powder leads to new phases in the coating: Cladding the original NiAl powder with phosphorus promotes the formation of a phase in the resulting coating based on phosphorus-containing compounds. This is confirmed by the presence of ~6.9 wt.% phosphorus and an elevated oxygen content (8.5 wt.%). The introduced phase is represented predominantly by oxide-phosphate formations uniformly distributed between the lamellae of the primary NiAl intermetallic.

2. Phosphorus changes the dominant wear mechanism: The addition of phosphorus alters the prevailing wear mechanism of the coatings. The pure NiAl coating is characterized by severe adhesive wear with pronounced grooves and significant depth variations (up to 12–15 μm). In contrast, after adding phosphorus, no adhesive wear mechanism is observed. The formation of a protective phosphate film ensures uniform wear with minimal depth variation (limited to about 5–7 μm).

3. Phosphorus markedly improves tribological performance: The use of phosphorus-containing (NiAl+P) coatings significantly improves tribological properties. The mass wear of the NiAl+P coating is more than two times lower compared to NiAl (approximately 97 mg/km vs 186.6 mg/km), and the total wear of the friction pair is reduced by a factor of 2.4. These results demonstrate the high effectiveness of phosphorus as an alloying additive for increasing the service life of NiAl-based coatings in tribological applications.

References

1. Chen, H., Luo, W. Effects of β-NiAl powder addition on the high temperature oxidation behaviour of thermally sprayed CoNiCrAlY coatings // Journal of Materials Research and Technology, 2025, Vol. 37, 1737–1747, https://www.doi.org/10.1016/j.jmrt.2025.06.140

2. Hardwicke C.U., Lau Y.-C., Advances in thermal spray coatings for gas turbines and energy generation: a review, Journal of Thermal Spray Technology 22 (2013) 564-576, https://www.doi.org/10.1007/s11666-013-9904-0

3. Hu, Q., Geng, S., Niu, X., Wang, J., Huang, Y., Wang, F. Effect of Y/Pt modification on high-temperature corrosion resistance of NiAl coatings in the environment of NaCl-humid air // Corrosion Science, 2025, Vol. 253, 113000, https://www.doi.org/10.1016/j.corsci.2025.113000

4. Ghara, T., Kuroda, S., Yanagisawa, T., Shahien, M., Suzuki, M., Inoue, T., Shinoda, K. Degradation behaviour of HVOF sprayed CoNiCrAlY coating in high-temperature ammonia environment towards its applicability in ammonia fueled gas turbines // International Journal of Hydrogen Energy, 2025, Vol. 130, 345–359, https://www.doi.org/10.1016/j.ijhydene.2025.04.277

5. Sun, H., Wan, S., Yi, G., Yang, J., Bai, L., Shi, P., Cheng, J. Friction and wear behaviors of NiAl–Bi_2O_3–Ag–Cr_2O_3 composite coating in the thermal cycle of RT–800 °C // Tribology International, 2021, Vol. 159, 106957, https://www.doi.org/10.1016/j.triboint.2021.106957

6. Zhou, X., Mukoyoshi, M., Kitagawa, H. Recent advances in high-entropy intermetallic nanoparticles: synthesis and electrocatalytic applications // Chemical Communications, 2025, Vol. 61, 10911–10930, https://www.doi.org/10.1039/D5CC00993F

7. Peng, J., Li, Z., Li, Y., Wang, Z., Tan, L., Wang, Y., Huang, L., Liu, F. Effect of in-situ growth Al_2O_3 on high-temperature oxidation performance and mechanism of NiAl // Journal of Alloys and Compounds, 2025, Vol. 1036, 181701, https://www.doi.org/10.1016/j.jallcom.2025.181701

8. Zhang, W.L., Li, S.M., Fu, L.B., Li, W., Sun, J., Wang, T.G., Jiang, S.M., Gong, J., Sun, C. Preparation and cyclic oxidation resistance of Hf-doped NiAl coating // Corrosion Science, 2022, Vol. 195, 110014, https://www.doi.org/10.1016/j.corsci.2021.110014

9. Zhang, L., Liao, X.-J., Chen, R., Luo, X.-T., Li, C.-J. Tribological behavior of NiAl coating deposited by plasma spraying of diamond-contained Ni/Al composite powder at a wide range temperature from 25 °C to 700 °C // Transactions of Materials Research, 2025, Vol. 1, 100100, https://www.doi.org/10.1016/j.tramat.2025.100100

10. Guo, H., Li, B., Yan, P., Wu, Z., Li, F., Liu, Z. Microstructures, mechanical properties and tribological behaviors of NiAl-based composite coatings with various addition of Nb // Surface and Coatings Technology, 2022, Vol. 449, 128977, https://www.doi.org/10.1016/j.surfcoat.2022.128977

11. Zhang, H., Zhu, H., Huang, J., Li, J., Xie, Z. In-situ TiB_2–NiAl composites synthesized by arc melting: Chemical reaction, microstructure and mechanical strength // Materials Science and Engineering: A, 2018, Vol. 719, 140–146, https://www.doi.org/10.1016/j.msea.2018.01.125

12. Sorokatyi, R., Chernets, M., Dykha, A., Mikosyanchyk, O. Phenomenological Model of Accumulation of Fatigue Tribological Damage in the Surface Layer of Materials // Mechanisms and Machine Science. – 2019. – Vol. 73. – P. 3761–3769, https://www.doi.org/10.1007/978-3-030-20131-9_371

13. Fan, X., Huang, W., Zhou, X., Zou, B. Preparation and characterization of NiAl–TiC–TiB_2 intermetallic matrix composite coatings by atmospheric plasma spraying of SHS powders // Ceramics International, 2020, Vol. 46, No. 8, 10512–10520, https://www.doi.org/10.1016/j.ceramint.2020.01.052

14. Bolelli, G.; Cannillo, V.; Lusvarghi, L.; Rosa, R.; Valarezo, A.; Choi, W. B.; Dey, R.; Weyant, C.; Sampath, S. Functionally graded WC-Co/NiAl HVOF coatings for damage tolerance, wear and corrosion protection // Surf. Coatings Technol. 2012, 206 (8–9), 2585–2601, https://www.doi.org/10.1016/j.surfcoat.2011.11.018

15. Sun, Y., Yuan, J., Wang, M., Wang, H., Chen, Z., Liu, X., Li, S., Zhao, W., Yang, J. Enhanced tribological performance of NiAl-based composite coatings: Design of the composition in coatings by addition of Mo and Nanodiamond // Tribology International, 2025, Vol. 203, 110405, https://www.doi.org/10.1016/j.triboint.2024.110405

16. O. Umanskyi, O.Poliarus, M. Ukrainets, O. Kostenko, M Antonov, I. Hussainova Influence of Cr, Ti and Zr Oxides Formation on High Temperature Sliding of NiAl-Based Plasma Spray Coatings // Journal "Key Engineering Materials", Trans Tech Publications, Switzerland, Vol. 674 (2016), pp 308-312, https://www.doi.org/10.4028/www.scientific.net/KEM.674.308

17. O. Umanskyi, O. Poliarus, M. Ukrainets, M. Antonov, I. Hussainova. High Temperature Sliding Wear of NiAl-based Coatings Reinforced by Borides // Materials Science (Medžiagotyra). – 2016. – Vol. 22, No. 1. – pp. 49-53, https://www.doi.org/10.5755/j01.ms.22.1.8093

18. O.Poliarus, J. Morgiel, O. Umanskyi, M. Pomorska, P. Bobrowski, M. Szczerba, O. Kostenko. Microstructure and wear of thermal sprayed composite NiAl-based Coatings // Archives of Civil and Mechanical Engineering, 19(4), pp. 1095-1103 (2019), https://www.doi.org/10.1016/j.acme.2019.06.002

Левчук Т.О., Полярус О.М., Коновал В.П., Макаренко О.С. Модифікація порошків інтерметаліду NiAl шляхом плакування фосфором для плазмових покриттів та дослідження їх структури і триботехнічних властивостей

У статті досліджено вплив додавання фосфору до інтерметалідного порошку NiAl на структуру, мікротвердість та триботехнічні властивості плазмових покриттів, які можуть бути рекомендовані для роботи в умовах тертя без мастила. Композиційний порошок NiAl+P отримано шляхом плакування NiAl фосфоровмісними сполуками. Встановлено, що додавання фосфору сприяє утворенню в покриттях фосфатних фаз, що знижує мікротвердість, але суттєво підвищує зносостійкість. В покритті NiAl+P при трибовипробуваннях на поверхні тертя формується захисна фосфатна плівка, яка виконує роль твердого мастила та зменшує інтенсивність зношування майже в 2,5 раза. Отримані результати свідчать про ефективність фосфору як легуючого елементу для підвищення експлуатаційної довговічності NiAl-покриттів у триботехнічних вузлах.

Ключові слова: інтерметалід NiAl, плакування фосфором, плазмове напилення, фосфатна плівка, триботехнічні властивості, зносостійкість, тверде мастило, мікроструктура

ISSN 2079-1372 ***Problems of Tribology****, V. 30, No 4/118-2025, 31-36*

Problems of Tribology
Website: http://tribology.khnu.km.ua/index.php/ProbTrib
E-mail: tribosenator@gmail.com

DOI: https://doi.org/10.31891/2079-1372-2025-118-4-31-36

Optical interferometry for assessing lubricating film properties

V. Akhmatov[0009-0003-6325-5262], **D. Stetskyi**[0009-0005-2610-1947]

National Transport University, Ukraine
E-mail: vladislavakhmatov1@gmail.com

Received: 05 September 2025: Revised 30 September 2025: Accept: 15 October 2025

Abstract

The study investigated the influence of rolling speed and lubricant properties on the formation of a lubricating film in point contacts. The film thickness was measured using optical interferometry, which provides high-precision, real-time data. Experimental tests were conducted on a specially designed rig simulating rolling conditions in bearing assemblies. Analysis of various lubricants showed that kinematic viscosity, base oil type, and chemical composition significantly affect the lubrication behavior and film formation regime. It was found that increasing rolling speed leads to a transition from boundary to hydrodynamic lubrication, with substantial changes in film thickness. The results can be applied to optimize lubricant selection in bearings of precision mechanisms.

Key words: tribological system, point contact, friction unit, lubricating film, optical interferometry, EGD lubrication.

Introduction

Various methods are used in modern tribology to measure lubricating film thickness, differing in the physical principles that determine this parameter. One of the most precise methods is optical interferometry [1].

This technique is based on the phenomenon of light interference - the superposition of coherent waves forming an interference pattern. Using this method, it is possible to obtain data on changes in the lubricating film thickness with nanometer precision in real time, which is a critical aspect in studying tribological processes in precision mechanisms.

Experimental results obtained using interferometry are the most accurate among other widely applied optical methods for investigating lubricating film thickness.

The purpose of the work

The aim of this study is to evaluate the influence of rolling speed on the formation of a lubricating film in local contact zones when using lubricants with different operational characteristics.

This work also highlights the effectiveness of optical interferometry in tribological research. Wider adoption of this method allows for non-contact measurements and real-time data acquisition under dynamic conditions in rolling bearing mechanisms. This, in turn, improves the capability to accurately assess lubricant performance, supports the development of new lubricant formulations, and aids in predicting the service life of friction units.

Methodical

The optical interferometry method for measuring lubricant film thickness makes it possible to determine the value of the lubricating film while accounting for the pattern of lubricant supply and distribution in the vicinity of the friction contact and the actual contact area. The use of a glass disk or glass cylinder (transparent material) as the indenter, together with a steel ball or steel cylinder as the counterbody—whose properties are nearly identical—enables the optical interferometry method to find its widest application in model experiments.

To obtain a clear colored interference pattern, a white light source is required, unlike monochromatic light. Each color interferes at a specific wavelength, so each lubricating film thickness in the friction contact corresponds to a specific color [2].

The schematic diagram of the interferometric system is shown in

Fig. . To enhance visibility, a semi-transparent chromium coating, 170 A° thick, is deposited on the surface of the glass disk by vacuum evaporation. This provides an optimal reflectivity of approximately 18% (with an absorption of about 25%).

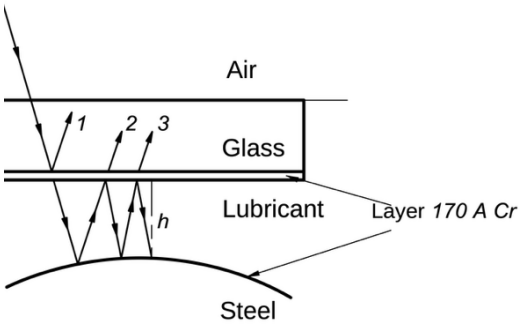

Fig. 1. Schematic diagram of the interferometric system

Investigation of the lubrication process in point contact using pptical interferometry

Experimental investigations were conducted using a test rig designed to enable precise measurement of ultrathin lubricating films via optical interferometry. The system accounts for the lubrication supply and distribution within the point contact region, as well as the actual contact area, and allows for real-time recording of results through video capture. The contacting pair, comprising a steel ball and a glass disk, is shown in **Fig. 3**. A general view of the test rig, which reproduces conditions analogous to the rolling contact between surfaces of the outer ring of a self-aligning ball bearing, is presented in **Fig. 2**.

Fig. 1. General view of the setup with auxiliary equipment

Fig. 2. Contacting pair: steel ball – glass disk

The object of investigation (**Fig. 3**) is the contact zone between a glass disk (1) and a standard steel ball (10) with a diameter of 25.4 mm and surface finish Ra < 0.025 μm, pressed against the disk by a load.

To enhance the visibility of interference fringes, a thin chromium layer of approximately 170 A° was deposited on the disk surface via vacuum evaporation. The steel ball was mounted on freely rotating supports (8) to minimize frictional resistance. These supports were fixed in a housing (2), which, together with the lubricant bath (9), was fabricated as a single structural element. This design allowed for near-ideal rolling conditions with minimal sliding, preventing excessive lubricant heating that could reduce viscosity in the contact zone. High sliding would cause additional energy dissipation due to viscous friction, adversely affecting experimental accuracy.

Disk rotation was driven by an electric motor (7) transmitting torque through a single-stage transmission (6). Contact load was controlled via a lever mechanism, where the primary pressure was applied through a movable bearing (3) mounted on shaft (4). Rotational speed was monitored with a non-contact electronic tachometer (5),

recording the disk's revolutions. Lubricant temperature was measured using a thermocouple positioned close to the friction contact area.

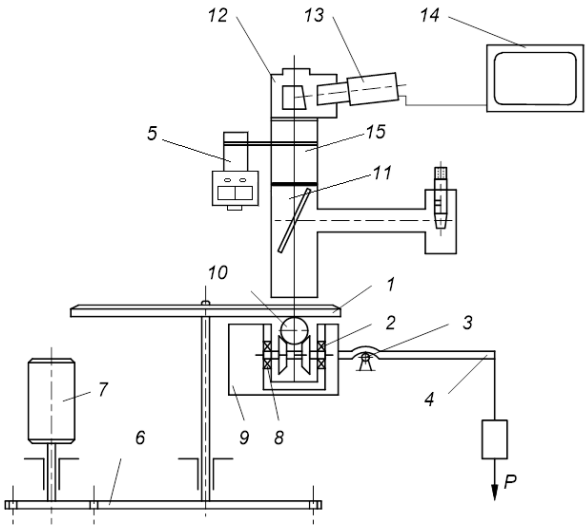

Fig. 3. Schematic of the friction unit

The contact zone (ball–plane) is observed using a microscope objective (11). To analyze the interference pattern in the friction area, a video recording system is employed, consisting of a transition tube (15), a microphotoadapter (12), a video camera (13), and a television monitor (14) on which the image is displayed.

Influence of lubricant components on the formation of lubricant film thickness under pure rolling conditions

An important factor determining the elastohydrodynamic (EHD) lubrication of a point contact is the dependence of the lubricant film thickness on the rolling speed [3]. Analyzing the variation of this thickness makes it possible to evaluate the influence of the rheological characteristics of different lubricants on the performance efficiency of mechanisms equipped with rolling bearings [4].

Maintaining pure rolling conditions is essential to prevent lubricant overheating, which can lead to a decrease in its viscosity at the inlet to the contact zone. This phenomenon results from slip and the dissipation of energy due to viscous friction. To ensure pure rolling in a ball–disk contact, the condition $V_1 = V_2$ must be satisfied in the following equation:

$$V_1 - V_2 = \frac{2\pi}{60} \cdot (\omega_1 \cdot r_1 - \omega_2 \cdot r_2), \tag{1}$$

Where V_1, V_2 are the linear velocities of the ball and the disk; r_1, r_2 are their radii; ω_1 i ω_2 – the angular velocities of the ball and the disk.

To ensure pure rolling, the condition $\omega_1 = 3\omega_2$ must be satisfied, meaning that the angular velocity of the ball should be three times greater than that of the disk. Under these conditions, equation (1) takes the following form:

$$r_2 = 3r_1 \tag{2}$$

To ensure the condition of pure rolling, the ball must be positioned at a distance from the center of disk rotation equal to three times its own radius.

The study focuses on evaluating the influence of rolling speed on the formation of the lubricant film in the central contact area. Five types of lubricants were analyzed experimentally: 1. transmission fluid Total SAE 85W90, 2. automatic transmission fluid Total SAE ATF, 3. engine oil Total SAE 15W40, 4. engine oil Total SAE 10W40, 5. universal motor–transmission oil Total SAE 25W. The experiments were carried out within a speed range from 0 to 1.8 m/s at a constant temperature of 20 °C. The contact stress reached 251.5 MPa. The lubricant film thickness was measured using optical interferometry.

To describe the lubrication process, a dimensionless parameter λ is used, which characterizes the lubrication regime and is calculated by the following expression:

$$\lambda = \frac{h}{\sqrt{R_{a1}^2 + R_{a2}^2}} \tag{3}$$

where h – the lubricant film thickness (μm),

R_{a1} – the arithmetic average surface roughness of the glass disk (μm),
R_{a2} – the arithmetic average surface roughness of the steel ball (or roller) (μm).
The classification of lubrication regimes according to the value of λ is as follows: λ= 0 – 1 – semi-dry; λ= 1– 1,5 – boundary; λ= 1,5 – 3 – mixed with boundary predominance; λ= 3 – 4 – elastohydrodynamic; λ≥ 4 – hydrodynamic.

Results of studying

When using Total SAE ATF, it was found that the lubricant film forms at a speed of $V_{\Sigma\kappa}$=0,24 m/s, and the actual film thickness reached h_d=0,128×10^{-6}m (**Fig. 4**), corresponding to a boundary lubrication regime with λ =1,28 (**Fig. 5**).

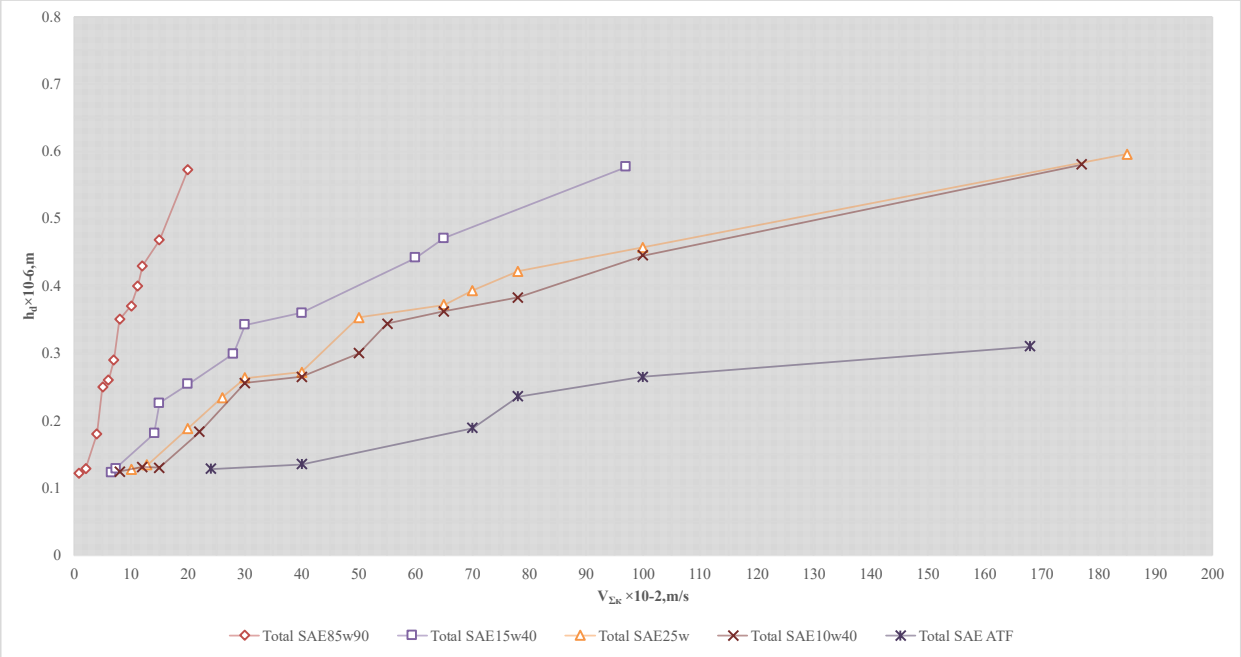

Fig. 4. Dependence of the actual lubricant film thickness h_d on the total rolling speed $V_{\Sigma\kappa}$

As the rolling speed increases, the lubricant film thickness also grows, reaching h_d=0,31×10^{-6}m at $V_{\Sigma\kappa}$=1,68 m/s, corresponding to a hydrodynamic lubrication regime with λ=3,10 (**Fig. 5**).
Experimental data show that when using the transmission oil Total SAE 85W90 at a total rolling speed of $V_{\Sigma\kappa}$=0,08 m/s a lubricant film with a thickness of h_d=0,122×10^{-6}m (**Fig. 4**), forms, corresponding to a boundary lubrication regime with λ=1,22 (**Fig. 5**). Upon reaching $V_{\Sigma\kappa}$=0,112 m/s, the film thickness increases to h_d=0,4×10^{-6}m (**Fig. 4**), establishing a hydrodynamic lubrication regime with λ=4 (**Fig. 5**) which persists for $V_{\Sigma\kappa}$ >0,2 m/s.
Analysis of Total SAE 85W90 characteristics compared to Total SAE ATF shows that the former provides a lubricant film thickness that is 79% greater than that of Total SAE ATF.

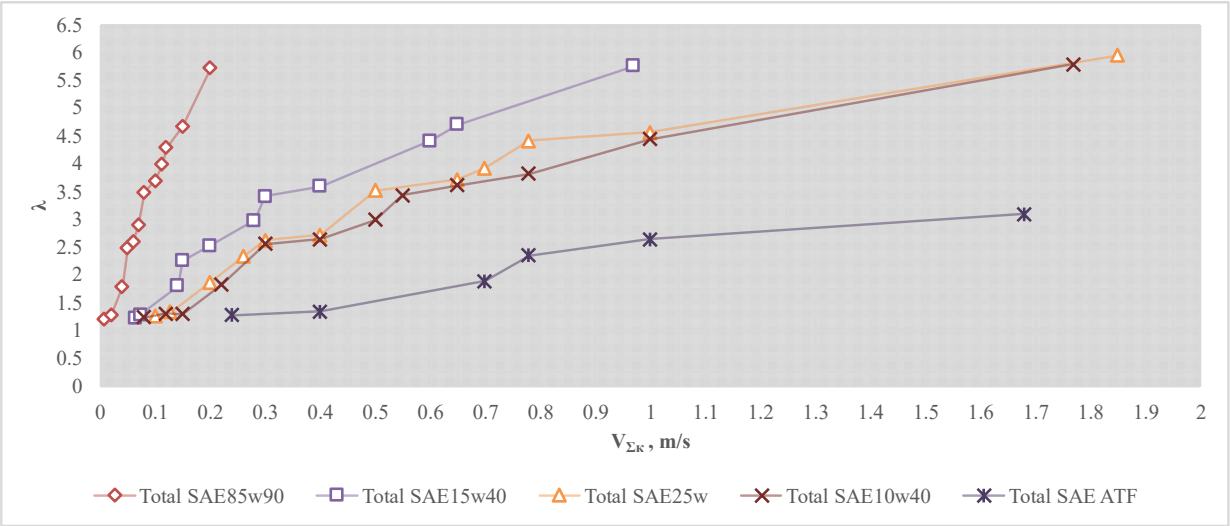

Fig. 5. Dependence of the lubrication regime λ on the total rolling speed $V_{\Sigma\kappa}$

The study using the engine oil Total SAE 15W40 showed that at a rolling speed of $V_{\Sigma к}$=0,065 m/s, a lubricant film with a thickness of h_d=0,123×10^{-6}m (**Fig. 4**) is formed, corresponding to a boundary lubrication regime with λ=1,23 (**Fig. 5**). When the rolling speed reaches $V_{\Sigma к}$=0,60 m/s, the lubricant film thickness increases to h_d=0,442×10^{-6}m (**Fig. 4**), establishing a hydrodynamic lubrication regime with λ=4,22 (**Fig. 5**), which remains dominant up to $V_{\sum к}$ = 1,05 m/s.

When using the engine oil Total SAE 10W40 as a lubricant, it was found that the film begins to form at a total rolling speed of $V_{\Sigma к}$=0,08m/s, with a film thickness of h_d=0,124×10^{-6}m (**Fig. 4**), corresponding to a boundary lubrication regime with λ=1,24 (**Fig. 5**). Upon reaching $V_{\Sigma к}$=1m/s, the film thickness increases to h_d=0,445×10^{-6}m (**Fig. 4**), resulting in a hydrodynamic lubrication regime with λ=4,45 (**Fig. 5**), which persists up to $V_{\sum к}$=1,96m/s.

Comparing the properties of this oil with those described above, it can be noted that Total SAE 10W40 produces nearly the same lubricant film thickness (according to the interferometric method) as Total SAE 15W40, with a difference of only 1–2%. However, film formation occurs at higher rolling speeds (by about 67%), indicating the use of a different base oil. Total SAE 15W40 employs mineral base oil I-40, while Total SAE 10W40 is formulated with synthetic base oil PAO-8.

The use of the universal motor–transmission oil Total 25W made it possible to determine that the lubricant film formation begins at a rolling speed of $V_{\Sigma к}$ = 0.1, m/s corresponding to a boundary lubrication regime with λ = 1.27 (**Fig. 5**), and an actual film thickness of h_d=0,127×10^{-6}m (**Fig. 4**). When the rolling speed reaches $V_{\Sigma к}$= 0.78m/s, the film thickness increases to h_d=0,422×10^{-6}m , establishing a hydrodynamic lubrication regime with λ = 4.2 (**Fig. 5**), which remains dominant up to $V_{\sum к}$ = 1.39 m/s.The experimental results indicate that this lubricant provides a film thickness 47% greater than that of Total SAE ATF, while its film formation rate exceeds that of Total SAE 10W40 by 14%. At the same time, it is inferior to oils such as Total SAE 85W90 (by 92%) and Total SAE 15W40 (by 31%).

The conducted studies show that the process of lubricant film formation during start-up is directly related to the rolling speed. As this speed increases, the film thickness in the center of the contact grows, allowing a transition from boundary to hydrodynamic lubrication. In this process, the kinematic viscosity of the oil, which largely depends on its base composition, plays an important role. The additive content in such oils typically ranges from 10–15%. Total SAE 85W90, containing high-molecular-weight petroleum fractions (up to 80%), forms the lubricant film thickness optimally.

Compared to other lubricants, Total SAE 25W accelerates the process due to a viscosity modifier of up to 8%, which increases the time required for film formation. It acts effectively at temperatures above 50 °C, promoting a significant increase in film thickness.

A comparison of the mineral oil Total SAE 15W40 with semi-synthetic oils Total SAE 10W40 and Total SAE 25W is also of interest. The lower efficiency of synthetic oils in film formation may be associated with the adhesion properties between polyalphaolefins and glass surfaces, where the interaction force is weaker than between petroleum components and glass. Total SAE ATF exhibits the fastest lubricant film formation among all tested samples, ensuring the quickest transition to the boundary lubrication regime. This is likely explained by its low kinematic viscosity, which is on average 60% lower than that of the other oils.

Conclusions

From this, it follows that when selecting a lubricant for a specific component, it is important to consider not only the kinematic viscosity but also the chemical composition of the oil and the properties of the interacting surface materials. This approach allows achieving optimal conditions for the rapid formation of the lubricant film during start-up and for maintaining a stable lubrication regime during operation, which ultimately ensures the durability and reliability of the friction system.

References

1. Milanenko A.A. The lubricating effect of oils under point contact friction conditions: abundant lubrication and lubricant starvation: Ph.D. thesis: 05.02.04 / A.A. Milanenko; National Aviation University. – Kyiv, 2000. – 214 p.

2. Savchuk A.N. Kinetics of changes in lubricating properties of transmission and motor oils under conditions of abundant and limited lubrication: Ph.D. thesis: 05.02.04 / A.N. Savchuk; National Transport University. – Kyiv, 2010. – 210 p.

3. Dmytrychenko M.F., Milanenko O.A. Lubricating action of oils under elastohydrodynamic lubrication conditions / M.F. Dmytrychenko, O.A. Milanenko // Monograph. – Kyiv: Ukravtodor, 2009. – 184 p.

4. Dmytrychenko M.F. Elastohydrodynamics: theory and practice / M.F. Dmytrychenko // Monograph. – Lviv: Publishing House of Lviv Polytechnic National University, 2000. – 224 p.

Ахматов В., Стецький Д. Оптична інтерферометрія як засіб оцінки характеристик мастильного шару.

У роботі досліджено вплив швидкості кочення та властивостей мастильного матеріалу на утворення мастильного шару в точковому контакті. Для вимірювання товщини мастильної плівки застосовано метод оптичної інтерферометрії, що забезпечує високу точність у реальному часі. Експериментальні дослідження проводилися на спеціально розробленому стенді, який моделює умови кочення в підшипникових вузлах. Аналіз різних типів мастильних матеріалів показав, що кінематична в'язкість, базова основа та хімічний склад олив істотно впливають на характер змащення та режим утворення плівки. Встановлено, що зі збільшенням швидкості кочення відбувається перехід від граничного до гідродинамічного режиму змащення, а мастильна плівка значно змінює свою товщину. Отримані результати можуть бути використані для оптимізації вибору мастильних матеріалів у підшипникових вузлах точних механізмів.

Key words: триботехнічна система, точковий контакт, вузол тертя, мастильний шар, оптична інтерферометрія, ЕГД мащення

ISSN 2079-1372 Problems of Tribology, V. 30, No 4/118-2025, 37-41

Problems of Tribology
Website: http://tribology.khnu.km.ua/index.php/ProbTrib
E-mail: tribosenator@gmail.com

DOI: https://doi.org/10.31891/2079-1372-2025-118-4-37-41

The influence of high-entropy alloys on the abrasive wear index of ultra-high-molecular-weight polyethylene

A.-M.V. Tomina[1]0000-0001-5354-0674, **V.Yu. Shurpik[1]**0009-0002-8007-8088, **Ye.A. Yeriomina[1]**0000-0001-8595-5735, **Predrag Dašić[2]**0000-0002-9242-274X, **V.B. Burzaiev[1]**0009-0000-6725-4003

[1]Dniprovsk State Technical University, Kamyanske, Ukraine
[2]Academy of Professional Studies Šumadija – Department in Trstenik, Trstenik, Serbia
E-mail: an.mtomina@gmail.com

Received: 10 October 2025: Revised 30 October 2025: Accept: 15 November 2025

Abstract

This work examines the influence of high-entropy alloys $Fe_{20}Ni_{20}Co_{20}Be_{20}Si_{14}B_6$ and : $Al_{40}Co_{12}Cu_{12}Cr_{12}Ni_{12}Fe_{12}$ on the abrasive wear index of ultrahigh-molecular-weight polyethylene. The effective filler content that ensures the minimum wear rate has been determined. For the $Fe_{20}Ni_{20}Co_{20}Be_{20}Si_{14}B_6$ alloy, the optimal concentration is 25 wt.%, whereas for the: $Al_{40}Co_{12}Cu_{12}Cr_{12}Ni_{12}Fe_{12}$ alloy it is 20 wt.%. The overall improvement in abrasive resistance reaches 35–45% compared to unfilled polyethylene. The enhancement in wear resistance is attributed to the strengthening of the polymer matrix by hard particles of the high-entropy alloys, whose microhardness exceeds 10000 MPa. Their introduction significantly increases the material's ability to resist mechanical degradation of the surface layers during friction against rigidly fixed abrasive particles. The obtained results confirm the feasibility of using high-entropy alloys as effective functional fillers for the development of wear-resistant polymer composites based on ultra-high-molecular-weight polyethylene and open up promising directions for further research in this field.

Keywords: ultra-high-molecular-weight polyethylene, abrasive wear index, high-entropy alloy, polymer composite material

Introduction

A major part of modern industrial equipment in Ukraine and around the world operates in conditions of severe abrasive wear. As a result, enterprises incur significant economic losses due to their downtime and repair. This problem is especially acute in the mining, automotive, and agricultural industries, where equipment operates in environments saturated with solid abrasive particles: sand, mineral inclusions, and rocks. An effective solution to this problem is introducing new wear-resistant polymer composite materials (PCMs) based on thermoplastic polymers containing dispersed metal filler (Fl). Such materials combine high strength, resistance to wear, corrosion and many chemical reagents with low density and technological ease of forming products, particularly, parts of complex geometry. Due to this, these composites are characterised by high functional properties, therefore they are an excellent alternative to traditional metals and alloys operating in conditions of intense abrasive wear. As the analysis of literary sources [1-3] has shown, using such materials instead of traditional ones (bronzes of the BrAZh brand, aluminium alloys, Gr3 and Gr2D2.5 cermets) allows for an increase in the durability of high-performance equipment by six times. Among the large number of polymer materials, we can distinguish ultra-high-molecular-weight polyethylene (UHMWPE), which is one of the most widely used technical polymers today. Composites based on it, including those containing dispersed Fl (in particular, liquid-quenched binary alloys of the Al-Ni, Al-Cr, Al-Co system, hydrogenated diamond-like carbon, metal oxides and sulfides, and graphite), are characterised by a combination of high functional properties, especially increased wear resistance, chemical inertness, and resistance to shock loads [4-7]. Given the above, searching for new compositions of composites based on UHMWPE is a relevant and promising task aimed at expanding the possibilities of their use in conditions of intensive wear in the mining, automotive, and agricultural industries.

The purpose of the work

Considering the above, the aim of this work is to investigate the influence of the percentage content of dispersed fillers–high-entropy alloys on the abrasive wear index of UHMWPE under conditions of rigidly fixed abrasive particles.

Objects and methods of research

UHMWPE (manufactured by Jiujiang Zhongke Xinxing New Material Co., Ltd., China) was used as a polymer matrix to create new wear-resistant PCMs [6].

Two high-entropy alloys (HEAs) were chosen as dispersed Fls for UHMWPE: $Al_{40}Co_{12}Cu_{12}Cr_{12}Ni_{12}Fe_{12}$ and $Fe_{20}Ni_{20}Co_{20}Be_{20}Si_{14}B_6$. These alloys usually contain from 5 to 13 elements in equiatomic or close to equiatomic concentrations. High-entropy (multicomponent) alloys are currently attracting considerable attention from researchers due to several improved physical and operational properties, including high corrosion resistance. Five or more components in the alloy in an equiatomic ratio ensure high entropy of the alloys. The difference in the atomic radii of the elements gives the crystal lattice a very high level of stresses (partly microstresses), which provides a high level of hardness and wear resistance. A certain ratio of elements leads to the formation of alloys with bcc, fcc or a mixture of crystal lattices. It is known [8] that bcc and fcc lattices are characterised by a different number of slip planes: it is the largest in the fcc lattice. Due to this, the hardness of the HEAs with the bcc lattice is the largest with relatively low plasticity, and vice versa. Therefore, in some cases, it is useful to obtain alloys with a mixture of bcc and fcc lattices, which allows combining relatively high hardness and plastic characteristics in the HEAs. It should be noted that obtaining structures close to the microcrystalline state is possible because of the significant difference in atomic radii. This can be traced by broad diffraction lines. As it is known, such a state provides a high level of corrosion resistance. It is worth noting that the recorded high level of microstresses can exceed $2{,}7\cdot10^{-3}$, which provides microhardness over HV=10000 MPa. Positive prospects are based on the fact that an amorphous structure, which will naturally combine high physical, tribological, and corrosion-resistant properties, may form in the structure of the HEAs during quenching from the melt. Currently, HEAs are receiving significant attention worldwide because of the possibility of using various elements in their equiatomic amount, as well as due to the prospects for implementing HEAs and developing the latest technologies [9]. Creating products and studying the abrasive wear index of new wear-resistant PCMs based on ultra-high-molecular-weight polyethylene was performed according to the method given in [6], which includes the activation of the HEAs in the magnetic field of a vortex mixer. The study of the roughness (R_a scale, μm) and the morphology of the friction surfaces of pure UHMWPE and PCMs based on it was done using a 170621 probe profilometer and a BIOLOM-M microscope. The hardness of the PCMs was measured on the Rockwell scale (HRR, hardness units) using a 2074 TPR device [9].

Results analysis and discussion

Evaluating the results of tribological properties (Fig. 1) of dispersion-strengthened PCMs shows that using high-entropy alloys (at.%) $Al_{40}Co_{12}Cu_{12}Cr_{12}Ni_{12}Fe_{12}$ (alloy №1) and $Fe_{20}Ni_{20}Co_{20}Be_{20}Si_{14}B_6$ (alloy №2) as Fls is an effective way to reduce the abrasive wear index of ultra-high-molecular-weight polyethylene by 30–45%

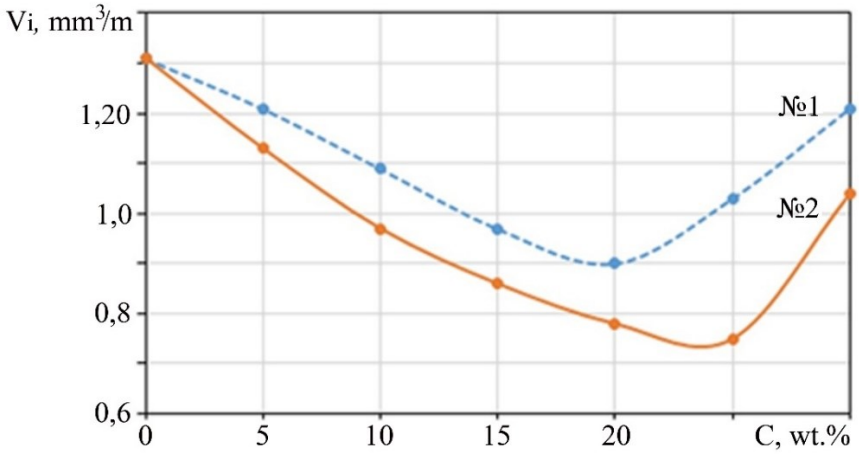

Fig. 1. The influence of the percentage content (C, wt.%) of HE alloys 1 and №2 on the abrasive wear index (V_i, mm³/m) of UHMWPE

The increase in wear resistance of UHMWPE to the action of abrasive particles is because dispersion-reinforced PCM fillers acquire high strength and resistance to mechanical damage. This occurs because there is a

mixture of fcc and bcc lattices in the structure of HEAs, which provides a high level of microstresses (≥2.7 10^{-3}) and microhardness (~10000 MPa). The established increase in PCM hardness by 1.6 g. (Fig. 2), a decrease in PCM roughness by 45% (see Fig. 3), and a comparison of friction surfaces confirm this. Fig. 4 shows that deep ploughing of UHMWPE is observable on the friction surface of UHMWPE, while the PCM surfaces are more uniform and homogeneous [10], which indicates an increase in wear resistance [11].

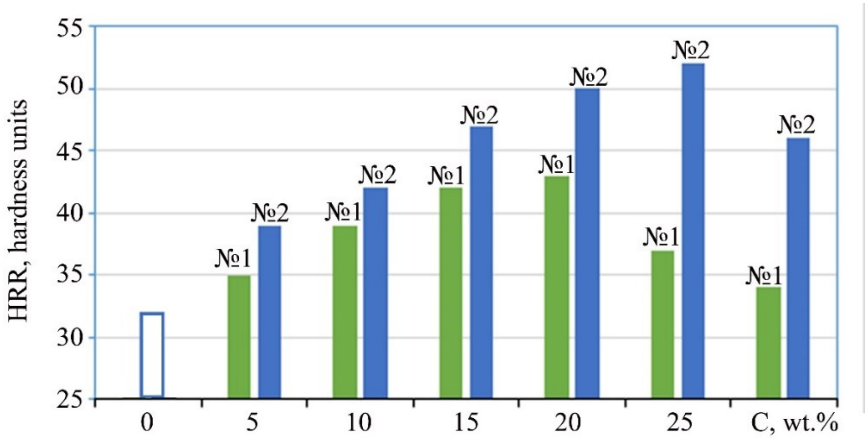

Fig. 2. The influence of percentage content (C, wt.%) of HE alloys №1 and №2 on hardness (HRR, hardness units) of UHMWPE

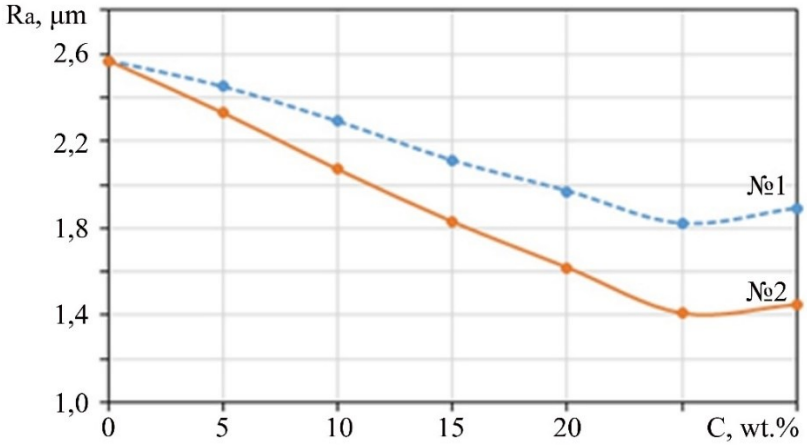

Fig. 3. The influence of the percentage content (C, wt.%) of high-entropy alloys №1 and №2 on the roughness (R_a, μm) of UHMWPE

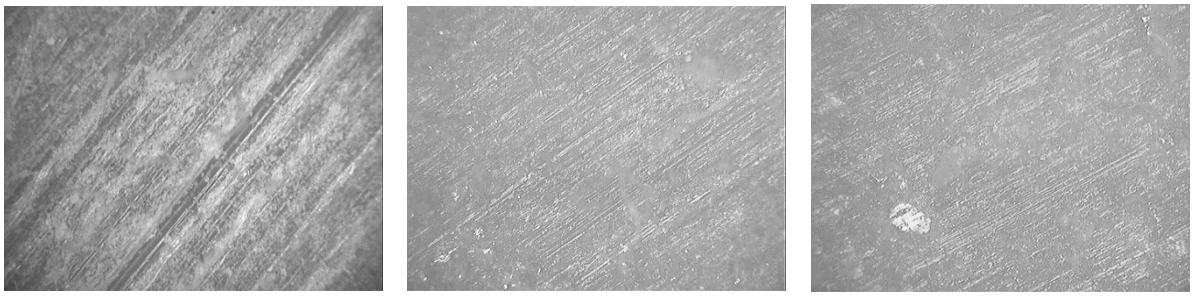

a b c

Fig.4. Friction surfaces (×200) of UHMWPE (a) and composites based on it containing 20 wt.% of alloy №1 (b) and 25 wt.% of alloy №2 (c)

It should be noted that with an increase in the percentage of alloy №1 and №2 in the UHMWPE to 25–30 wt.% and 30 wt.%, respectively, a decrease in the abrasive wear resistance of the developed PCMs is observed. This is probably a consequence of the increased defects in the material: the formation of voids, pores, and microcracks. A comparison of the experimental (1) and theoretical (2) densities of the developed PCMs (Fig. 5) can confirm this conclusion [11].

The dependences in Fig. 4 clearly show that when the content in the PCMs is 5–20 wt.% of alloy №1 and 5–25 wt.% of alloy №2, the experimental density of the PCMs is somewhat higher than the theoretical one. This indicates a more ordered supramolecular structure of the developed PCMs because of the strong intercomponent interaction at the "UHMWPE-high-entropy alloy" interface. With a further increase in the amount of HEAs in the volume of the UHMWPE, an inverse ratio is observed. This can be explained by the fact that the HEA particles of

alloys №1 and №2 find it difficult to achieve uniform distribution in the volume of UHMWPE as a result of the strong intermolecular energy of their components (E(Fe)=4.04·10^5 J/mol, E(Al)=3.11·10^5 J/mol, E(Co)=4.39·10^5 J/mol, E(Cu)=3.39·10^5 J/mol and E(Ni)=4.22·10^5 J/mol) [12].

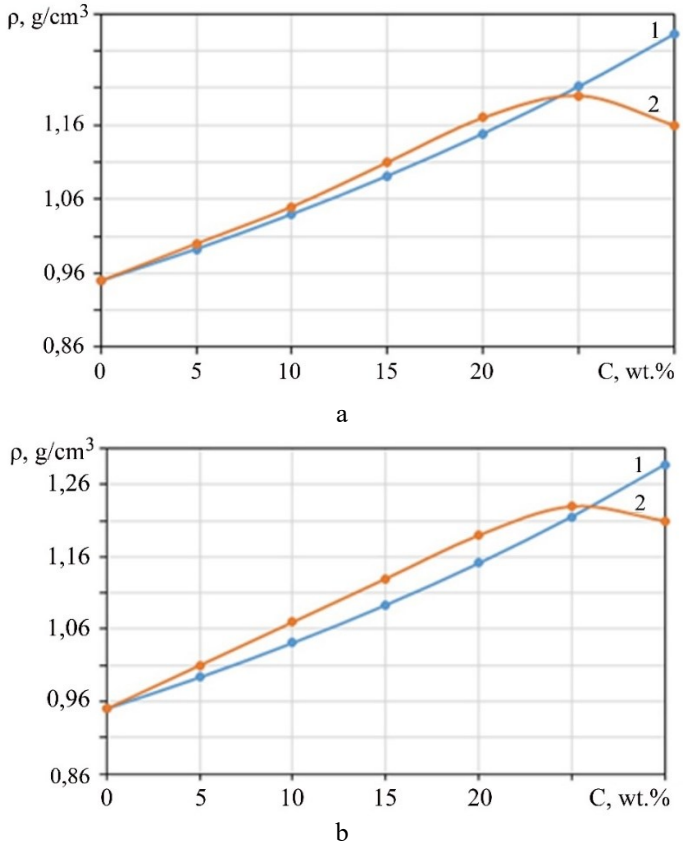

Fig. 5. Dependence of theoretical (1) and experimental (2) density (ρ, g/cm^3) of UHMWPE on the percentage content (C, wt. %) of high-entropy alloys №1 (a) and №2 (b)

Subsequently, the filler particles stick together, forming agglomerates (clusters) with a smaller contact surface with UHMWPE.

Conclusions

Analysis of the results of the conducted research showed that using high-entropy (multicomponent) alloys $Fe_{20}Ni_{20}Co_{20}Be_{20}Si_{14}B_6$ and $Al_{40}Co_{12}Cu_{12}Cr_{12}Ni_{12}Fe_{12}$ as Fls for UHMWPE is an effective way to improve its tribological properties by reducing the abrasive wear and roughness index by 45%. We established that the effective Fl content is 25 wt.% $Fe_{20}Ni_{20}Co_{20}Be_{20}Si_{14}B_6$ and 20 wt.% $Al_{40}Co_{12}Cu_{12}Cr_{12}Ni_{12}Fe_{12}$. The developed PCM compositions can be used in the manufacture of tribotechnical parts for the agricultural, mining, and automotive industries, which operate in aggressive conditions (under the influence of UV radiation, variable temperatures, moisture, and abrasive particles). Applying them will not only reduce the mass of the structure, but also increase the service life of the equipment.

References

1. A.S. Kobets Application of polymer composites in the agricultural industry. Monograph. Dnipro: Zhurfond, 2022. 356 p. https://dspace.dsau.dp.ua/handle/123456789/7031

2. V.O. Melnyk Causes of wear of parts of friction units of aviation equipment and methods of ensuring their operability. Problems of friction and wear. Problems of Friction and Wear. 2020. Vol.86, No1. P. 87–92. https://doi.org/10.18372/0370-2197.86.14491

3. O. Shevchuk, U.Wagenknecht, S. Wiessner, N. Bukartyk, M. Chobit, V. Tokarev Flame-retardant polymer composites on the basis of modified magnesium hydroxide. Chemistry & Chemical Technology 2015. Vol. 9, No 2. P. 149–155. https://ena.lpnu.ua/handle/ntb/28323

4. T. Chang, C. Yuan, Z. Guo Tribological behavior of aged UHMWPE under water-lubricated condition. Tribology International. 2019. Vol. 133. P. 1–11. https://doi.org/10.1016/j.triboint.2018.12.038

5. Anuj Bellare, Alessandro Bistolfi, Saverio Affatato Ultra-High Molecular Weight Polyethylene: Influence of the Chemical, Physical and Mechanical Properties on the Wear Behavior. Materials. 2017, Vol.7, No10. P. 791. https://doi.org/10.3390/ma10070791

6. V.F. Bashev, A.-M.V. Tomina, K.A. Mykyta, T.V. Kalinina, S.I. Riabtsev, O.I. Kushnerov The influence of a rapidly-quenched filler on the wear resistance of ultrahigh molecular weight polyethylene. Functional Materials. 2024. Vol.31, №3. P. 387–390. http://functmaterials.org.ua/contents/31-3/387

7. M.M. Bratychak, N.V. Chopyk, V.M. Zemke Technological features of polymer blends processing based on ultra-high molecular weight polyethylene. Chemistry, Technology and Application of Substances. 2018. Vol.1, №1. P. 127–132. https://ena.lpnu.ua/handle/ntb/45022

8. O.I. Kushnerov, V.F. Bashev, S.I. Ryabtsev Structure and Properties of Nanostructured Metallic Glass of the Fe–B–Co–Nb–Ni–Si High-Entropy Alloy System. Nanomaterials and Nanocomposites, Nanostructure Surfaces, and Their Applications, Springer Proceedings in Physics. 2021. Vol.246. P.557–567. https://link.springer.com/chapter/10.1007/978-3-030-51905-6_38

9. O.I. Kushnerov, V.F. Bashev, S.I. Ryabtsev Structure and Properties of Melt-Quenched $Al_4CoCrCuFeNi$ High Entropy Alloy. Defect and Diffusion Forum. 2024. Vol.431. P.47–54. https://doi.org/10.4028/p-4GvJbC

10. Ye.A. Yeriomina, O.B. Lysenko, V.K. Nosenko, Ya.E. Yarovyi Study of the influence of quick-hardened alloy on the properties of metal polymers. Journal Of Physics And Electronics. 2021. Vol. 29, No.1. P. 41–44. https://doi.org/10.15421/332105

11. Ya.E. Yarovyi, Ye.A. Yeriomina, A.-M.V. Tomina The influence of nickel-clad chromium carbide on the tribological properties of composite based on phenylone aromatic polyamide. Functional Materials. 2025. Vol.32, No.1. P. 72–76. https://doi.org/10.15407/fm32.01.72

12. V.I. Dvoruk, Kindrachuk M.V. Physical nature of abrasive wear resistance of commercially pure metals. Problems of Tribology, 2011, No. 2. P. 79–85. https://tribology.khmnu.edu.ua/index.php/ProbTrib/article/view/335

Томіна А-М.В., Шурпік В.Ю., Єрьоміна К.А., Predrag Dašić, Бурзав В.Б. Вплив високоентропійних сплавів на показник абразивного стирання надвисокомолекулярного поліетилену

У роботі розглянуто вплив високоентропійних сплавів $Fe_{20}Ni_{20}Co_{20}Be_{20}Si_{14}B_6$ та $Al_{40}Co_{12}Cu_{12}Cr_{12}Ni_{12}Fe_{12}$ на показник абразивного стирання надвисокомолекулярного поліетилену. Зокрема, встановлено ефективний вміст наповнювачів, при яких досягається мінімальне значення показника абразивного стирання. Для сплаву $Fe_{20}Ni_{20}Co_{20}Be_{20}Si_{14}B_6$ такі значення спостерігаються при концентрації 25 мас.%, тоді як для сплаву $Al_{40}Co_{12}Cu_{12}Cr_{12}Ni_{12}Fe_{12}$ – при 20 мас.%. У досліджених інтервалах концентрацій спостерігається загальне покращення абразивної стійкості на 35–45% порівняно з вихідним ненаповненим поліетиленом, що свідчить про високу ефективність обраних порошкових наповнювачів. Підвищення зносостійкості пояснюється особливостями взаємодії твердих часток високоентропійних сплавів з полімерною матрицею. Завдяки мікротвердості, що перевищує 10000 МПа, такі частки виконують роль армуючих елементів, які рівномірно розподіляються в об’ємі поліетилену та сприяють формуванню більш стабільної та жорсткої структурної сітки. Це забезпечує ефективний опір механічному руйнуванню поверхневих шарів під час тертя по жорсткозакріплених абразивних частках, що особливо важливо для роботи вузлів тертя в умовах інтенсивних навантажень. Додатково встановлено, що твердість отриманих композитів зростає приблизно у 1,6 рази, що підтверджує підсилюючий вплив високоентропійних наповнювачів та позитивно відображається на експлуатаційній довговічності матеріалу. Отримані результати підтверджують доцільність використання порошків високоентропійних сплавів як перспективних функціональних наповнювачів для створення зносостійких полімерних композиційних матеріалів на основі надвисокомолекулярного поліетилену та окреслюють подальші напрями удосконалення технологій модифікації полімерів.

Ключові слова: надвисокомолекулярний поліетилен, показник абразивного стирання, високоентропійний сплав, полімерний композиційний матеріал

ISSN 2079-1372 Problems of Tribology, V. 30, No 4/118-2025, 42-49

Problems of Tribology
Website: http://tribology.khnu.km.ua/index.php/ProbTrib
E-mail: tribosenator@gmail.com

DOI: https://doi.org/10.31891/2079-1372-2025-118-4-42-49

Study of the wear process and damage characteristics of the "stationary shaft–bushing" tribological pair

A. Gypka*[0000-0002-7565-5664], D. Stukhliak[0000-0002-9404-4359], D. Mironov[0000-0002-5717-4322], O. Totosko[0000-0001-6002-1477], R. Khoroshun[0000-0002-1862-7640], L. Slobodian[0000-0002-9191-6801], M. Kostyuk

Ternopil Ivan Puluj National Technical University , Ukraine
**E- mail : Gypkab@gmail.com*

Received: 12 October 2025: Revised 30 October 2025: Accept: 20 November 2025

Abstract

The article investigates the causes of surface degradation in the "stationary shaft–bushing" tribological pair of the roller assembly of a diesel engine fuel pump plunger in a heavy-duty truck, operating under increased loads and boundary lubrication conditions. A surface damage passporting methodology was applied, including analysis of microhardness, surface roughness, geometrical accuracy, and structural transformations within surface layers of the components, supplemented by elements of X-ray diffraction analysis.

It was established that the dominant wear mechanism is hot scuffing (adhesive wear of the second kind), driven by irregular lubricant supply, chemical affinity of the materials of both components (bearing steel 100Cr6/ШХ15), localized load concentration, and the stationary configuration of the shaft. The formation of secondary hardened "white layers" was observed, indicating thermal overloading and a reduced load-bearing capacity of the surface layers after prolonged service.

A set of design, technological, and operational measures is proposed to improve the reliability and durability of this friction pair.

Keywords: hot scuffing, tribological pair, fuel pump, microhardness, secondary structures, surface damage.

Introduction

The increasing requirements for fuel efficiency and environmental performance of diesel engines necessitate higher fuel delivery per cycle and higher injection pressures in fuel injection systems. This results in elevated mechanical and thermal loads on the components of the plunger pump, particularly on the "stationary shaft–bushing" friction pair in the roller assembly of the tappet. Operational experience shows that with an increase in plunger diameter and the corresponding rise in axial loads, intensive surface damage due to hot scuffing occurs within this tribological pair. Premature failure of these components limits the service life of the fuel pump, reduces engine reliability, and leads to economic losses.

The complexity of this issue is further aggravated by boundary lubrication conditions and the structural and chemical similarity of the materials in frictional contact. Such operating conditions promote the formation of welding bridges between the asperity peaks in the contact zone of the surfaces. Therefore, there is a growing need for scientifically justified methods and design solutions aimed at improving the durability and performance of the "shaft–bushing" friction pair under the operating conditions of diesel fuel systems.

Literature Review

In modern research on diesel engine fuel injection equipment, significant attention is paid to the tribotechnical characteristics of the "cam–roller–shaft" contact pair in high-pressure fuel pumps. Increased injection pressures and stricter environmental emission requirements lead to higher mechanical loads on these components. In the studies by [1], the wear and running-in behavior of cam–roller systems in diesel engines was

analyzed, demonstrating the development of complex surface topography under operating conditions and local variations in hardness in mixed lubrication regimes, which determine the further evolution of frictional interaction and the risk of scuffing. Research conducted by [2] for the "cam–roller tappet" pair in heavy-duty diesel fuel pumps, based on numerical modeling and lubrication analysis, revealed that boundary lubrication zones form already at the running-in stage, where load is transmitted through individual asperities, and local temperature spikes may initiate damage due to the onset of adhesive interaction followed by scuffing. A considerable amount of studies also focuses on the influence of fuel type and lubricants on the reliability of friction units in diesel fuel injection equipment. The review by [3] summarizes current understanding of the mechanisms of ZDDP additive action, the formation of protective tribofilms, and their role in preventing scuffing under boundary lubrication conditions. Recent works by [4-6]and others have shown that the kinetics of tribofilm growth, as well as its thickness and morphology, are strongly dependent on surface topology, loading regime, and additive chemistry. It has also been demonstrated that tribofilm breakdown may occur locally under severe loading, reopening direct metallic contact and promoting scuffing in frictional interfaces. Reviews concerning friction reduction in internal combustion engines emphasize that the friction units of fuel injection equipment — where high contact stresses, low sliding speeds, and boundary lubrication are combined — remain among the most critical elements in terms of scuffing and service life reduction. Another direction of research concerns surface modification of components — the application of hard wear-resistant coatings, surface texturing, deep thermal and cryogenic treatment, as well as the use of composite materials and coatings. PVD-coatings such as BALINIT applied to fuel pump components, rollers, and tappets have demonstrated a significant reduction in friction coefficient and increased scuffing resistance due to modifications in the chemical composition and thermophysical properties of protective surface layers. Research in the field of cryogenic treatment of tool and bearing steels has proven that deep cooling after quenching promotes more complete transformation of retained austenite into martensite and the formation of a more stable structure with enhanced wear resistance. This is particularly important for steels such as 100Cr6 (ШХ15), which are widely used in highly loaded bearing and plunger units. In the study [8], a comprehensive methodology for evaluating the tribological efficiency of automotive component couplings was proposed, combining experimental research, modeling, and diagnostic criteria for assessing the performance of surface layers. This approach enables an in-depth analysis of friction conditions and identification of the most vulnerable tribosystems. In the article [9], tribodiagnostics of surface damage during operation was examined based on changes in the structural and mechanical properties of surface layers, ensuring early detection of failure initiation and forecasting of remaining service life. The research conducted [10] established the patterns of variation in the lubrication degree of crankshaft bearings depending on engine load and speed regimes. The influence of the hydrodynamic lubrication film on reliable bearing operation was demonstrated, and methods were proposed to enhance durability by optimizing operating parameters. The summarized findings confirm the relevance of further development of diagnostic approaches and measures to improve the reliability of tribological components in automotive systems, particularly those operating under boundary lubrication, high contact loads, and significant thermal gradients. Studies [11–14] demonstrate the effectiveness of various protective coatings — including Fe–Mn–C–B–Si–Ni–Cr eutectic welding layers and polymer-modified thermosetting composites — in improving wear resistance, enhancing antifriction performance, and stabilizing adhesion properties of friction surfaces under elevated temperature and boundary lubrication conditions, which is relevant for extending the durability of highly loaded tribological contacts in automotive systems

Purpose of the study

To determine the dominant mechanism of surface damage in the "stationary shaft–bushing" tribological pair of the roller tappet assembly of a diesel engine fuel pump under increased loading and restricted lubrication supply, in order to provide a scientific rationale for a set of design and technological measures aimed at improving its operational reliability and service life.

Research results

Improving the reliability and service life of friction units in fuel injection equipment is only possible with a thorough investigation of the damage mechanisms of the most heavily loaded and vulnerable tribological contacts that determine system operability. These include the sliding "stationary shaft–bushing" tribological pair in the roller tappet assembly of the plunger pump of a heavy-duty diesel engine.

Intensification of fuel pump operation through an increase in plunger diameter from 9 to 10 mm leads to a 28% rise in maximum chamber pressure (from 42.4 to 54.2 MPa) and a 57% increase in cyclic axial force (from 2.7×10^3 to 4.25×10^3 N). As a result of such loading, premature surface failure of the tribological pair occurs: hot scuffing is detected after only 4 hours of pump operation on a calibration test bench. Therefore, it is crucial to identify the dominant wear mechanism and determine the causes of damage in this tribological contact. A surface damage passporting method was applied, involving a comprehensive assessment of: compliance of component geometry with design requirements, loading and lubrication conditions, and the actual state of working surfaces after operation. Three groups of tribological pairs were compared in the study: damaged shaft–bushing pairs after 4 hours of bench testing under elevated axial load; field-operated pairs with 1330 hours of service (≈50,000 km

mileage) under optimal loading conditions; and new components. The obtained results of tribosystem passporting were summarized in the form of a technical function for the “stationary shaft–bushing” friction pair of the roller tappet assembly in the fuel pump (Table 1). Roundness profiles of the internal surfaces of the bushings for the different groups are presented in Fig. 1, and the quantitative results of form deviation analysis are shown in Fig. 2. It was determined that all examined bushings exhibit deviations from ideal geometry in the form of polygonalization; however, the nature and severity of deformation differ significantly depending on the loading conditions and service duration.

Table 1

Technical passport of the “stationary shaft–bushing” tribosystem of the roller tappet assembly of a diesel engine fuel pump

Section	Parameter	Description / Value
I. Analysis of friction and wear conditions	Type of interaction	Sliding friction
	Lubrication regime	Boundary (limited lubricant supply)
	Axial load	2.7×10^3…4.25×10^3 N
	Sliding speed	0.1…2.5 m/s
	Contact zone temperature	1073…1123 K
	Operating time	4 h (bench test), 1330 h (in service)
II. Material and component characteristics	Shaft material	Bearing steel 100Cr6 (ШХ15)
	Bushing material	Bearing steel 100Cr6 (ШХ15)
	Initial surface roughness	Ra = 1.6 μm
	Shaft geometry (working dimensions)	$Ø9^{-0.01}$ mm / $Ø10^{-0.01}$ mm
	Bushing geometry (tolerances)	$Ø9^{+0.033-0.013}$ mm / $Ø10^{+0.033-0.013}$ mm
	Density	$\rho = 7811$ kg/m³
	Chemical composition (100Cr6), wt.%	C 0.95–1.05; Si 0.17–0.37; Mn 0.20–0.40; Cr 1.30–1.65; P ≤0.027; S ≤0.02; Ni ≤0.30
	Mechanical properties	$\sigma_v \approx 730$ MPa; $\sigma_{0.2} \approx 420$ MPa; $\delta \approx 21\%$; $\psi \approx 46\%$
	Thermophysical properties	$\alpha_n = 45\times10^4$ J/(m²·K)
III. Environmental factors	Contamination	Dusty air, impurities in fuel
IV. Risks and expected damage mechanisms	Potential wear types	Scuffing (adhesive wear of the second kind), fretting, abrasive wear
	Critical conditions	Surface overheating, direct metallic contact, local peak stresses at asperity tips
V. Geometry and surface heat treatment	Contact geometry	Cylindrical surfaces, line contact footprint
	Heat treatment	Hardening at 850 °C (210 min) + oil quenching; cold treatment at –30…–60 °C (200 min); tempering at 180 °C (200 min); air cooling
	Lubrication regime	Boundary friction
	Lubricant supply	“Splash lubrication” (insufficient and unstable lubricant flow to the upper contact zone)
VI. Tribological interactions	Contact interfaces	“Shaft–bushing”, “bushing–environment”, “shaft–environment”; load directions and displacements illustrated in Fig. 1a–c
VII. Tribological characteristics	Dominant wear mechanism	Adhesive wear (hot scuffing, Type II), thermal softening, formation of “white layers”
	Contact conditions	Cylindrical contact between shaft (1) and bushing (2); critical load zone located in the upper part of the bushing (minimum lubrication)
	Controlled parameters	Wear rate; coefficient of friction; contact temperature; contact electrical resistance (CER); specific damage energy; load-bearing capacity reserve of the surface layers

Bushings that have operated for 1330 hours under normal service conditions demonstrated the smallest non-uniformity of profile deviation — the polygonalization in this case is practically reduced to minor ovality

(Fig. 2, curve 1). New bushings are characterized by a tetragonal profile shape (Fig. 2, curve 2), indicating manufacturing inaccuracies and insufficient quality of finishing operations. The most pronounced multi-polygonal deformation was observed in bushings damaged during bench operation under increased axial loads (Fig. 2, curve 3), which leads to localized increases in contact stresses and promotes the development of hot scuffing.

Thus, the analysis of internal bushing geometry based on roundness profiles confirms that increased mechanical loading and unstable lubrication result in accelerated wear of the working surfaces, which consequently causes failure of the friction unit.

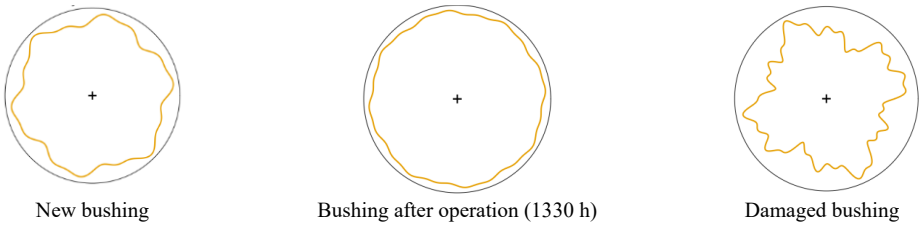

Fig. 1. Roundness profiles of the internal surface of bushings in the "shaft–bushing" friction pair after different operating conditions

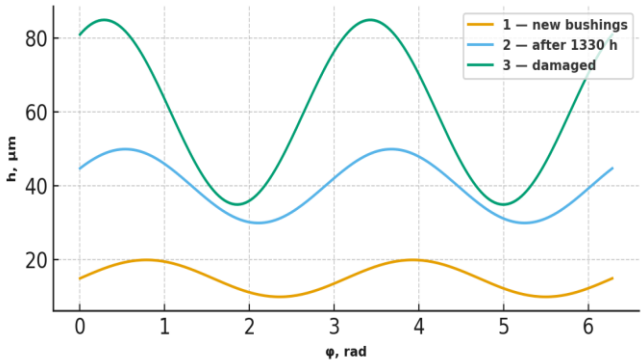

Fig. 2. Form deviation of the internal bushing surface after different operating conditions: 1 - new bushings; 2 - bushings after 1330 h of operation; 3 - bushings damaged during bench testing under increased loads

The surface topography analysis of the shafts in the new condition, after 1330 hours of operation, and after damage under increased loading conditions (Fig. 3) showed that normal operation results in a significant reduction of surface roughness compared to the new component due to running-in processes and plastic smoothing of asperities under mixed friction conditions. The machining quality of the new shaft's outer surface ($R_a \approx 1.6$ μm) is significantly higher compared to the bushing's internal surface ($R_a \approx 58$ μm), which does not meet the requirements of technical specifications stating that the roughness parameters of contacting elements must be compatible. Such inconsistency deteriorates the formation of a stable lubricant film and promotes localized concentration of contact stresses. The microhardness characteristics of the shaft surface layer are shown in Fig. 4. The average surface microhardness of the new shaft is approximately 5500 MPa (Fig. 4, curve 1), and the microstructure consists of hardened martensite with a high level of residual stresses. This provides increased initial wear resistance; however, it also creates susceptibility to thermal cracking and the formation of "white layers" in cases of overheating under boundary lubrication conditions.

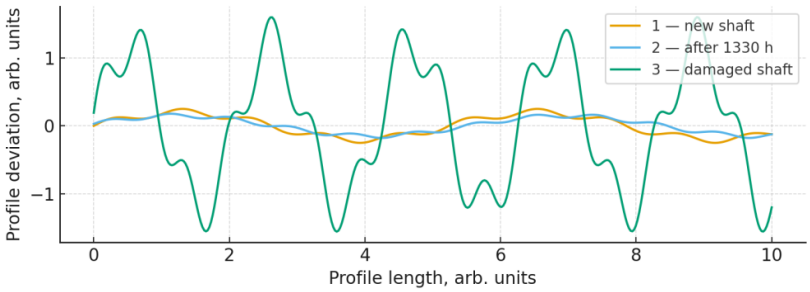

Fig. 3. Profilograms of the working surface of shafts in the "shaft–bushing" friction pair: 1 - new shaft (vertical scale ×10 000; horizontal scale ×80); 2 - shaft after 1330 h of operation (vertical scale ×10 000; horizontal scale ×80); 3 - shaft damaged during bench testing under increased loads (vertical scale ×4000; horizontal scale ×80).

After 1330 hours of operation, strengthening of the shaft surface layer was observed, associated with work hardening and phase transformations under variable loading. In contrast, the damaged components show the formation of a secondary-hardened "white layer" with an abrupt increase in hardness, which indicates thermal overload and serves as an initiator of hot scuffing.

During normal operation of the assembly, strengthening of the surface layers occurs due to work hardening and stabilization of secondary structures. It was established that after 1330 hours of operation, the surface microhardness of the shaft increases to approximately 6060 MPa (Fig. 4, curve 2), indicating partial transformation of the material into martensite, which is more resistant to wear. In this case, a reduction in micro-relief depth was observed already at the running-in stage.

In contrast, on the surfaces of damaged bushings and shafts that operated under increased mechanical and thermal loads, localized formation of a densified "white layer" with significantly higher hardness was detected (Fig. 4, curve 3). The microhardness of this layer exceeds the initial value nearly twofold, indicating the development of secondary hardening and the formation of a brittle structure with a high tendency to delamination. The presence of a white layer implies that temperatures in specific contact points reached levels sufficient to initiate thermal plasticity of the surface layers, reducing their strengthening and followed by rapid cooling when metallic junctions are ruptured. Such thermodynamic instability is the major driving factor behind the development of hot scuffing.

The results of X-ray diffraction analysis confirm the formation of new Fe_γ-type phases characteristic of rapid surface cooling after localized overheating, which is consistent with the mechanism of secondary hardening under boundary friction conditions.

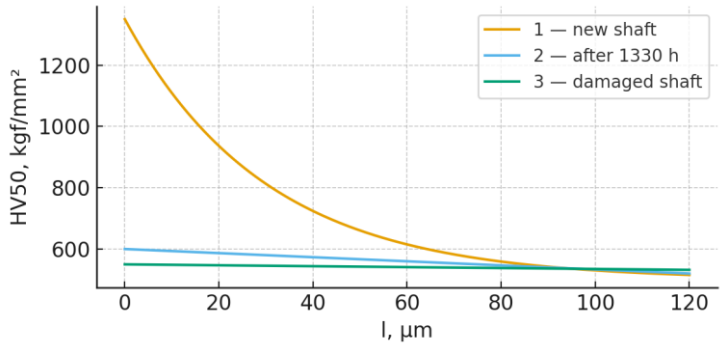

Fig. 4. Distribution of HV50 microhardness within the surface layer of the shafts in the "shaft–bushing" friction pair after different operating conditions: 1 - damaged shaft (secondary hardening, "white layer"); 2 - shaft after 1330 h of normal operation; 3 - new shaft.

Based on a set of experimental and diagnostic investigations, it was determined that the dominant surface damage mechanism limiting the serviceability of the "stationary shaft–bushing" friction pair in the roller tappet assembly of the fuel pump is adhesive wear of the second kind (hot scuffing). The development of hot scuffing is induced by boundary lubrication conditions, in which the lubricant supply to the contact zone is unstable or insufficient. Under such circumstances, the dynamic balance between the formation and removal of secondary structures in the surface layers of the frictional contact is disrupted. As the lubricant film collapses, contact occurs between nascent metallic asperities of both elements.

Since the shaft and the bushing are manufactured from the same steel grade (100Cr6), the chemical affinity of the materials promotes the formation of welding bridges at the interface. The action of tangential forces that cause relative displacement leads to rupture of these junctions, accompanied by sharp localized temperature rises. As a result, the surface layers undergo thermal softening and plastic deformation, local melting, and a decrease in load-bearing capacity, followed by secondary hardening during cooling (formation of a "white layer").

Consequently, the surface loses structural stability. Repeated initiation and accumulation of these processes lead to accelerated degradation and eventual failure of the friction pair. The severity of hot scuffing is strongly influenced by the thermophysical properties of the material (thermal conductivity, heat capacity, high-temperature strength), which determine the ability of the surface layers to dissipate heat from the contact zone. In the analyzed friction pair, hot scuffing most frequently develops under boundary or starved lubrication; during rapid load increases at start-ups and transient modes; and under disrupted lubricant supply, as in the present study.

Thus, the combination of elevated mechanical loads, chemical affinity of the contacting materials, and limited lubrication is a decisive factor driving the failure of this friction pair due to the development of hot scuffing. Based on the established damage mechanism, a physical model of adhesive wear of the second kind was proposed, comprising five stages: breakdown of boundary lubrication layers and secondary structures due to irregular lubricant supply; approach of metallic asperities to contact distances and collapse of the lubricant film; intensive plastic deformation in microcontacts with the formation of dislocation-active zones and increased vacancy

concentration; mutual diffusion of metallic surfaces and formation of metallic junctions in the true contact region; rupture of metallic junctions accompanied by material transfer and generation of wear debris.

The practical significance of this model is that the prevention of hot scuffing is governed by the durability and stability of secondary protective structures, and the thermophysical properties of the contacting materials determining heat dissipation capabilities.

To reduce the intensity of adhesive wear of the second kind, engineering solutions must be implemented to: suppress activation of metallic contact (strengthening of surface layers, improvement of high-temperature resistance); promote surface passivation, which ensures the formation of stable secondary structures and efficient heat removal.

Passivation control may be achieved by increasing the thermal conductivity and heat capacity of the materials in the friction pair; using lubricants with functional additives that promote the formation of robust anti-scuffing films on the contacting surfaces.

Generalization of the results confirms the feasibility of applying a set of design, technological, and operational solutions to eliminate or significantly reduce damage in the "stationary shaft–bushing" friction pair of the roller tappet assembly of a fuel pump. Based on the obtained results, a comprehensive set of measures for improving durability of the friction pair is justified and summarized in Table 2.

Table 2

A set of measures aimed at improving the durability of the "stationary shaft–bushing" friction pair in the roller tappet assembly of a fuel pump

№	Category of measures	Recommendation	Expected technical effect
1	Design-related	Introduction of axial lubrication grooves and eccentric relief in the upper zone of the shaft	Improved lubricant supply, reduction of boundary friction
		Use of dissimilar materials for the shaft and the bushing	Reduced chemical affinity, lower risk of metallic adhesion and scuffing
2	Optimization of load conditions	Parametric optimization of fuel injection equipment to increase delivery without additional load growth	Reduction of peak axial loads and thermal overload
3	Technological surface strengthening	Deep cryogenic treatment (≈ −90 °C) immediately after quenching	Strengthening and stabilization of surface layers, reduced susceptibility to scuffing
		Optimization of finishing operations and sealing technologies	Formation of favorable surface topography and durable secondary structures
4	Modification of operating media	Use of anti-scuffing and antiwear additives in lubricating and fuel media	Accelerated formation of protective tribofilms in the contact zone

Conclusions

It has been established that the dominant surface damage mechanism in the "stationary shaft–bushing" friction pair of the roller tappet assembly in a fuel pump is adhesive wear of the second kind (hot scuffing), which develops rapidly under boundary lubrication and increased axial loading.

It has been shown that bushings operated for 1330 hours under normal conditions exhibit minimal form deviations, whereas damaged bushings demonstrate pronounced polygonal deformation of the cylindrical surface profile, indicating intensive plastic deformation in the contact zone.

Analysis of surface topography and microhardness confirmed the formation of a localized densified "white layer" after failure, whose microhardness is nearly twice the initial value. This indicates secondary hardening of the surface layer caused by localized thermal overload.

It was determined that the primary cause of scuffing is insufficient lubricant supply during periods of maximum cyclic loading, resulting in direct contact between nascent metallic asperities and the formation of welding bridges.

The mechanism of hot scuffing has been defined, allowing the identification of key factors governing the progression of surface damage, including the strength of secondary structures and the thermophysical properties of the material.

A set of design, technological, and operational measures has been justified to reduce the intensity of hot scuffing in the studied friction pair, including the introduction of lubrication grooves and eccentric relief, the use of dissimilar materials in the pair, deep cryogenic treatment, and modification of the working media with functional additives.

Further experimental studies on tribological test benches are required to validate the proposed solutions and to optimize the parameters of the design and technological improvements of the assembly.

References

1. Lindholm P. Characterisation of wear on a cam follower system in a diesel engine. *Wear*. 2003. https://doi.org/10.1016/S0043-1648(03)00335-1

2. Alakhramsing S. S., de Rooij M. B., Schipper D. J., van Drogen M. Lubrication and frictional analysis of cam–roller follower mechanisms. *Proc. IMechE Part J: J. Engineering Tribology*. 2018. https://doi.org/10.1177/1350650117718083

3. Spikes H. Mechanisms of ZDDP—An update. *Tribology Letters*. 2025. https://doi.org/10.1007/s11249-025-01968-3

4. Tsai A. E. et al. Dynamics of tribofilm formation in boundary lubrication. *Tribology International / Materials*. 2024. https://doi.org/10.3390/ma17061335

5. Dawczyk J. Film thickness and friction of ZDDP tribofilms. *Tribology Letters*. 2019. https://doi.org/10.1007/s11249-019-1148-9

6. Bai, L., Meng, Y., Zhang, V. *et al.* Effect of Surface Topography on ZDDP Tribofilm Formation During Running-in Stage Subject to Boundary Lubrication. *Tribol Lett* **70**, 10 (2022). https://doi.org/10.1007/s11249-021-01552-5

7. Akchurin A. A mixed-TEHL analysis of cam–roller contacts considering thermal and roughness effects. *Journal of Tribology*. 2018. https://doi.org/10.1115/1.4040979

8. Aulin, V., Gypka, A., Liashuk, O., Stukhlyak, P., & Hrynkiv, A. (2024). A comprehensive method of researching the tribological efficiency of couplings of parts of nodes, systems and aggregates of cars. Problems of Tribology, 29(1/111), 75-83. https://tribology.khmnu.edu.ua/index.php/ProbTrib/article/view/943

9. Aulin, V., Lyashuk, O., Gupka, A., Tson, O., Dmitro, M., Sokol, M., ... & Yarema, I. (2024). Tribodiagnosis of the surface damage of tribo-coupling parts materials during machine operation. Procedia Structural Integrity, 59, 428-435. https://doi.org/10.1016/j.prostr.2024.04.061

10. Gypka, A., Aulin, V., Lyashuk, O., Hrynkiv, A., & Hud, V. (2024). The patterns of changes in the degree of lubrication of the crankshaft bearings of car engines depending on the parameters of the load-speed modes of operation. Problems of Tribology, 29(3/113), 72-78. https://tribology.khmnu.edu.ua/index.php/ProbTrib/article/view/965

11. Pashechko, M., Dziedzic, K., Stukhliak, P., Barszcz, M., Borc, J., & Jozwik, J. (2022). Wear Resistance of Eutectic Welding Coatings of Iron-Based Fe–Mn–C–B–Si–Ni–Cr at Increased Temperature. Journal of Friction and Wear, 43(1), 90–94. https://doi.org/10.3103/S106836662201010X

12. Stukhlyak, P. D., & Bliznets, M. M. (1987). Wear resistance of epoxyfuran composites modified with polyvinyl alcohol. Soviet Journal of Friction and Wear (English translation of Trenie i Iznos), 8(3), 122–124. Scopus.

13. Stukhlyak, P. D. (1986b). Antifriction and adhesive properties of coatings of thermosetting plastics modified with thermoplastic polymers. Soviet Journal of Friction and Wear (English translation of Trenie i Iznos), 7(1), 138–141. Scopus.

14. Stukhlyak, P. D. (1986a). Antifriction and adhesion performances of thermosetting coatings modified by thermoplastics. TRENIE & IZNOS, 7(1, 1986), 173–177.

Гупка А.Б. , Стухляк Д.П. , Міронов Д.В. , Тотосько О.В. , Хорошун Р.В. , Слободян Л.М., Костюк М.В. Дослідження процесу зношування та характеру пошкоджуваності трибоспряження «нерухома вісь-втулка»

У статті досліджено причини поверхневого руйнування трибоспряження «нерухома вісь – втулка» роликового вузла штовхача паливного насоса дизельного двигуна вантажного автомобіля за умов підвищених навантажень і граничного мащення. Застосовано метод паспортизації поверхневого руйнування з аналізом мікротвердості, шорсткості, геометричної точності та структурних змін у поверхневих шарах деталей, включаючи елементи рентгеноструктурного аналізу. Встановлено, що основним видом руйнування є гарячий задир (схоплювання II роду), зумовлений нерегулярним підведенням мастильного матеріалу, хімічною спорідненістю матеріалів обох деталей (Сталь ШХ15), локальною концентрацією навантажень та нерухомим положенням осі. Показано формування вторинно-загартованих «білих шарів», що свідчить про теплове перевантаження та зниження запасу несучої здатності поверхневих шарів після тривалої експлуатації. Запропоновано комплекс конструктивних, технологічних і експлуатаційних заходів для підвищення надійності й довговічності пари тертя.

Ключові слова: гарячий задир, трибоспряження, паливний насос, мікротвердість, вторинні структури, поверхневе руйнування.

ISSN 2079-1372 Problems of Tribology, V. 30, No 4/118-2025, 50-56

Problems of Tribology
Website: http://tribology.khnu.km.ua/index.php/ProbTrib
E-mail: tribosenator@gmail.com

DOI: https://doi.org/10.31891/2079-1372-2025-118-4-50-56

Enhancement of corrosion–mechanical wear resistance of metallic alloys by glow-discharge nitriding

M.S. Stechyshyn[1]0000-0001-5780-2790, **N.S. Mashovets**[*1]0000-0001-9181-5253, **S.Ya. Pidhaichuk**[1]0000-0002-9868-6447, **V.M. Shevchuk**[2]0000-0002-0436-1183, **A.V. Korinnyi**[1]0009-0000-9445-5054

[1]*Khmelnitskyi National University, Ukraine*
[2]*Bohdan Khmelnytskyi National Academy of State Border Guard Service of Ukraine, Khmelnytskyi, Ukraine*
**E- mail : mashovetsns@ukr.net*

Received: 20 October 2025: Revised 30 October 2025: Accept: 25 November 2025

Abstract

The aim of this work is to provide a comprehensive analysis of hydrogen-free nitriding and nitrocarburizing processes in a glow discharge, to summarize the regularities of nitride and carbonitride layer formation on steels and titanium alloys, and to evaluate their corrosion–mechanical wear resistance under conditions of sliding, fretting, cavitation, and exposure to aggressive media. Particular attention is given to the application of Pastukh's I.M. model for interpreting the kinetics and energy mechanisms of diffusion processes. The study presents a comparative analysis of the structural–phase transformations during nitriding and nitrocarburizing in a hydrogen-free glow discharge and systematizes experimental data on microhardness, electrochemical behavior, and corrosion–mechanical wear resistance.

The methodological basis of the theoretical part is the energy-exchange model developed by I. M. Pastukh, which describes the influence of active plasma species on the diffusion rate and phase formation. It is shown that hydrogen-free nitriding provides intensified nitrogen diffusion, the formation of stable nitrides TiN, Ti_2N, ε-($Fe_{2–3}N$), γ′-(Fe_4N), and the elimination of hydrogen embrittlement. It is established that nitrocarburizing produces multilayer carbonitride structures with hardness values of 900–1300 HV and high adhesion to the substrate. The modified layers demonstrate a 3–6-fold increase in wear resistance, a 2.5–4-fold reduction in cavitation damage, and a significant decrease in corrosion current in NaCl and NaOH solutions. A transition of the dominant failure mechanisms from brittle and adhesive to plastic-deformation dominated modes has been identified. The obtained results confirm the experimentally observed regularities of carbonitride-layer formation and demonstrate the key role of ion bombardment in generating the defect-subzone that governs diffusion kinetics and phase stability.

The findings may be applied in the design of wear-resistant machine components, medical implants, and elements of cavitation units operating in alkaline and chloride environments. Hydrogen-free nitriding and nitrocarburizing technologies are identified as highly efficient, economically feasible, and suitable for industrial implementation.

Keywords: glow discharge, hydrogen-free nitriding, nitrocarburizing, nitride layers, titanium, steel, corrosion–mechanical wear

Introduction

Surface strengthening of titanium alloys and structural materials remains one of the key directions for improving the operational reliability of machine components, technological equipment, and critical-purpose products. Among the known surface-modification methods, a special place is occupied by nitriding and nitrocarburizing, which enable the formation of hard diffusion layers with high wear resistance, corrosion resistance, and fretting resistance. The use of glow discharge significantly expands the capabilities of these processes by intensifying diffusion, activating plasma-chemical reactions, and reducing the treatment temperature.

Traditional plasma nitriding technologies are based on hydrogen-containing gas mixtures, which facilitate surface cleaning but may simultaneously induce several undesirable effects, including hydrogen uptake, embrittlement, phase-structure changes, and reduced service life of components. For this reason, considerable

attention is devoted to the development of hydrogen-free nitriding and nitrocarburizing processes, which eliminate unwanted side effects and ensure the formation of stable nitride layers with predictable properties.

In recent years, substantial experimental data have been accumulated regarding the influence of glow-discharge parameters on the structure and properties of nitride layers formed on titanium alloys and steels, as well as on the dependence of corrosion–mechanical wear resistance, fretting resistance, and wear behavior in corrosive environments on these parameters.

Glow-discharge nitrocarburizing is a surface-modification process for steels and alloys that combines the advantages of nitriding and carburizing. Its effectiveness is determined by the active interaction of nitrogen and carbon, which in the glow-discharge plasma form complex carbonitride phases characterized by high hardness, corrosion resistance, and fretting resistance.

Despite significant progress in studying nitriding and nitrocarburizing processes, a number of fundamental and applied aspects of these technologies in hydrogen-free glow discharges remain insufficiently clarified. In particular, the influence of the absence of hydrogen on the activation mechanisms of nitrogen and carbon, the formation of the defect sublayer, and the kinetics of diffusion in the near-surface region of metals require further refinement, as do the regularities of phase formation in hydrogen-free environments, including the stability of nitride and carbonitride phases and their correlation with plasma parameters.

Special attention should be devoted to correlating experimental results with the energy-exchange model developed by I. M. Pastukh, which describes the interaction of active plasma species with the metal surface, with practical validation for hydrogen-free nitrogen–carbon (N–C) media, and to understanding how the structural–phase characteristics of modified layers influence their wear resistance.

Literature review

Nitriding and nitrocarburizing in a glow discharge remain among the most effective surface-modification methods for steels and titanium alloys due to their ability to form hard, wear-resistant, and corrosion-resistant nitride and carbonitride phases. Recent review studies [1–7] indicate a significant increase in interest in hydrogen-free technologies, which eliminate the problem of hydrogen embrittlement and provide more intensive ionic activation of the surface.

In study [1], it was shown that low-temperature nitriding of titanium in a glow discharge leads to the formation of TiN–Ti_2N layers with a pronounced microhardness gradient, where ion bombardment plays a key role by determining defect formation and the initial stage of diffusion. Works [2–5] investigated the influence of the main glow-discharge nitriding parameters—pressure, gas composition, temperature, and treatment duration—on the evolution of surface structure and properties of stainless steels. The authors demonstrate that variations in nitriding regimes control the nitrogen diffusion rate, the formation of nitride and nitrogen-enriched solid-solution layers, as well as the final performance characteristics of the material, including hardness, wear resistance, and corrosion resistance. Accurate control of process parameters is essential for obtaining stable and optimized properties of nitrided steels, which aligns with current trends in enhancing the efficiency of glow-discharge surface modification. The research demonstrates that discharge parameters significantly influence the phase composition of layers on stainless steels. A correlation between discharge power and the ε/γ′-phase ratio was identified, which is consistent with the energy-exchange model proposed by I. M. Pastukh.

Study [6] emphasizes that not only the external processing parameters (pressure, gas composition, voltage, time) determine the final surface properties, but also the quantitative characteristics of the flux and dose of plasma particles that actually reach the treated surface. Article [7] shows that for titanium alloys, glow discharge provides deep nitrogen saturation without overheating the material, which is particularly important for medical implants.

A comprehensive analysis of the influence of hydrogen-free nitrogen–carbon media on titanium alloys was performed in study [8]. The authors demonstrated that a hydrogen-free atmosphere promotes stabilization of the Ti_2N phase and prevents degradation of α-titanium, which is typical for hydrogen-containing discharges. Several works, including [8, 9], systematized the kinetic features of nitrogen diffusion in titanium alloys using the energy model of I. M. Pastukh, which describes the interaction of the flux of active particles with the surface through the balance of ion-impact energy and defect generation. The model has received experimental confirmation in subsequent studies [10–13], highlighting its universality for hydrogen-free media.

Studies [14, 15] demonstrated that combined nitrogen and carbon saturation provides a more ductile and crack-resistant layer compared with pure nitriding. Carbon promotes the formation of a stable ε-phase with a modified lattice structure, reducing residual stresses and improving resistance to fretting and cavitation damage. These findings agree with modern results reported in [16], where it was shown that Fe–(N,C) carbonitrides exhibit superior tribocorrosion performance compared to nitrides.

Investigations of the corrosion–mechanical stability of plasma-modified layers in works [17,18,19] revealed that nitrocarburized layers on steels show significantly increased wear resistance and 1.5–3-fold higher cavitation resistance compared to conventional nitriding.

Analysis of current data confirms that hydrogen-free nitriding and nitrocarburizing in a glow discharge are promising surface-engineering methods that ensure intensive surface activation, formation of stable nitride and carbonitride phases, improved tribocorrosion and cavitation resistance, and complete elimination of hydrogen embrittlement.

Objectives of the Study

The primary objective of this study is to provide a comprehensive analysis of hydrogen-free nitriding and nitrocarburizing processes under glow-discharge conditions, with particular attention to the mechanisms of nitrogen and carbon activation, diffusion kinetics, and the formation of nitride and carbonitride layers on steels and titanium alloys. The research aims to clarify how the absence of hydrogen influences surface activation, phase stability, and defect formation, as well as to determine how these factors affect the microstructure and operational performance of the modified layers.

The study seeks to formulate well-grounded conclusions regarding the technological advantages, limitations, and practical applicability of hydrogen-free nitriding and nitrocarburizing for enhancing the durability of machine components, titanium elements, and structural units operating in aggressive chemical or dynamic environments.

Purpose of work

To determine the technological advantages and limitations of hydrogen-free nitriding and carbonitriding compared to traditional hydrogen-containing methods.

Methods

This research is based on the analysis of scientific studies published in recent years, as well as on experimental results in the fields of glow-discharge nitriding, nitrocarburizing, and surface modification of titanium and steels. The article summarizes data on the modification of the following materials: α–β titanium alloys VT3-1 and VT8, austenitic stainless steels 08Kh18N10 and 12Kh18N9T, structural steels 38KhMYuA, 40Kh, 20Kh, and carbon steels. The main variable processing parameters include: gas pressure in the vacuum chamber of 80–400 Pa; treatment temperature of 500–700 °C; gas-mixture composition (N_2, N_2 + Ar, N_2 + C); discharge voltage of 400–1200 V; current density of 1–10 mA/cm²; and treatment duration of 1–10 hours. To analyze the properties of the modified surface layer, the following methods are employed: surface microhardness measurement using a PMT-3 microhardness tester; nitride-layer thickness determination using microstructural analysis on an MIM-10 microscope; phase-composition analysis of the surface layer using a DRON-3M X-ray diffractometer; X-ray photoelectron spectroscopy (XPS); and electron Auger spectroscopy performed using a JAMP-10S scanning Auger microprobe and electrochemical examinations in chloride and alkaline environments.

Research

Activation of nitrogen in a hydrogen-free glow-discharge environment differs fundamentally from classical hydrogen-containing nitriding technologies. The absence of hydrogen alters the energy exchange at the gas–solid interface, affects the composition of active plasma species, and determines the diffusion–kinetic regularities of nitrogen penetration into the metal. Based on analytical developments by Pastukh I.M. and their further extension in a series of subsequent works [10,11], a model was substantiated that describes the mechanism of nitride layer formation in hydrogen-free gas-discharge media through a system of interrelated processes such as electron-impact activation, surface energy exchange, ion-stimulated diffusion, and the thermodynamics of nitride formation.

The absence of hydrogen leads to a sharp increase in the fraction of heavy ions N_2^+ and N^+, which carry high impulse energy. This enhances the bombardment of the metal surface and results in intensified surface cleaning, oxide-film destruction, formation of active adsorption centers, and active nitrogen diffusion. Studies on titanium alloys [13] and steels confirm the presence of an intensive primary stage of surface activation, during which a sharp increase in the nitrogen uptake rate is observed in the first 10–20 minutes of treatment. This effect was first quantitatively described in the works of Pastukh I.M. [10], where the dependence of the flux of active species on electron energy and cathode potential was demonstrated.

According to Pastukh's energy model, a distinctly non-uniform energy distribution of active particles is formed in the glow discharge, with a pronounced increase in their energy within the near-surface cathode sheath. Calculations showed that it is the cathode potential drop that ensures the acceleration of nitrogen ions, while the electron component of the plasma determines the intensity of molecular N_2 dissociation. Thus, the flux of active particles reaching the surface consists of N_2^+/N^+ ions, metastable N atoms, as well as fast neutral atoms formed due to charge exchange in the cathode sheath. This combined energetic action determines the nature of the primary activation of the metallic surface and the subsequent rate of diffusion saturation.

Under hydrogen-free glow-discharge nitriding, the process of hydrogen saturation is absent, which is confirmed by studies [8,15]. In this case, a more homogeneous composition of surface layers is formed; no black (brittle) zones typical of hydrogen-containing mixtures appear; adhesion of nitride phases to the substrate increases; and corrosion–mechanical resistance in chloride and alkaline environments improves. This is consistent with Pastukh's model [10]: under hydrogen-free conditions, the surface energy of the system increases, promoting the formation of thermodynamically stable mononitrides rather than metastable hydrogen-defective structures.

X-ray diffraction analysis of the VT8 titanium alloy showed that, depending on the nitriding regime, diffraction peaks of α-Ti, TiN (δ-phase), and Ti_2N (ε-phase) appear on the surface of the nitrided titanium alloy, whereas on the surface of the non-nitrided titanium alloy only α-Ti and β-Ti peaks are present (Fig. 1).

In a hydrogen-free glow discharge, the diffusion coefficient of nitrogen may increase by a factor of 2–4 compared to hydrogen-containing environments. This is associated with the higher energetic potential of N^+ ions, a greater number of direct impact processes, and an increased rate of vacancy generation in the near-surface zone of the metal. Studies on steels and titanium alloys (8; 22) recorded a sharp increase in microhardness and in the thickness of nitride layers specifically under hydrogen-free conditions, which fully corresponds to the predictions of Pastukh's model regarding the role of ion bombardment.

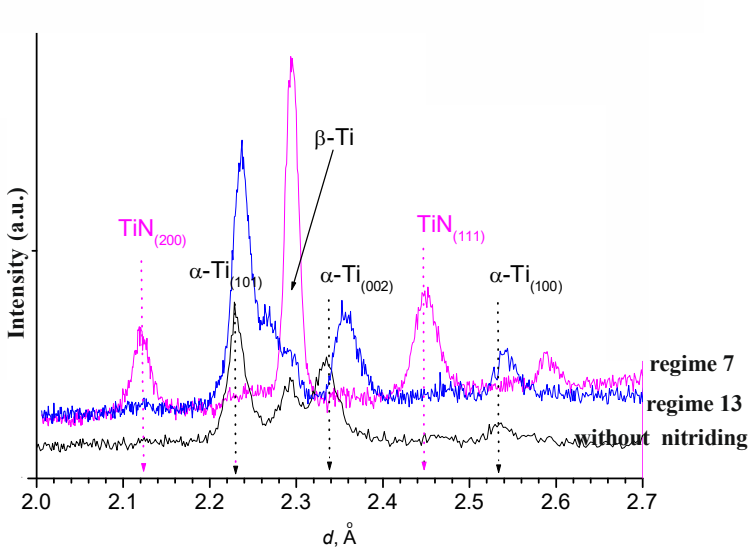

Fig.1. Radiographs for the VT8 titanium alloy: without nitriding, under the №7 regime (epy surface temperature of 660°C and pressure of 160 Pa, nitriding duration of 75 minutes) and the № 13 regime (the surface temperature of 620°C, pressure of 240 Pa, the duration of the nitriding for 20 minutes).

Based on the conducted research [15], the following regularities of nitride phase formation in hydrogen-free discharge can be distinguished: in steels, ε-($Fe_{2–3}N$) and γ'-(Fe_4N) phases with high hardness of 900–1200 HV are formed; in titanium alloys, a gradient layer TiN → Ti_2N → α-Ti(N) is formed [9]. Particularly important is the fact that under hydrogen-free conditions the Ti_2N phase becomes stabilized, which is an indicator of an optimal energetic regime, as experimentally confirmed in works [8,13].

After glow-discharge nitriding, the nitride layers on the surface of structural steels consist of an outer ε-phase ($Fe_{2–3}N$) — hard and wear-resistant; an inner γ'-phase (Fe_4N) — more ductile; and a diffusion zone with a nitrogen–graphite-type distribution. On the surface of titanium alloys, TiN (golden color), Ti_2N (light yellow), and a solid-solution zone of N in α-Ti are formed. These layers are characterized by high adhesion and thermal stability. At the same time, glow-discharge carbonitriding allows the formation of ε-($Fe_{2–3}N_{1–x}C_x$), γ'-($Fe_4N_{1–x}C_x$) phases, and complex carbonitride structures on steels. Such layers exhibit higher hardness and improved performance in highly aggressive environments.

Carbonitriding occurs in mixtures of the N_2–C_xH_y or N_2–CO–CO_2 type, where sources of carbon are fragmented molecules of CH_4, C_2H_2, CO, and CO_2 in metastable states. The kinetics of carbonitriding involves simultaneous saturation of the surface with nitrogen and carbon, followed by the formation of carbonitrides Fe(C,N) as well as a carbon-enriched ε-phase. Studies [15,22] show that under glow-discharge conditions it is possible to form a three-phase gradient layer in which the outer zone contains a carbon–nitrogen enriched layer with increased hardness up to 900–1300 HV.

The formation process of carbonitrides in a glow discharge consists of the following stages: primary cleaning and activation of the surface, bombardment by N^+, C^+, and N_2^+ ions, which leads to the destruction of the oxide film, the appearance of voids and vacancies, and the activation of chemisorption of C and N. The publication [22] demonstrated that ion bombardment at the initial stages creates defect subsurface zones that sharply increase the diffusion rate of carbon and nitrogen into steel. Unlike conventional gas carbonitriding, in a glow discharge this process occurs predominantly due to the ion flux rather than molecular diffusion. According to the model by Pastukh I.M., the total flux of active particles in hydrogen-free environments provides conditions under which the chemical activity of the elements exceeds the activation energy of nitride and carbonitride formation. The ε-phase $Fe_{2–3}$(N,C) forms first under high surface saturation, followed by the γ'-phase Fe_4(N,C), carbonitride inclusions in α-Fe, and nanocrystalline mixed-composition zones. It has been established that the presence of carbon stabilizes the ε-phase, increases its thickness, and prevents local failures under dynamic loading.

According to research data [15], the structure of the strengthened layer includes an outer saturated ε-zone, where C and N occupy mixed lattice positions; an intermediate γ'-layer with increased hardness and a quasi-monolithic structure; and a diffusion subzone with a gradual decrease in C and N concentrations. This combination ensures the absence of sharp hardness transitions, high adhesion of the layer to the substrate, low tendency to delamination, and enhanced resistance to corrosion–mechanical wear.

It has been established that hydrogen-free carbonitriding significantly reduces the coefficient of friction (down to 0.11) at a sliding speed of 0.5 m/s and a contact pressure of 12 MPa. Increasing pressure leads to plastic flow and an increase in the actual contact area on the one hand, and to deformation strengthening of the metal on the other. Although the rate of electrochemical corrosion increases in the presence of plastic deformation of surface layers, it still lags behind the rate of mechanical damage — the higher the contact pressure, the greater this difference becomes (Table 1) [17].

Table 1

Dependence of the corrosion component of damage during corrosion–mechanical wear of 40X steel in an alkaline environment (v = 0.05 m/s)

Pressure, MPa	Corrosion current, A/m^2	Corrosion rate, g/(m^2·год)	Total mass loss, g/(m^2·год)	Corrosion loss rate, %
1	0.183	0.190	0.223	85
2	0.296	0.308	0.376	82
4	0.456	0.474	0.640	74
8	2.493/0.550	2.593/0.573	5.403/0.924	48/62
12	2.718/0.970	3.027/1.010	10.095/2.062	30/49

Note: Numerator – improvement, denominator – nitriding (793 K, 75% N2 + 25% Ar, 265 Pa + 10% propane).

Studies [15, 17] have shown that carbonitrided layers exhibit significantly increased wear resistance and resistance to corrosion–mechanical degradation. It has been established that under abrasive–corrosive and cavitation wear conditions, carbonitride layers demonstrate stability unattainable for purely nitride surfaces. This is due to the fact that the presence of carbon reduces internal stresses in the ε-phase, improves the plasticity of the layer, and promotes the formation of Fe(C,N) phases that are more resistant to micro-fracture [23–25].

Conclusions

1. The data obtained and summarized in this work indicate that the efficiency of hydrogen-free nitriding and carbonitriding in a glow discharge is determined by a complex interaction of plasma, surface, and diffusion processes. The modified layers produced by glow-discharge nitriding and carbonitriding exhibit high corrosion–mechanical wear resistance in all investigated environments. Glow-discharge carbonitriding ensures the formation of a multiphase strengthened layer with superior wear resistance and corrosion–mechanical durability. The combined incorporation of nitrogen and carbon stabilizes the ε-phase, improves the plastic characteristics of the layer, and enhances its long-term wear resistance in corrosion-active environments.

2. The experimental regularities are fully consistent with the energy model proposed by Pastukh I.M., which explains the kinetics of metal saturation with nitrogen and carbon through the balance of active particle fluxes and the energetic stability of the resulting phases, thus confirming the adequacy of the theoretical description of the processes.

3. Glow-discharge carbonitriding is an optimal strengthening method for structural steels operating under conditions of cavitation, fretting, abrasive wear, and corrosion-induced degradation.

4. Glow discharge is one of the most effective methods for producing wear-resistant, corrosion-resistant, and stable surface layers on steels and titanium alloys.

References

1. Kamiński, J., Sitek, R., Adamczyk-Cieślak, B., & Kulikowski, K. (2024). *Impact of glow-discharge nitriding technology on the properties of 3D-printed Grade 2 titanium alloy*. Materials, 17(18), 4592. https://doi.org/10.3390/ma17184592

2. Bolotov M.G., Bolotov G.P., Rudenko M.M. The Impact of Nitriding Parameters on Evolution of Properties of Stainless-Steel Surface Plasma-Nitrided in Glow Discharge. Progress in Physics of Metals, 25(1), 74–113 (2024). https://doi.org/10.15407/ufm.25.01.074

3. Sitek, R., Kamiński, J., Kulikowski, K., & Adamczyk-Cieślak, B. (2022). *Effect of plasma nitriding on the structure and properties of titanium Grade 2 produced by DMLS*. Surface & Coatings Technology, 433, 128119. https://doi.org/10.1007/s13632-022-00903-5

4. Yang, S., Kitchen, M., Luo, Q., Ievlev, D., & Cooke, K. (2016). Effect of Nitriding Time on the Structural Evolution and Properties of Austenitic Stainless Steel Nitrided Using High Power Pulsed DC Glow

Discharge Ar/N2 Plasma. *Journal of Coating Science and Technology*, *3*(2), 62–74. https://doi.org/10.6000/2369-3355.2016.03.02.3

5. Frączek, T., Prusak, R., Ogórek, M., & Skuza, Z. (2022). Nitriding of 316L Steel in a Glow Discharge Plasma. *Materials*, *15*(9), 3081. https://doi.org/10.3390/ma15093081

6. Mozetič, M. Low-pressure non-equilibrium plasma technologies: scientific background and technological challenges. *Rev. Mod. Plasma Phys.* **9**, 25 (2025). https://doi.org/10.1007/s41614-025-00201-x

7. Liu, M., Tan, Z., Xu, S., Zhao, Y., Wang, H., Zhang, S., Ma, R., Jiang, T., Ma, Z., Zhong, N., & Li, W. (2025). Correction: Liu et al. Synthesis and Characterization of Silane-Coupled Sodium Silicate Composite Coatings for Enhanced Anticorrosive Performance. *Coatings* 2025, *15*, 428. *Coatings*, *15*(5), 515. https://doi.org/10.3390/coatings15050515

8. Mashovets N.S., Pastukh I.M., Voloshko S.M. (2017) *Aspects of the practical application of titanium alloys after low temperature nitriding glow discharge in hydrogen- free -gas media*. Applied Surface Science (392). 356–361 https://doi.org/10.1016/j.apsusc.2016.08.180

9. Mashovets N. S. (2019) *Analysis of the influence of nitriding in a glow discharge on the properties of a titanium alloy*. Problems of Tribologyy. 24 (3/93), 39–44. https://doi.org/10.31891/2079-1372-2019-93-3-39-44

10. Pastukh, I.M. Energy model of glow discharge nitriding. *Tech. Phys.* **61**, 76–83 (2016). https://doi.org/10.1134/S1063784216010151

11. Stechyshyna, N.M., Stechyshyn, M.S., Oleksandrenko, V.P. *et al.* Influence of the Power Parameters of Hydrogen-Free Nitriding in Glow Discharge on the Physicochemical Properties of 40Kh Steel. *Mater Sci* **57**, 484–491 (2022). https://doi.org/10.1007/s11003-022-00569-y

12. Sokolova, H.M., Pastukh, I.M. Energy Aspects of the Modeling of Nitriding in Glow Discharge. Mater Sci 53, 368–373 (2017). https://doi.org/10.1007/s11003-017-0084-9

13. Stechyshyn, M. S., Dykha, O. V., Skyba, M. Ye., Zdorenko, D. V., & Liukhovets, V. V. (2025). *Theoretical foundations of glow discharge nitriding of internal local recesses on metallic surfaces*. Problems of Tribology, 30(3/117), 6–12. https://doi.org/10.31891/2079-1372-2025-117-3-6-12

14. Skyba M., Stechyshyn M., Lukianiuk M., Kurskoi V., Mashovets N., Lyukhovets' V. (2021) Physico-chemical properties and wear resistance of nitrided steel 38KhMUA. Scientific Journal of TNTU (Tern.), vol 103, no 3, pp. 63–69. https://doi.org/10.33108/visnyk_tntu2021.03.063

15. Stechyshyn, M.S., Stechyshyna, N.M., Mashovets, N.S. et al. Corrosion-mechanical wear of carbonitrided steel in an alkaline environment. Mater Sci 60, 536–542 (2025). https://doi.org/10.1007/s11003-025-00916-9

16. Boztepe E., Alves A.C., Ariza E., Rocha L.A., Cansever N., Toptan F. A comparative investigation of the corrosion and tribocorrosion behaviour of nitrocarburized, gas nitrided, fluidized-bed nitrided, and plasma nitrided plastic mould steel. *Surface & Coatings Technology*, 2018, 334**:** 116-123. https://doi.org/10.1016/j.surfcoat.2017.11.033

17. M.S. Stechyshyn, M.Ye. Skyba, N.S. Mashovets', V.S. Kurskoy, and M.I. Tsepenyuk, The Effect of Pre-Hydrogenation on Thermodiffusion Chromizing and Cavitation Resistance of Carbon Steels and Gray Cast Iron, *Metallofiz. Noveishie Tekhnol.*, 46, No. 12: 1173–1183 (2024) (in Ukrainian). https://doi.org/10.15407/mfint.46.12.1173

18. Jiang, M., Li, Y., & Zhang, H. (2025). Corrosion Resistance and Plasma Surface Treatment on Titanium and Titanium Alloys: A Review. *Coatings*, *15*(10), 1180. https://doi.org/10.3390/coatings15101180

19. Klimenko, I. O., Marinin, V. G., Ovcharenko, V. D., Kovalenko, V. I., Kuprin, A. S., Reshetnyak, O. M., Belous, V. A., Rostova, H. Y. (2022). Resistance of titanium alloys to cavitation wear. *Voprosy Atomnoj Nauki I Tekhnik*i, no.1-137, p. 130–135. https://doi.org/10.46813/2022-137-130

20. Stechyshyn, M. S., Skyba, M. E., Stechyshyna, N. M., Martynyuk, A. V., & Mardarevych, R. S. (2020). *Physicochemical properties of the surface layers of 40Kh steel after hydrogen-free nitriding in glow discharge.* Materials Science, 55(6), 892–898. https://doi.org/10.1007/s11003-020-00384-3

21. Stechyshyn, M. S., Skyba, M. E., Sukhenko, Yu. G., & Tsepeniuk, M. I. (2019). *Fatigue strength of nitrided steels in corrosion-active media of the food enterprises.* Materials Science, 55(1), 136–141. https://doi.org/10.1007/s11003-019-00261-8

22. Stechyshyn, M.S., Skyba, M.Y., Stechyshyna, N.M., Mashovets N. S; *al.* Wear Resistance of Glow-Discharge Nitride 08Kh18N10 Steel. *Mater Sci* (2024). 59 (2) pp. 249-255 https://doi.org/10.1007/s11003-024-00770-1

23. Stechyshyn, M. S., Skyba, M. E., Student, M. M., Oleksandrenko, V. P., & Luk'yanyuk, M. V. (2018). Residual stresses in layers of structural steels nitrided in glow discharge. *Materials Science, 54*(3), 395–399. https://doi.org/10.1007/s11003-018-0197-9

24. Stechyshyn, M. S., Stechyshyna, N. M., Martynyuk, A. V., & Luk'yanyuk, M. M. (2018). Strength and plasticity of the surface layers of metals nitrided in glow discharge. *Materials Science, 54*(5), 55–60. https://doi.org/10.1007/s11003-018-0156-5

25. Stechyshyn, M. S., Martynyuk, A. V., Bilyk, Y. M., Oleksandrenko, V. P., & Stechyshyna, N. M. (2017). Influence of the ionic nitriding of steels in glow discharge on the structure and properties of the coatings. *Materials Science, 53*(3), 343–349. https://doi.org/10.1007/s11003-017-0081-z

М.С. Стечишин, Н.С. Машовець, С.Я. Підгайчук, В.М. Шевчук, А.В. Корінний Підвищення корозійно-механічної зносостійкості металевих сплавів азотуванням в тліючому розряді

Метою роботи є комплексний аналіз процесів безводневого азотування та карбоазотування у тліючому розряді, узагальнення закономірностей формування нітридних і карбонітридних шарів на сталях і титанових сплавах, а також оцінювання їх корозійно-механічної зносостійкості в умовах тертя, фретингу, кавітації та дії агресивних середовищ. Окрема увага приділена застосуванню моделі Пастуха І.М. для інтерпретації кінетики та енергетичних механізмів дифузійних процесів. У статті проведено порівняльний аналіз структурно-фазових перетворень при азотуванні і карбоазотуванні в безводневому тліючому розряді, виконано систематизацію експериментальних даних щодо мікротвердості, електрохімічних характеристик і корозійно-механічної зносостійкості. Методологічною основою теоретичної частини є енергообмінна модель Пастуха І.М., що описує вплив активних частинок плазми на швидкість дифузії та фазоутворення. Показано, що безводневе азотування забезпечує інтенсифіковану дифузії азоту, формування стабільних нітридів TiN, Ti_2N, ε-($Fe_{2–3}N$), γ'-(Fe_4N) та усунення водневої крихкості. Установлено, що карбоазотування створює багатошарові карбонітридні структури з твердістю 900–1300 HV та високою адгезією до основи. Модифіковані шари демонструють 3–6-кратне підвищення зносостійкості, 2,5–4-кратне зменшення кавітаційного руйнування та значне зниження корозійного струму у NaCl та NaOH. Виявлено зміну механізмів руйнування з крихкого та адгезійного на пластично-деформаційний. Показано відповідність експериментальних закономірностей для формування карбоазотованих шарів. Доведено ключову роль іонного бомбардування у формуванні дефектної підзони, що визначає кінетику дифузії та стабільність фаз. Результати можуть бути використані при проектуванні зносостійких елементів машин, медичних імплантів, деталей для кавітаційних вузлів, що працюють у лужних та хлоридних середовищах. Технології безводневого азотування та карбоазотування визначені як високоефективні, економічно доцільні та придатні до промислового застосування.

Ключьові слова: тліючий розряд, безводневе азотування, карбоазотування, нітридні шари, титан, сталь, корозійно-механічне зношування

ISSN 2079-1372 Problems of Tribology, V. 30, No 4/118-2025, 57-61

Problems of Tribology
Website: http://tribology.khnu.km.ua/index.php/ProbTrib
E-mail: tribosenator@gmail.com

DOI: https://doi.org/10.31891/2079-1372-2025-118-4-57-61

Influence of surfacing modes on the properties of high-carbon coatings

V. Shenfeld * 0000-0002-5548-6971, **O. Bodnar** 0009-0002-4400-9173 **O. Shylina** 0009-0082-4123-5822

Vinnytsia National Technical University, Vinnytsia,Ukraine
**E-mail: leravntu@gmail.com*

Received: 30 October 2025: Revised 10 November 2025: Accept: 02 December 2025

Abstract

The paper presents the results of a study of the influence of surfacing modes on the hardness and wear intensity of high-carbon coatings under dry friction. The coatings were deposited by electric-arc surfacing using carbon fibrous materials. A mathematical model is proposed that describes the influence of the selected parameters ($v_н$, U, I) on the hardness of the surfaced layer (*HRC*) and the wear intensity I_3. Using the obtained mathematical models, it is possible to solve current problems of obtaining coatings with a given hardness and wear resistance, which arise during the design of technological processes that use the deposition of coatings. For real technological processes, the problems should be solved by the graph-analytical method or linear programming methods using response surfaces. Analysis of response surfaces showed that increasing the deposition rate increases the hardness of the deposited coating and the intensity of wear under dry friction conditions.

Keywords: Surfacing, hardness, wear resistance, friction, coatings, regression analysis

Introduction and review of publications

At present, a wide range of methods is used under industrial conditions to deposit high-carbon layers with good wear resistance. First and foremost, this refers to laser surfacing [1–3], as well as electron-beam, plasma, and electric-arc surfacing processes [4–10]. The lifetime of the weld pool in the liquid state, the cooling rate and the crystallisation time of the surfaced metal depend on the parameters of the surfacing process. As a result, the structure of the obtained coatings, their hardness and wear intensity will change. Among the main factors that affect these characteristics are the surfacing speed $v_н$, the electrode wire feed rate $v_д$, the arc voltage U and the surfacing current I [11–13].

Aims of the paper

In this connection, an urgent task is to determine the optimal values of the surfacing process parameters that ensure the required hardness of the surfaced layer (*HRC*) and minimal wear intensity I_3 under conditions of dry and abrasive friction.

Results

The wire feed speed in the UD-209M unit is structurally linked to the surfacing speed. Therefore, the following parameters were chosen as variable factors: surfacing speed $v_н$, arc voltage U and surfacing current I.

To solve the stated problem a mathematical model was developed that describes the influence of the selected parameters ($v_н$, U, I) on the hardness of the surfaced layer *(HRC)* and the wear intensity I_3. It is expedient to use a full factorial experimental design and regression analysis.

The methodology of regression analysis is described in detail in a number of works, and therefore only the results of its application are presented here.

The experiments were carried out using the UD-209M unit. Surfacing was performed with NP-30HGSA electrode wire and carbon fabric on flat specimens made of 45 steel. Carbon dioxide was used as the shielding atmosphere, and reverse polarity was applied.

The preliminarily obtained linear model was found to be inadequate. Therefore, it is reasonable to approximate the response functions y_{HRC} and y_{I_3} by a second-order polynomial of the form.

$$y = b_0 + \sum_{1 \le i \le k} b_i x_i + \sum_{1 \le i \le l \le k} b_{il} x_i x_l + \sum_{1 \le i \le k} b_{il} x_i^2 \ , \tag{1}$$

The intervals of variation and factor levels are given in Table 1.

Table 1

Intervals of variation and factor levels influencing the hardness and wear intensity of the high-carbon surfaced layer are shown below

Factors	Variation interval	Factor levels		
		Base 0	Upper +1	Lower -1
x_1 – arc voltage, V	4	28	32	24
x_2 – surfacing speed, m/h	7.5	18.5	26	11
x_3 – current, A	20	100	120	80

Four samples were cut from each surfaced specimen, on which the hardness of the surfaced layer and the wear intensity were measured. The TK-2M hardness tester was used to measure the hardness of the surfaced layer.

A rotatable second-order experimental design matrix for three factors was compiled.

For each macrosection the hardness *HRC* was determined as the average of 10 measurements, and the wear intensity $I_з$ was determined from the mass loss measurements. The columns y_{HRC} and y_{I_3} in Table 2 present the average values of hardness HRC and wear intensity $I_з$, respectively.

Table 2

Central composite second-order design matrix for three factors

Plan structure	Test No.	x_0	x_1	x_2	x_3	x_1x_2	x_1x_3	x_2x_3	x_1^2	x_2^2	x_3^2	y_{HRC}	y_{I_3}, mg/km
Design 2^3	1	+	+	+	+	+	+	+	+	+	+	54	0,06
	2	+	-	+	+	-	-	+	+	+	+	56	0,05
	3	+	+	-	+	-	+	-	+	+	+	46	0,09
	4	+	-	-	+	+	-	-	+	+	+	44	0,08
	5	+	+	+	-	+	-	-	+	+	+	52	0,07
	6	+	-	+	-	-	+	-	+	+	+	48	0,08
	7	+	+	-	-	-	-	+	+	+	+	42	0,1
	8	+	-	-	-	+	+	+	+	+	+	40	0,12
Star points	9	+	+α	0	0	0	0	0	α^2	0	0	45	0,09
	10	+	-α	0	0	0	0	0	α^2	0	0	48	0,08
	11	+	0	+α	0	0	0	0	0	α^2	0	56	0,05
	12	+	0	-α	0	0	0	0	0	α^2	0	40	0,12
	13	+	0	0	+α	0	0	0	0	0	α^2	44	0,08
	14	+	0	0	-α	0	0	0	0	0	α^2	42	0,1
Centre point	15	+	0	0	0	0	0	0	0	0	0	46	0,09
	16	+	0	0	0	0	0	0	0	0	0	44	0,08
	17	+	0	0	0	0	0	0	0	0	0	42	0,1
	18	+	0	0	0	0	0	0	0	0	0	45	0,09
	19	+	0	0	0	0	0	0	0	0	0	44	0,08
	20	+	0	0	0	0	0	0	0	0	0	48	0,07

The coefficients of the regression equations for the functions $y_{HRC} = f(U, v_н, I)$, $y_{I_3} = f(U, v_н, I)$, as well as the dispersions of the regression coefficients, were determined. The calculation results are summarised in Table 3.

Taking into account the significance of the regression coefficients, the equations assume the form:

$$y_{HRC} = 44{,}8 - 4{,}753 \cdot x_2 - 1{,}564 \cdot x_3 - 0{,}75 \cdot x_1 \cdot x_3 - 0{,}25 \cdot x_2 \cdot x_3 - 0{,}256 \cdot x_3^2 . \tag{2}$$

$$y_{I_3} = 0{,}523 + 0{,}203 \cdot x_1 + 0{,}172 \cdot x_3 + 0{,}131 \cdot x_1 \cdot x_3 - 0{,}111 \cdot x_3^2 \tag{3}$$

Table 3

Results of the study according to the experimental design

Regression coefficient	y_{HRC}				y_{I3}			
	Coeff. value	$s^2\{b\}$ $\cdot 10^{-3}$	Δb $\pm$	Significance	Coeff. value	$s^2\{b\}$ $\cdot 10^{-3}$	Δb $\pm$	Significance
b_0	44,8	0,69	2,142	+	0,523	1,35	0,094	+
b_1	0,07	0,3	1,419	-	0,203	0,59	0,063	+
b_2	4,753	0,3	1,419	+	0,062	0,59	0,063	-
b_3	1,564	0,3	1,419	+	0,172	0,59	0,063	+
b_{12}	-0,25	0,52	1,855	-	0,041	1,01	0,082	-
b_{13}	-0,75	0,52	1,855	+	0,131	1,01	0,082	+
b_{23}	0,25	0,52	1,855	+	0,0013	1,01	0,082	-
b_{11}	0,983	0,29	1,383	-	0,032	0,56	0,061	-
b_{22}	1,514	0,29	1,383	-	0,0024	0,56	0,061	-
b_{33}	-0,26	0,29	1,383	+	-0,111	0,56	0,061	+

The adequacy of the obtained models was checked using the Fisher criterion. At the 5% significance level the tabulated value of the criterion is $F_T = 4,7$. The calculated values were $F_{HRC} = 0,3$ and $F_{i3} = 0,8$. Since the calculated values are lower than the tabulated one, the models can be considered adequate.

Using the obtained models (regression equations), and fixing one of the surfacing process parameters, response surfaces can be obtained that clearly show the influence of the other parameters on the hardness of the surfaced layer and the wear intensity under dry friction.

By using the obtained mathematical models (equations (2) and (3)), a number of problems arising in the design of technological processes involving surfacing of coatings can be solved. Among them, the most common are problems related to obtaining coatings with specified hardness and wear resistance.

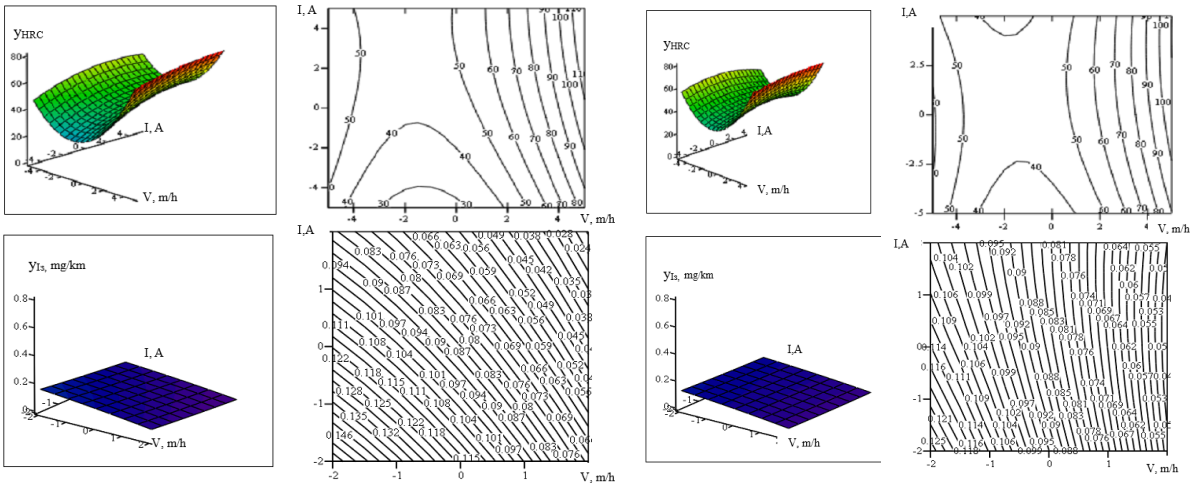

a **b**

Fig. 1. Response surfaces of the functions y_{HRC} and y_{I3} at: a – U_{min}; b – U_{max}

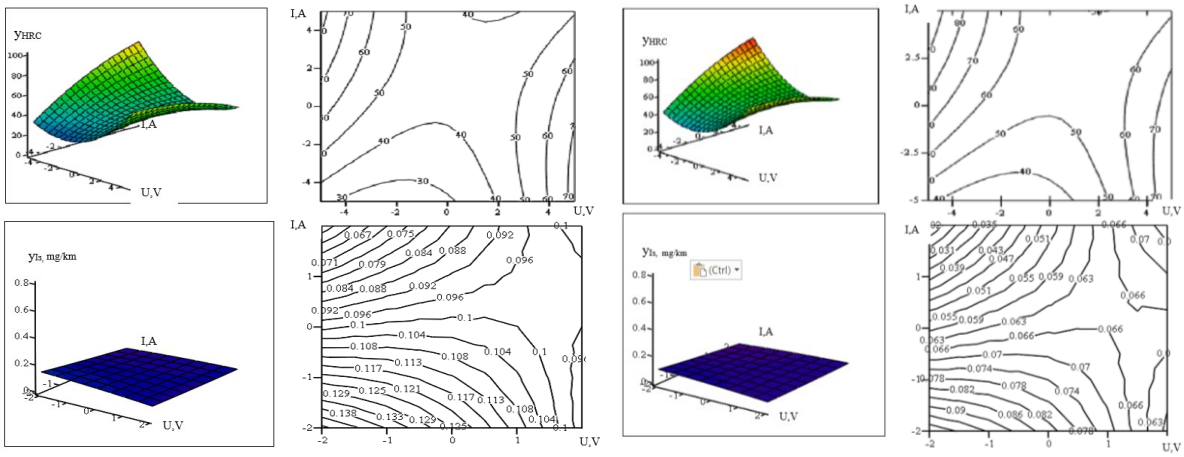

a **b**

Fig. 2. Response surfaces of the functions y_{HRC} and y_{I3} at: a – V_{min}; b – V_{max}

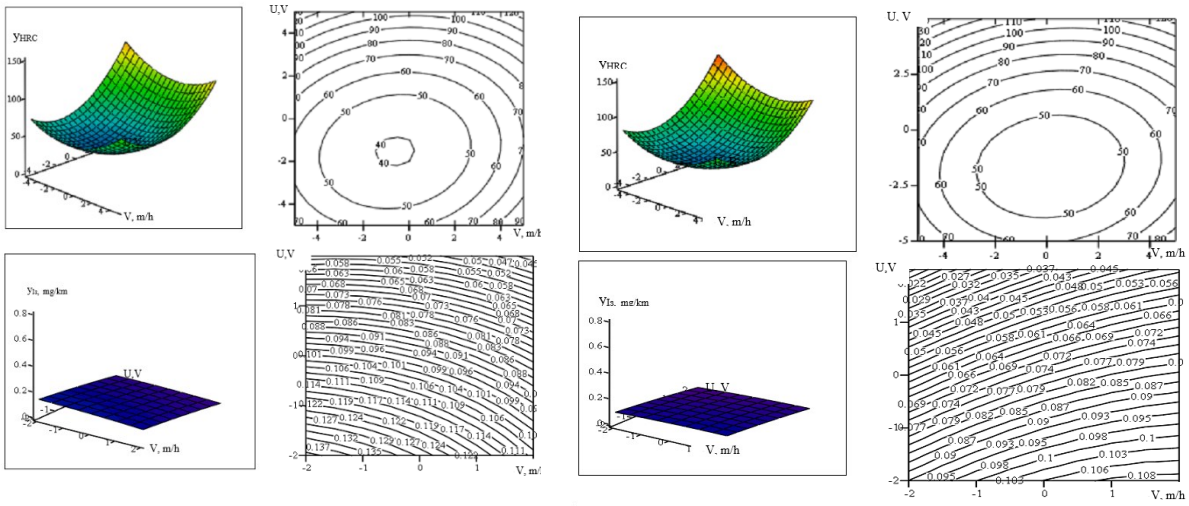

Fig. 3. Response surfaces of the functions y_{HRC} and y_{I3} at: a – I_{min}; b – I_{max}

Figures 1–3 show the response surfaces that illustrate the influence of arc voltage, surfacing speed and current on the hardness of the surfaced layer and on the wear intensity**.**

Conclusions

The influence of the voltage on the welding arc and the deposition rate on the hardness of the deposited coating is nonlinear, and on the wear intensity - linear. Response surfaces (Fig. 1-2) show the presence of extrema, the smallest and largest values of functions in the area of parameter variation. It is advisable for real technological processes to solve the problems set by the graph-analytical method or linear programming methods using response surfaces.

From the analysis of the response surfaces (Fig. 3) it follows that an increase in the deposition rate increases the hardness of the deposited coating and the wear intensity under dry friction conditions.

The determination of surfacing modes for applying wear-resistant high-carbon coatings under dry friction conditions should reasonably be based on regression equations. This makes it possible to obtain the required hardness and wear resistance in accordance with the requirements imposed on the working surfaces of the part.

References

1. Das D. K. Prior Austenite Grains in Steels laser Surface Alloyed with Carbon // Materials characterization.– 1997. – V. 38, No 3. – P. 135–141. https://doi.org/10.1016/S1044-5803(97)00002-8

2. Abboud J. H. Laser surface treatments of iron-based substrates for automotive application / J. H. Abboud, K. Y. Benyounis, A. G. Olabi, M. S. J. Hashmi // Journal of Materials Processing Technology. – 2007. – V. 182, No 1. – P. 427–431. https://doi.org/10.1016/J.JMATPROTEC.2006.08.026

3. Khalfallah I. Y. Microstructure and corrosion behavior of austenitic stainless steel treated with laser / I. Y. Khalfallah, M. N. Rahoma, J. H. Abboud, K. Y. Benyounis // Optics&Laser Technology. – 2011. – V. 43. – P. 806–813. https://doi.org/10.1016/j.optlastec.2010.11.006

4. Dariusz Bartkowsksi Microstructure, microhardness and corrosion resistance of Stellite-6 coatings reinforced with WC particles using laser cladding / Dariusz Bartkowski, Andrzej Młynarczak, Adam Piasecki, Bartłomiej Dudziak, Marek Gościański, Aneta Bartkowska // Optics & Laser Technology. – 2015. – V. 68. – P. 191–201. https://doi.org/10.1016/j.optlastec.2014.12.005.

5. Zeyu Hu Effect of WC content on microstructure and properties of high-speed laser cladding Ni-based coating / Zeyu Hu, Yang Li, Bingwen Lu, Na Tan, Lanrong Cai, Qingsong Yong // Optics & Laser Technology. – 2022. – V. 155. – 108449. https://doi.org/10.1016/j.optlastec.2022.108449.

6. Xinxin Guo Microstructure and wear resistance of tungsten carbide particle reinforced titanium alloy coating by WAAM / Xinxin Guo, Ming Ma, Shuaifeng Zhang, Zhengying Wei // Tribology International. – 2024. – V. 194. – 109536. https://doi.org/10.1016/j.triboint.2024.109536.

7. Bataev I. A. Non-vacuum electronbeam boriding of low-carbon steel / I. A. Bataev, A. A. Bataev, M. G. Golkovsky, A.Yu. Teplykh, V. G. Burov, S. V. Veselov // Surface and Coatings Technology. – 2012. – V. 207. – P. 245–253. https://doi.org/10.1016/j.surfcoat.2012.06.081

8. Katsamas A.I. Laser-beam carburizing of low-alloy steels / A.I Katsamas, G.N Haidemenopoulos // Surface and Coatings Technology. – 2001. – V. 139. – P. 183–191. https://doi.org/10.1016/S0257-8972(00)01061-6

9. Niroj Maharjan, Direct laser hardening of AISI 1020 steel under controlled gas atmosphere / Niroj Maharjan, Wei Zhou, Naien Wu // Surface and Coatings Technology. – 2020. – V. 385. 125399. https://doi.org/10.1016/j.surfcoat.2020.125399.

10. Eroglu M. Tungsten-inert gas surface alloying of a low carbon steel / M. Eroglu, N. Ozdemir // Surface and Coatings Technology. – 2002. – № 154. – P. 209–217. https://doi.org/10.1016/S0257-8972(01)01712-1

11. Savuliak V. I. Vplyv mikrostruktury vysokovuhletsevykh shariv, otrymanykh metodom elektroduhovoho naplavlennia z vykorystanniam vuhletsevykh voloknystykh materialiv, na parametry znosostiikosti v umovakh sukhoho tertia kovzannia / V. I. Savuliak, V. Y Shenfeld, S. O. Panasiuk //Naukovi notatky. / vypusk 49, chastyna 1 – Lutsk, 2015 – S.139–143. https://ir.lib.vntu.edu.ua/bitstream/handle/123456789/7059/%d0%92%d0%bf%d0%bb%d0%b8%d0%b2%20%d0%bc%d1%96%d0%ba%d1%80%d0%be%d1%81%d1%82%d1%80%d1%83%d0%ba%d1%82%d1%83%d1%80%d0%b8.pdf?sequence=1&isAllowed=y

12. Savulyak V. I. Obtaining high-carbon coatings from martensite-austenitic structure for work under conditions of sliding friction without lubricants / V. I. Savulyak, V. Y. Shenfeld, S. O. Panasyuk // TEHNOMUS «New Technologies and Products in Machines Manufacturing Technologies» journal / Romania, 2015 – s462–468. https://ir.lib.vntu.edu.ua/bitstream/handle/123456789/18450/82.pdf?sequence=1&isAllowed=y

13. Savuliak V. I. Vplyv shvydkosti naplavlennia na znosostiikist vysokovuhletsevykh shariv, nanesenykh metodom elektroduhovoho naplavlennia z vykorystanniam vuhletsevykh voloknystykh materialiv / V. I. Savuliak, V. Y Shenfeld, O. B. Yanchenko // «Naukovi notatky» mizhvuzivskyi zbirnyk (za haluziamy znan «mashynobuduvannia ta metaloobrobka», «inzhenerna mekhanika», «metalurhiia ta materialoznavstvo») / vypusk 41 chastyna 1 – Lutsk, 2013 – S.224–229. https://ir.lib.vntu.edu.ua/bitstream/handle/123456789/7058/%d0%92%d0%bf%d0%bb%d0%b8%d0%b2%20%d1%88%d0%b2%d0%b8%d0%b4%d0%ba%d0%be%d1%81%d1%82%d1%96.pdf?sequence=1&isAllowed=y

Шенфельд В.Й., Боднар О.І., Шиліна О.П. Вплив режимів наплавлювання на властивості високовуглецевих покриттів

У статті подано результати дослідження впливу режимів наплавлення на твердість та інтенсивність зношування високовуглецевих покриттів в умовах сухого тертя, нанесених методом електродугового наплавлення з використанням вуглецевих волокнистих матеріалів. Показані математичні моделі, які описують вплив визначених параметрів ($v_н$, *U, I*) на твердість наплавленого шару *(HRC)* та інтенсивність зношування $I_З$. За допомогою отриманих математичних моделей можна розв'язувати актуальні задачі отримання покриттів із заданою твердістю та зносостійкістю, які виникають під час проектування технологічних процесів, що використовують наплавлення покриттів. Для реальних технологічних процесів поставлені задачі потрібно розв'язувати графо-аналітичним методом або методами лінійного програмування з використанням поверхонь відгуків. Аналіз поверхонь відгуків показав, що збільшення швидкості наплавлення збільшує твердість наплавленого покриття та інтенсивність зношування в умовах сухого тертя.

Ключові слова: наплавлення, твердість, зносостійкість, тертя, покриття, регресійний аналіз

ISSN 2079-1372 ***Problems of Tribology****, V. 30, No 4/118-2025, 62-71*

Problems of Tribology
Website: http://tribology.khnu.km.ua/index.php/ProbTrib
E-mail: tribosenator@gmail.com

DOI: https://doi.org/10.31891/2079-1372-2025-118-4-62-71

Analytical study of an improved mathematical model of the hydraulic drive of the garbage truck's sealing plate mechanism, taking into account the wear of its hydraulic cylinder

O.V. Bereziuk [1] 0000-0002-2747-2978, **V.I. Savulyak** [1] 0000-0002-4278-5155, **V.O. Kharzhevskyi** [2] 0000-0003-4816-2781, **S. Cv. Ivanov** [3] 0000-0002-7719-6086, **A.Ye. Alekseiev** [1] 0009-0009-0485-9414

[1] *Vinnytsia National Technical University, Ukraine*
[2] *Khmelnytskyi National University, Ukraine*
[3] *Technical University Sofia, Branch Plovdiv, Bulgaria*
E-mail: berezyukoleg@i.ua

Received: 10 November 2025: Revised 30 November 2025: Accept:10 December 2025

Abstract

The article is dedicated to the analytical study of the improved mathematical model of the hydraulic drive of the garbage truck's sealing plate mechanism, in which the influence of the wear of the hydraulic cylinder on its operation is additionally taken into account. On the basis of the numerical studies of the improved nonlinear mathematical model of the hydraulic drive of the garbage truck's sealing plate mechanism, which takes into account the wear of the hydraulic cylinder, its linearized modification was created, presented in the form of a system of ordinary linear differential equations of the second order. To perform design calculations of new modifications of garbage trucks, approximate analytical expressions were obtained that describe the change in time of the pressure in the hydraulic cylinder's pressure line, as well as the speed and movement of the sealing plate based on the proposed linearized mathematical model of the hydraulic drive of the garbage truck's sealing plate mechanism, taking into account the wear of the hydraulic cylinder. The obtained regression equation that provides the possibility of an approximate determination of the duration of the process of compacting municipal solid waste in a garbage truck, taking into account the wear of the hydraulic cylinder. This equation can be used during the design process of new garbage truck, allowing to take into account the change in the technical condition of the actuators without the need to analyze the full nonlinear mathematical model of the drive of the working bodies. In addition, it is suitable for the usage in the optimization procedures of the main parameters of the hydraulic drive. It was found that the creation of an improved methodology for design calculations of new garbage truck constructions, taking into account the wear of the actuators, requires additional scientific research and further development of the corresponding theoretical methodology.

Keywords: linearized mathematical model, consideration of wear, Laplace transformation, hydraulic drive, wear, hydraulic cylinder, sealing plate mechanism, garbage truck, municipal solid waste.

Introduction

One of the important directions of development of modern municipal engineering in Ukraine is to increase the efficiency and modernization of mobile equipment of garbage trucks, which determines the topicality of relevant scientific and engineering research [1]. In this area, it is so important to ensure high wear resistance, reliability and long service life of machine elements, because those parameters determine the efficiency of equipment operation. Increasing these characteristics helps to reduce maintenance and repair costs, reduce the number of equipment downtimes, and also extend its overall service life under conditions of significant and frequently repeated loads that are typical for intensive operation of municipal vehicles [2, 3]. In Ukraine, most of the work involved in collecting and transporting municipal solid waste (MSW) to landfills or processing plants is carried out using garbage trucks. An important element of such vehicles is the sealing plate mechanism, which is operated by a hydraulic drive [4, 5]. Today, Ukraine has about 3,700 garbage trucks in operation, which perform

not only the function of transporting MSW, but also carry out their preliminary compaction. The use of such equipment makes it possible to significantly reduce the costs associated with MSW transportation, as well as reduce the required area of landfills for their disposal. This provides a significant economic effect and helps reduce the negative anthropogenic impact on the environment. During the compaction of MSW in a garbage truck, the highest loads are observed in the friction units, in particular in the hydraulic cylinder. Intensive wear of these elements is caused by several factors: significant weight of MSW in the body, the need for mechanisms to operate in reverse mode with repeated reciprocating movements, as well as high repetition of operating cycles during a single trip. An additional factor complicating operation is the influence of variable environmental conditions, in particular significant fluctuations in relative humidity and temperature, as well as a high level of their contamination. The combination of these factors causes accelerated wear of working surfaces, which negatively affects the reliability and durability of garbage trucks. Deterioration of the operational properties of the materials of parts or insufficient lubrication leads to an increase in friction forces in friction pairs. As a result, system vibrations increase, which negatively affects its dynamic stability and reduces the mechanism's ability to withstand high loads during operation in reverse mode. Accelerated wear of friction units reduces the efficiency of the garbage truck and increases potential risks to the safety of its operation. This can cause emergency operating modes that threaten the health of operators and at the same time negatively affect the environment in the event of uncontrolled spillage or leakage of solid waste. According to the provisions of the Resolution of the Cabinet of Ministers of Ukraine No. 265 [6], one of the priority areas for the development of municipal services is the introduction of modern highly efficient garbage trucks. These machines play a key role in the system of technical means intended for collection, transportation and primary processing of solid waste. The introduction of modern models of garbage trucks allows not only to optimize logistics processes and reduce operating costs, but also contributes to a comprehensive solution to important environmental problems associated with waste management. In addition, the renewal of the fleet of equipment increases the overall reliability and efficiency of municipal services, which is of strategic importance for ensuring the sustainable development of settlements. Planning the renewal, maintenance and repair of garbage trucks is significantly facilitated by using approximate analytical dependencies of the main power and kinematic characteristics of the hydraulic drive of the garbage truck's sealing plate mechanism, taking into account the wear of its hydraulic cylinder.

Analysis of recent research and publications

Vehicles that collect and transport solid waste are equipped with complex systems that perform the loading of waste from stationary collection containers, the reception and pre-compaction of the material, compaction in the body of the garbage truck and, finally, the disposal of the collected waste at a landfill. Of all these operations, the compaction process is the most mechanically demanding. In the article [7], a structural analysis of the compaction sealing plate of a garbage truck is presented. In the first stage, a parametric modeling of the assembly consisting of the sealing plate, the counter-pressure plate, the rear part of the garbage truck and the material to be compacted was carried out. Dynamic modeling of the MSW compaction process in a garbage truck was carried out, and the mechanical stresses for the compaction sealing plate were used into the modeling module of the SOLIDWORKS 2016 CAD/CAE software, with the help of which a finite element analysis was performed. As a result, the equivalent stresses distribution that were calculated using the von Mises criterion, displacements, and relative deformations of the sealing plate of the analyzed garbage truck were obtained.

In the scientific work [8], a detailed structural analysis of the main elements of a garbage truck that are subject to intensive wear during operation was carried out. The work considered the design features of these parts, the conditions of their operation and the factors that most significantly affect the speed and nature of the degradation of friction surfaces. Particular attention was paid to the definition of vulnerable zones that limit the durability of garbage truck mechanisms, as well as the systematization of typical manifestations of wear that occur under the influence of loads, operating modes and external operating conditions. In the study [9], the authors proposed an improved method for technical diagnostics of hydraulic cylinder malfunctions associated with wear of sealing elements and the appearance of internal leaks of the working fluid. The method is based on the analysis and integration of the energy characteristics of the hydraulic drive, which allows to increase the sensitivity of detecting defects at the early stages of their development. The usage of an approach based on the merging of energy parameters provides a more comprehensive assessment of the technical condition of the hydraulic cylinder, enables the detection of hidden signs of deviations in the system's operation, and increases the accuracy of predicting its remaining service life.

The study [10] comprehensively analyzes the kinematics and dynamics of the scraping mechanism for compacting MSW in a garbage truck using numerical methods. To study the operation of the mechanism under actual working conditions during a full cycle lasting 18 seconds, a multi-body structure integrated with a hydraulic simulation model was created. The model was verified by calculation at stationary moments in time, which showed high consistency. The results show that the pressing mechanism operates in steady-state modes almost all the time, with cylinder speeds ranging from 0.08 to 0.15 m/sec. The speed and acceleration of the hydraulic cylinder fluctuate greatly when the mechanism accelerates or decelerates, but the effect of inertia is negligible. The forces applied to the joints are maximum at the end of the pressing process. It is notable that the force applied to the connection between the scraper plate and the sliding plate is the highest: three times higher than that applied to the

connection between the sliding plate and the press cylinder, and one and a half times higher than that applied to the connection between the scraper plate and the scraper cylinder. The results of the study can be applied to the design process of garbage trucks in specialized vehicles, or used as a basis for improving productivity and optimizing the weight, strength, and materials of the mechanism.

The study [5] provides a detailed analysis of hydrodynamic processes occurring during the flow of working fluid through a water seal using computer modeling methods. By means of numerical experiments, the authors were able to establish the nature of hydraulic losses in local narrowings and channels of the water seal, as well as quantitatively estimate the level of pressure loss resulting from these processes. The results obtained made it possible to comprehensively characterize the interaction of fluid flows with the structural elements of the internal cavities of the water seal and to identify the most critical areas where an intense pressure drop occurs. Based on the analysis, a number of design improvements to the hydraulic lock were proposed, aimed to optimize the shape of its channels and improve fluid flow conditions. The proposed changes do not affect the functional purpose of this element, but ensure a more uniform distribution of velocities in the flow and a reduction in local turbulent zones. The implementation of such design solutions makes it possible to reduce pressure losses in the working part of the hydraulic distributor, which is an important factor in increasing the energy efficiency of the hydraulic drive. As a result, the overall energy losses in the system are reduced, which has a positive effect on its performance, stability, and durability.

Scientific publication [11] provides an in-depth study of the specifics of the wood chip pressing process in screw presses. The authors analyzed the sequence of physical and mechanical phenomena occurring in different functional areas of the screw during the movement and compaction of raw materials. Particular attention is paid to describing the behavior of wood chips under conditions of variable pressure and intense friction that arise in the areas of feeding, transportation, compaction, and briquette formation. The dependencies that were obtained in the study made it possible to establish methods for engineering calculations of the loads acting on the screw turns and to determine the dependencies that define the optimal design parameters of the screw press. In addition, based on theoretical analysis and experimental observations, the required drive power was determined to ensure a stable pressing process under various operating modes. The thermal processes accompanying the compaction of wood chips were studied separately. The dependencies of change in the temperature of raw materials along the length of the screw were established and the factors influencing the intensity of its heating were determined. The specific energy costs required for the formation of the pressed product were also calculated, which allows to increase the energy efficiency of the technological process and ensure a rational choice of operating modes for the pressing equipment.

The scientific article [12] establishes that the wear rate of the working hydraulic cylinder of the garbage truck's compactor sealing plate mechanism is exponentially dependent on the pressing force. Taking this dependency into account allows for the optimization of maintenance and repair planning, which, in turn, increases the overall efficiency of garbage truck operation. To illustrate this process, a graph was constructed showing the change in the wear rate of the hydraulic cylinder as a function of the pressing force, which confirmed the good correlation between the obtained model and the experimental data. In particular, for the serial Ukrainian garbage truck model KO-436, the wear rate of the working hydraulic cylinder according to this dependency is 0.257 μm/h. At the same time, increasing the pressing force from 30 MN to 150 MN reduces the wear rate of the hydraulic press cylinder by 3.6 times. This effect is explained by the specifics of contact processes between working surfaces and the peculiarities of the mechanism's operation at different load levels.

The analysis of the causes of typical technical failures of garbage truck units, presented in [13], shows that a significant percentage of malfunctions (about 45%) are happened due to hydraulic drive failures. The main factors contributing to these failures are manufacturing defects associated with the usage of low-quality components, as well as significant fluctuations in the loads on the working parts. A study of the causes of working body failures showed that the dominant factors are heat treatment defects and deviations from design parameters during mechanical processing (35%), mistakes in the assembly process, adjustment, and tightening of threaded connections (30%), and poor-quality welding (30%). It has been established that the majority of failures (80–90%) occur as a result of wear and corrosion of the working surfaces of parts, with failure occurring after a critical level of degradation has been reached, i.e., when the unit or machine reaches its limit technical condition. In particular, up to 28% of all failures of hydraulic drive elements occur in hydraulic cylinders, which is caused by wear of mating surfaces and deformation of the rod and cylinder during operation. Durability analysis shows that the average service life of hydraulic drive components, in particular hydraulic cylinders, is only about one-third of their maximum service life, i.e., the service life specified by the manufacturer is not achieved by 45-55%. The highest percentage of hydraulic cylinder failures in the early stages of operation or after repair occurs in the rods (31%) and sealing sleeves (42%). In addition, a common form of failure of hydraulic system components is the loss of external and internal tightness caused by contamination of the working fluid, which leads to malfunctioning of the units.

According to the results of research [14], it has been established that among the main elements of side-loading garbage trucks, the hydraulic system has the shortest service life. It is the key factor in the intensive wear and tear of these vehicles and determines their operational reliability. An analysis of the causes of failures, presented in [15], has made it possible to develop a structural overview of the most common malfunctions of hydraulic equipment in garbage trucks. In particular, the largest percentage is accounted for by failures of hydraulic cylinders – 34.92%, caused by wear of seals, gaskets, rods, destruction of the piston mounting nut, bending of the rod, or mechanical damage. Hydraulic pump failures account for 16.40% and are most often associated with body

wear, gear wear, seal damage, or cracks in the body. Next in order of frequency are pipes and hoses – 15.34%, whose failures are caused by breakage and wear. A significant proportion is also accounted for by malfunctions of hydraulic distributors – 13.23%, associated with wear of seals and spools or the formation of cracks in the housing.

A scientific article [16] has established that "conical" wear of the hydraulic cylinder rod within the range of 0.2–0.4 mm along its length before the first major overhaul causes a 7.2% decrease in pressure in the hydraulic system, an increase in specific fuel consumption by 11.4%, and an increase in the carbon monoxide content in exhaust gases by 26%. A further increase in rod wear in the working area to 0.6–0.7 mm leads to a 13.4% drop in pressure, a 21.3% increase in specific fuel consumption, and a sharp increase in the toxicity of exhaust gases—from 25% to 59%, which significantly exceeds the permissible norms. The maximum permissible value of wear of the geometric parameters of the hydraulic cylinder rod of the hydraulic drive of construction and road machines is proposed to be considered to be no more than 0.4 mm. In addition, it has been established that rod wear negatively affects the physical and chemical characteristics of the working fluid: the content of iron and mechanical impurities in it doubles. In turn, it requires more frequent fluid replacement and leads to its overconsumption, which significantly reduces the efficiency and durability of the hydraulic drive, shortening the service life of the machines.

The materials of work [17] point out that the wear of sealing elements in hydraulic systems causes the gradual penetration of working fluid into the non-working cavities of hydraulic machines. Although this process often has no external manifestations, it causes unproductive losses of hydraulic drive power, which, in turn, leads to increased consumption of fuel and lubricants and reduced energy efficiency of the working mechanisms. Power losses associated with seal wear can cause deviations in the operating modes of the hydraulic motor from the optimal ones, which negatively affects the overall performance of the hydraulic drive. The study examines the mechanical system "hydraulic cylinder – sealed piston – compressed hydraulic fluid" and establishes the dependence of the hydraulic cylinder's efficiency on the amount of leakage. Additionally, the process of piston settling during the use of VMGZ working fluid was analyzed and the mechanism of fluid leakage through the hydraulic cylinder seal was investigated.

A scientific article [18] notes that the results of long-term observations of garbage trucks show that the largest percentage of failures is associated with wear and corrosion of the working surfaces of their working equipment parts. In particular, failures of hydraulic cylinders caused by wear of mating surfaces and deformation of the rod and cylinder during operation account for about 32% of the total number of hydraulic drive component failures. Such a high failure rate is explained by uneven loading of the body and intense abrasive wear, which is characteristic of the difficult operating conditions of garbage trucks. An analysis of the causes of failures showed that the key factor in degradation is the wear of the working surfaces of the main parts of the hydraulic drive, in particular the spools and housings of the hydraulic distributors, as well as the rods of the hydraulic cylinders. It has been established that the determining mechanism of wear is hydroabrasive damage, which develops as a result of untimely replacement of the working hydraulic fluid and the use of low-quality or already partially destroyed sealing elements, primarily hydraulic cylinder seals. Dust, mechanical impurities, and wear products enter the sliding zone under such conditions, which significantly accelerates the destruction of working surfaces. The authors propose the usage of chrome plating in a cold self-regulating electrolyte as one of the most effective methods for restoring worn parts. This technology provides the formation of high-quality chrome coatings with increased wear resistance and high process productivity, which makes it a promising alternative to traditional repair methods.

An analytical study of the mathematical model of the process of grinding polymer waste in the grinding chamber of a rotary crusher with continuous classification of the finished product, carried out in the work [19], which provide a detailed understanding of the grinding process based on a comprehensive description of the interaction of particles with the working elements of the crusher. The developed model covers both the dynamics of particle motion in the grinding chamber and the processes of destruction of polymer raw materials under the action of impact, compressive, and shear loads, which makes it possible to accurately predict the parameters of the input material. The authors of the study found that the proposed approach ensures high accuracy in determining the geometric dimensions of the final product particles by taking into account a complex of factors: the angular velocity of the rotor, the initial dimensions of the waste, the geometry and design characteristics of the crusher's working parts, the intensity of raw material feed, and the loading modes of the grinding chamber. In addition, the obtained model made it possible to determine the productivity of the equipment depending on the parameters of the working process, to establish the influence of the classification speed of the finished product on the stability of the crusher, and to estimate the energy costs required to achieve the specified grinding quality. Thanks to the combination of analytical methods and consideration of a wide range of technological parameters, the results of the study can be used to optimize the design of rotary crushers, increase their energy efficiency, and ensure the stability of the particle size distribution of the final product during the processing of polymer waste.

The article [20] presents an algorithm for numerical and analytical research of dynamic processes of a planar six-bar linkage mechanism of a sewing machine's thread puller. The proposed approach involves solving the differential equation of motion of the mechanism using numerical methods, which provides calculation of the kinematic and dynamic characteristics of the system. To verify the accuracy of the obtained results and to visualize the behavior of the mechanism, computer modeling was created in Mathcad software, which made it possible to analyze the trajectories of the links, the velocities and accelerations of the joints, and to identify possible critical points in the mechanism's operation. Such a complex approach ensures both the accuracy of calculations and the

possibility of their usage in the optimization of the thread puller design to increase the reliability and productivity of sewing equipment.

In the work [21], an analytical study of a mathematical model was carried out, which made it possible to identify the main dependencies of operation of vibration and vibration-impact machines that use a hydraulic pulse drive with a single-stage pulsator valve. The study covers the analysis of the dynamic characteristics of such machines, in particular the frequency of oscillations, vibration amplitudes, and the periodicity of pulses generated by the pulsator valve. The results obtained allow to estimate the influence of the drive design parameters on the efficiency of the equipment and can be used to optimize its operating modes in order to increase productivity, reduce energy consumption, and reduce wear on working parts.

The article [22] proposes an improved nonlinear mathematical model of the hydraulic drive of a garbage truck's sealing plate mechanism, which takes into account the effect of wear on its hydraulic cylinder. The usage of this model made it possible to conduct a numerical study of the dynamics of the drive, which allowed evaluating the change in the main characteristics of the system during operation. In particular, it was found that taking into account the wear of the hydraulic cylinder significantly affects such parameters as the speed and force of the plate movement, the working pressure in the pressure line, and the stability of the hydraulic fluid supply. It indicates the critical need to take into account operational wear when designing and optimizing hydraulic drives of garbage trucks to ensure their reliable and efficient operation for the entire service life.

The work [23] studies the dynamics of the hydraulic drive of a MSW pressing plate based on a nonlinear mathematical model described by a system of differential equations with corresponding boundary conditions. This model simulates the operation of the hydraulic drive of the garbage truck's pressing sealing plate mechanism, including for static waste compaction modes. In addition, the study proposes and analytically validates a linearized mathematical model of the plate's hydraulic drive, which provides a simplified analysis of the control processes and dynamic behavior of the system. At the same time, these mathematical models do not take into account the wear of the power hydraulic cylinder, one of the key elements of the hydraulic drive, which carries a significant part of the load during the pressing process. Ignoring this factor may limit the practical value of the model, especially regarding long-term prediction of the efficiency and stability of the mechanism in real operating conditions. Since the wear of the hydraulic cylinder significantly affects the performance and reliability of the system, its elimination may lead to appear the deviations between the calculated and actual performance parameters of the hydraulic drive.

However, during the analysis of known publications, the authors did not find a linearized improved mathematical model of the hydraulic drive of the garbage truck's sealing plate mechanism, taking into account the wear of its hydraulic cylinder and the results of its analytical study.

Aims of the article

Analytical study of a linearized improved mathematical model of the hydraulic drive of the garbage truck's sealing plate mechanism, taking into account the wear of its hydraulic cylinder, to obtain analytical dependencies of the main power and kinematic characteristics of this hydraulic drive in steady-state operation, which can be used during design calculations of new garbage truck designs, taking into account the wear of the working bodies.

Methods

During the analytical study of the linearized improved mathematical model of the hydraulic drive of the garbage truck's sealing plate mechanism, taking into account the wear of its hydraulic cylinder, the following methods were used: operator calculus using Laplace transformation to solve a system of ordinary linear differential equations, linearization of nonlinear dependencies, decomposition of complex expressions into simpler fractions, as well as computer modeling methods.

To plot graphs, the MatModel software was used, which implements the 4th order Runge-Kutta-Felberg numerical method with a variable integration step.

Results

Fig. 1 shows the calculation diagram of a linearized improved mathematical model of the hydraulic drive of the garbage truck's sealing plate mechanism, taking into account the wear of its hydraulic cylinder when using the rear loading scheme for solid waste during static compaction. The diagram shows the following structural elements: PP – pressing plate; HC – hydraulic cylinder; HD – hydraulic distributor; P – hydraulic pump; SV – safety valve; F – filter; T – working fluid tank, as well as the main geometric, kinematic and power parameters: p_1, p_2, p_3, p_4 – pressures at the pump outlet, hydraulic cylinder inlet, hydraulic cylinder outlet, and filter inlet, respectively; W_1, W_2, W_3, W_4 – volumes of pipelines between the pump and hydraulic distributor, hydraulic distributor and hydraulic cylinder inlet, hydraulic cylinder outlet and hydraulic distributor, hydraulic distributor and filter; Q_P – actual pump flow rate; S_P – cross-sectional area of the distributor opening; S_f – surface area of the filter element; k_f – specific filter capacity (not shown in the diagram); μ_d – dynamic viscosity coefficient (not shown in the diagram); D, d – diameters of the piston and rod; G_p – weight of the pressing plate; G_c – weight of the

hydraulic cylinder; G_{W1} – weight of the waste above the pressing plate; G_{W2} – weight of the waste outside the pressing plate; F_{FR} – friction force between the pressing plate and the guides; F_{TW} – the friction force between the MSW and the body; F_C – the force developed by the hydraulic cylinder; h_1, h_2 – the heights of the bottom and top of the press plate; b – the width of the press sealing plate (not shown in the diagram); δ – the thickness of the press plate; α – the angle of inclination of the press plate; x – the displacement of the press plate.

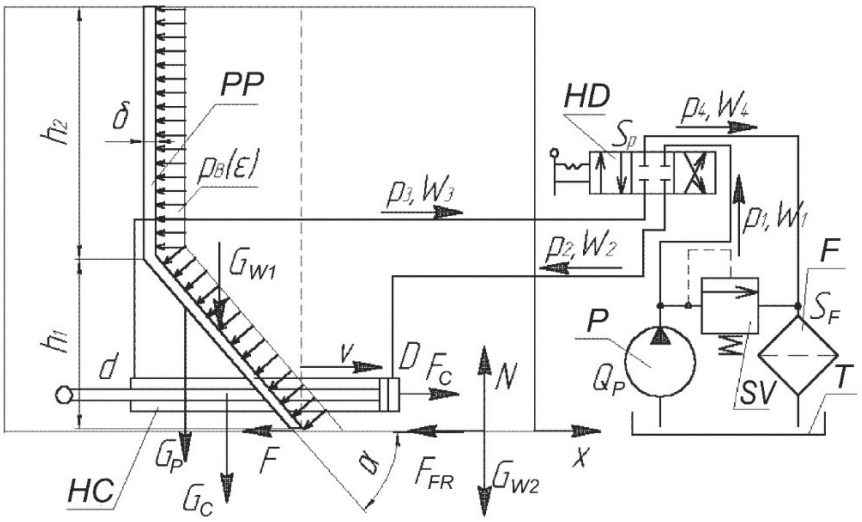

Fig. 1. Calculation scheme of the linearized improved mathematical model of the hydraulic drive of the garbage truck's sealing plate mechanism, taking into account the wear of its hydraulic cylinder

Analysis of the carried studies of the nonlinear mathematical model [22] showed that $p_1 \approx p_2 \approx p_{12}$, and the influence of pressure in the drain lines and viscous friction forces on the operation of the hydraulic drive is insignificant.

The process of MSW compaction in a garbage truck can be described by the following system of linearized differential equations:

$$\begin{cases} Q_P = vS_{C1} + \sigma_0 p_{12} + \alpha_\sigma + \beta_\sigma t + KW_{12}\dfrac{dp_{12}}{dt}; & (1) \\ p_{12}S_{C1} = m_m \dfrac{dv}{dt} + p_{B0}S_{P1}e^{\beta_p t}, & (2) \end{cases}$$

where $W_{12} = W_1 + W_2$; σ_0 – nominal coefficient of working fluid losses for flow from the high pressure region to the low pressure region, $m^5/(N \cdot sec)$; α_σ, β_σ – approximation coefficients of the dependence of working fluid losses on the duration of the hydraulic cylinder wear process ($\alpha_\sigma = -3.573 \cdot 10^{-9}$ m^3/sec; $\beta_\sigma = 1.443 \cdot 10^{-9}$ m^3/sec^2), m_m – reduced mass of moving parts, kg; v – speed of movement of the garbage truck's sealing plate, m/sec; p_{V0} – initial pressure of MSW compaction, Pa; β_p – approximation coefficient of dependence of MSW compaction pressure on the duration of the process ($\beta_p = 0.00217$).

For further study of the linearized mathematical model of the hydraulic drive of the garbage truck's sealing plate mechanism, taking into account the wear of its hydraulic cylinder, we will use the Laplace transformation, according to which we obtain the following:

$$\begin{cases} \dfrac{Q_P}{s} = V(s)S_{C1} + P(s)\sigma_0 + \dfrac{\alpha_\sigma}{s} + \dfrac{\beta_\sigma}{s^2} + P_{12}(s)sKW_{12}; & (3) \\ P_{12}(s)S_{C1} = V(s)sm_m + \dfrac{p_{B0}S_{P1}}{s-\beta_p}. & (4) \end{cases}$$

Substituting equation (3) into equation (4), we obtain the following:

$$P_{12}(s) = \frac{b_2 s^2 + b_1 s + b_0}{s(s-\beta_p)(a_2 s^2 + a_1 s + a_0)}, \quad (5)$$

where $a_2 = KW_{12}m_p$; $a_1 = \sigma_0 m_m$; $a_0 = S_{C1}^2$; $b_1 = p_{B0}S_{P1}S_{C1} - \beta_m m_m (Q_P - \alpha_\sigma) - \beta_\sigma m_m$; $b_0 = \beta_\sigma \beta_m m_m$; $b_2 = (Q_P - \alpha_\sigma)m_m$. (6)

By decomposing expression (5) into simpler fractions after reducing it to canonical form, we obtain:

$$P_{12}(s) = A\frac{1}{s} + B\frac{1}{s-\beta_p} + \frac{C}{a_2}\frac{s + a_1/(2a_2)}{\left[s + a_1/(2a_2)\right]^2 + \left(4a_0a_2 - a_1^2\right)/\left(4a_2^2\right)} + \\ + \frac{2D - Ca_1/a_2}{\sqrt{4a_0a_2 - a_1^2}}\frac{\sqrt{4a_0a_2 - a_1^2}/\left(2a_2\right)}{\left[s + a_1/(2a_2)\right]^2 + \left(4a_0a_2 - a_1^2\right)/\left(4a_2^2\right)}, \tag{7}$$

where $A = -\frac{b_0}{\beta_p a_0}$; $B = \frac{\beta_p^2 b_2 + b_0}{\beta_p\left(\beta_p^2 a_1 + \beta_p a_1 + a_0\right)}$; $C = \frac{a_2}{\beta_p}\left(\frac{b_0}{a_0} - \frac{\beta_p^2 b_2 + b_0}{\beta_p^2 a_1 + \beta_p a_1 + a_0}\right)$;

$$D = -\frac{b_1}{\beta_p} - \frac{b_0\left(a_0 - \beta_p a_1\right)}{\beta_p^2 a_0} + \frac{a_0\left(\beta_p^2 b_2 + b_0\right)}{\beta_p^2\left(\beta_p^2 a_1 + \beta_p a_1 + a_0\right)}. \tag{8}$$

Let's find the original image of (7):

$$p_{12}(t) = A + Be^{\beta_p t} + B_1\cos\left(\omega_0 t\right) + \frac{C}{a_2}e^{-\frac{a_1}{2a_2}t}\cos\left(\frac{\sqrt{4a_0a_2 - a_1^2}}{2a_2}t\right) + \frac{2D - Ca_1/a_2}{\sqrt{4a_0a_2 - a_1^2}}e^{-\frac{a_1}{2a_2}t}\sin\left(\frac{\sqrt{4a_0a_2 - a_1^2}}{2a_2}t\right). \tag{9}$$

Excluding insignificant coefficients of expression (9), which have a higher order of smallness, and taking into account the accepted designations according to (6), (8), the pressure in the pressure cavity of the hydraulic cylinder of the garbage truck's sealing plate mechanism, taking into account its wear, is described by the equation:

$$p_{12}(t) \approx \frac{m_m\left[\left(Q_P - \alpha_\sigma\right)\beta_m e^{\beta_p t} - \beta_\sigma\right]}{S_{C1}^2}. \tag{10}$$

Solving the system of equations (3, 4) with respect to $V(s) = X(s)s$, after reduction to the canonical form we obtain the following:

$$X(s) = \frac{V(s)}{s} = \frac{B\sigma_0 - C_x\beta_m}{S_{C1}\beta_p}\frac{1}{s} + \frac{Q_P - \alpha_\sigma}{S_{C1}}\frac{1}{s^2} - \frac{\beta_\sigma}{2S_{C1}}\frac{1}{s^3} - \frac{B\left(KW_{12} + \sigma_0/\beta_m\right)}{S_{C1}}\frac{1}{s - \beta_m} - \\ - \frac{D_x}{a_2 S_{C1}}\frac{s + a_1/(2a_2)}{\left[s + a_1/(2a_2)\right]^2 + \left(4a_0a_2 - a_1^2\right)/\left(4a_2^2\right)} - \frac{2E_x - D_x a_1/a_2}{S_{C1}\sqrt{4a_0a_2 - a_1^2}}\frac{\sqrt{4a_0a_2 - a_1^2}/\left(2a_2\right)}{\left[s + a_1/(2a_2)\right]^2 + \left(4a_0a_2 - a_1^2\right)/\left(4a_2^2\right)}, \tag{11}$$

where $A_x = -\sigma_0/\beta_m$; $B_x = KW_{12} + \sigma_0/\beta_m$; $C_x = D\sigma_0/a_0$; $D_x = CKW_{12} - a_2 D\sigma_0/a_0$;

$$E_{1p} = C\sigma_0 + DKW_{12} - a_1 D\sigma_0/a_0. \tag{12}$$

Next, we find the original image of (11)

$$x(t) = \frac{B\sigma_0 - C_x\beta_p}{S_{C1}\beta_p} + \frac{Q_H - \alpha_\sigma}{S_{C1}}t - \frac{\beta_\sigma}{2S_{C1}}t^2 - \frac{B\left(KW_{12} + \sigma_0/\beta_m\right)}{S_{C1}}e^{\beta_p t} + \\ - \frac{D_x}{a_2 S_{C1}}e^{-\frac{a_1}{2a_2}t}\cos\left(\frac{\sqrt{4a_0a_2 - a_1^2}}{2a_2}t\right) - \frac{2E_x - D_x a_1/a_2}{S_{C1}\sqrt{4a_0a_2 - a_1^2}}e^{-\frac{a_1}{2a_2}t}\sin\left(\frac{\sqrt{4a_0a_2 - a_1^2}}{2a_2}t\right). \tag{13}$$

Neglecting the insignificant coefficients of equation (13), which have a higher order of smallness, and taking into account the accepted designations according to (6), (8), (12) and the initial conditions $x(0) = 0$, the movement of the garbage truck's sealing plate, taking into account the wear of the hydraulic cylinder, can be described by the equation

$$x(t) \approx \frac{Q_P - \alpha_\sigma}{S_{C1}}t - \frac{\beta_\sigma}{2S_{C1}}t^2 + \frac{m_p\left(Q_P - \alpha_\sigma\right)\left(KW_{12} + \sigma_0\right)}{S_{C1}^3}\left(1 - e^{\beta_p t}\right). \tag{14}$$

After differentiating the equation (14) and taking into account the initial conditions $v(0) = 0$, the speed of movement of the garbage truck's sealing plate, taking into account the wear of the hydraulic cylinder, can be described by the following equation

$$v(t) \approx \frac{m_m \beta_m \left(Q_P - \alpha_\sigma\right)\left(KW_{12} + \sigma_0\right)}{S_{C1}^3}\left(1 - e^{\beta_m t}\right) - \frac{\beta_\sigma}{S_{C1}} t. \tag{15}$$

From equation (10), we can determine the duration of solid waste compaction in a garbage truck, taking into account the wear of the hydraulic cylinder of the sealing plate.

$$t \approx \frac{1}{\beta_m} \ln\left[\frac{p_{12} S_{C1}^2}{m_m \beta_m \left(Q_P - \alpha_\sigma\right)} + \frac{\beta_\sigma}{\beta_m \left(Q_P - \alpha_\sigma\right)}\right]. \tag{16}$$

A comparison of the results that were obtained using nonlinear and linearized mathematical models of the hydraulic drive of the garbage truck's sealing plate mechanism, taking into account the wear of its hydraulic cylinder, as well as using equations obtained as a result of the analytical solution of the linearized model, is shown in Fig. 2.

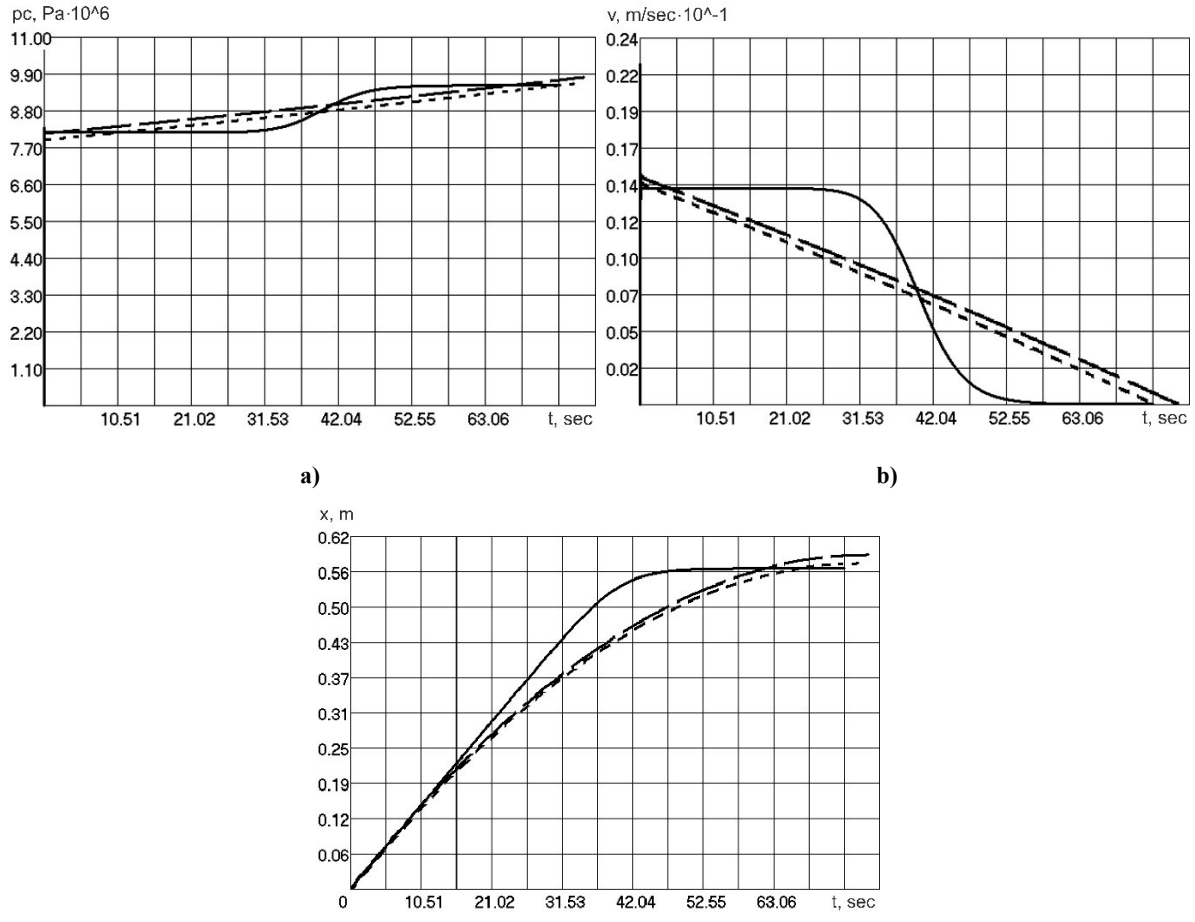

Fig. 2. Comparison of results obtained using nonlinear (——) and linearized (– – –) mathematical models of the hydraulic drive of the garbage truck's sealing plate mechanism taking into account the wear of its hydraulic cylinder, as well as using the equations obtained as a result of its analytical solution (···): a) –change in pressure in the hydraulic cylinder; b) –change in speed; c) –displacement

When comparing the characteristics of MSW compaction in a garbage truck obtained using a nonlinear mathematical model and equations (10), (14), (15), derived from the analytical solution of the linearized mathematical model of the hydraulic drive of the garbage truck's sealing plate mechanism, taking into account the wear of its hydraulic cylinder, the deviation is about 10% compared to the nonlinear mathematical model, which is acceptable for preliminary design calculations. If necessary, the values of the main parameters can be refined at the final stage of design using a nonlinear mathematical model.

The obtained regression equation (16) allows to approximately determine the duration of MSW compaction in a garbage truck, taking into account the wear of the hydraulic cylinder of the sealing plate, which can be used during design calculations of new garbage truck constructions, taking into account the wear of the working bodies without the need to research the nonlinear mathematical model of the drive of its working bodies, as well as during the optimization of the main parameters of the hydraulic drive.

The development of an improved methodology for design calculations of new garbage truck structures, taking into account the wear and tear of operational mechanisms, requires additional scientific research and further development of the relevant theoretical foundations.

Conclusions

To perform design calculations for new modifications of garbage trucks, approximate analytical equations were obtained that describe the change in pressure over time in the pressure line of the hydraulic cylinder, as well as the speed and displacement of the sealing plate based on the proposed linearized mathematical model of the hydraulic drive of the garbage truck's compaction sealing plate mechanism, taking into account the wear of the hydraulic cylinder. The resulting regression equation provides the ability to approximately determine the duration of the solid waste compaction process in a garbage truck, taking into account the wear of the hydraulic cylinder. This equation can be used when designing new garbage truck constructions, allowing for changes in the technical condition of the operational mechanisms without the need to analyze a complete nonlinear mathematical model of the drive of the working bodies. It has been established that the development of an improved methodology for design calculations of new garbage truck constructions, taking into account the wear of the operational mechanisms, requires additional scientific research and further development of the relevant theoretical foundations.

References

1. Holenko K., Dykha O., Koda E., Kernytskyy I., Horbay O., Royko Y., Fornalchyk Y., Berezovetska O., Rys V., Humenuyk R., Berezovetskyi S., Żółtowski M., Baryłka A., Markiewicz A., Wierzbicki T., Bayat H. (2024) Structure and strength optimization of the Bogdan ERCV27 electric garbage truck spatial frame under static loading. Applied Sciences, 14(23), 11012. https://doi.org/10.3390/app142311012

2. Dykha A., Sorokatyi R., Pasichnyk O., Yaroshenko P., Skrypnyk T. (2020, December) Machine wear calculation module in computer-aided design systems. In IOP Conference Series: Materials Science and Engineering, 1001(1), 012040, https://doi.org/10.1088/1757-899X/1001/1/012040

3. Kindrachuk M.V., Kharchenko V.V., Marchuk V.Y., Humeniuk I.A., Leusenko D.V. (2024) Methodology for Selecting Compatible Metal Materials for Friction Pairs During Fretting-Corrosion Wear. Metallophysics & Advanced Technologies, 46(7), 637-648, https://doi.org/10.15407/mfint.46.07.0637

4. Woods M.C., Brooks C.K., Pearce J.M. (2024) Open-source cold and hot scientific sheet press for investigating polymer-based material properties. HardwareX, 19, e00566, https://doi.org/10.1016/j.ohx.2024.e00566

5. Petrov O., Kozlov L., Lozinskiy D., Piontkevych O. (2019) Improvement of the hydraulic units design based on CFD modeling. Lecture Notes in Mechanical Engineering, 653-660, https://doi.org/10.1007/978-3-030-22365-6_65

6. The Cabinet of Ministers of Ukraine (2004) Resolution No. 265 "Pro zatverdzhennia Prohramy povodzhennia z tverdymy pobutovymyvidkhodamy" ["On Approval of the Program for Solid Waste Management"]. URL: http://zakon1.rada.gov.ua/laws/show/265-2004-%D0%BF.

7. Voicu G., Lazea M., Constantin G.A., Stefan E.M., Munteanu M.G. (2020) Finite element analysis of the compaction plate from a garbage truck. In E3S Web of Conferences, 180, 04006, https://doi.org/10.1051/e3sconf/202018004006

8. Lazea M., Constantin G.A., Stoica D., Voicu G. (2020) Analiza structurala cu elemente finite a pieselor de uzura de pe placa de contrapresiune a unei autogunoiere. Revista Romana de Materiale, 50(2), 283-293.

9. Qiu Z., Min R., Wang D., Fan S. (2022) Energy features fusion based hydraulic cylinder seal wear and internal leakage fault diagnosis method. Measurement, 195, 111042, https://doi.org/10.1016/j.measurement.2022.111042

10. Pham M.Q., Vu T.V., Tran L.Q., Nguyen H.H., Hong T.D. (2024) Study on Kinetics and Dynamics of the Scraping-pressing Mechanism of the Compactor Garbage Truck. FME Transactions, 52(4), p603, https://doi.org/10.5937/fme2404603Q

11. Tataryants M.S., Zavinsky S.I., Troshin A.G. (2015) Development of a methodology for calculating loads on the screw and energy consumption of screw presses. ScienceRise, 6 (2), 80-84, https://doi.org/10.15587/2313-8416.2015.44378

12. Bereziuk O.V., Savulyak V.I., Kharzhevskyi V.O., Alekseiev A.Ye. (2024) Determination of the regularity of the rate of wear of the working hydraulic cylinder of the mechanism of the sealing plate of the garbage truck from the pressing force. Problems of Tribology, 29(1/111), 38-44, https://doi.org/10.31891/2079-1372-2024-111-1-38-44

13. Kotomchin A.N., Lyakhov Yu.G. (2019) Analysis of failures of knots and units of construction, road, lifting and transport machines and specialized motor transport on the example of MUE «Communalderservice». Engineering & Computer science, 3, 174-178.

14. Nosenko A.S., Domnickij A.A., Altunina M.S., Zubov V.V. (2019) Theoretical and experimental research findings on batch-operation bin loader with hydraulically driven conveying element. MIAB. Mining Informational and Analytical Bulletin, 11, 119-130, http://dx.doi.org/10.25018/0236-1493-2019-11-0-119-130

15. Lobov N.V., Maltsev D.V., Genson E.M. (2019) Improving the process of transport of solid municipal

waste by automobile transport. Proceedings of IOP Conference Series: Materials Science and Engineering. IOP Publishing, 1(632), 012033, https://doi.org/10.1088/1757-899X/632/1/012033

16. Nurakov S.N., Savinkin V.V. (2008) About development methods for calculating the wear of the rod cylinder interface of hydraulic machines. Proceedings of the Karaganda State Technical University, 3 (32), 96.

17. Shalapai VV, Machuga OS (2023) Vtraty potuzhnosti u hidrotsylindri vnaslidok protikannia hidravlichnoi ridyny cherez neshchilnist [Power loss in the hydraulic cylinder due to hydraulic fluid leakage through non-tightness]. Comprehensive quality assurance of technological processes and systems –2023: Proceedings of the XIII International Scientific and Practical Conference, May 25-26, 2023, Chernihiv. National University "Chernihiv Polytechnic", 287-289.

18. Kargin R.V., Yakovlev I.A., Shemshura E.A. (2017) Modeling of workflow in the grip-container-grip system of body garbage trucks. Procedia Engineering, 206, 1535-1539, https://doi.org/10.1016/j.proeng.2017.10.727

19. Skyba M.Ye., Misiats O.V., Polishchuk A.O., Misiats V.P., Rubanka M.M. (2021). Systema adaptyvnoho chastotnoho keruvannia shvydkistiu obertannia asynkhronnoho tryfaznoho elektrodvyhuna pryvodu rotornoi drobarky [Adaptive frequency control system for the rotational speed of a three-phase asynchronous electric motor driving a rotary crusher]. Herald of of Khmelnytskyi National University. Technical Sciences, 2(295), 139-146. https://doi.org/10.31891/2307-5732-2021-295-2-139-146

20. Manoilenko O., Dvorzhak V., Horobets V., Panasiuk I., Bezuhlyi D. (2024) Assessing the impact of sewing machine thread take-up mechanism parameters on the magnitude and nature of thread take-up. Eastern European Journal of Enterprise Technologies, 2024, 6(1(132)), 64-75, https://doi.org/10.15587/1729-4061.2024.315129

21. Iskovich-Lototsky R., Kots I., Ivanchuk Y., Ivashko Y., Gromaszek K., Mussabekova A., Kalimoldayev M. (2019). Terms of the stability for the control valve of the hydraulic impulse drive of vibrating and vibro-impact machines. Przeglad Elektrotechniczny, 4(19), 19-23, https://doi.org/10.15199/48.2019.04.04

22. Bereziuk O.V., Savulyak V.I., Kharzhevskyi V.O., Alekseiev A.Ye. (2025) Improved mathematical model of the hydraulic drive of the garbage truck's sealing plate mechanism taking into account the wear of its hydraulic cylinder. Problems of Tribology, 30(2/116), 34-41, https://doi.org/10.31891/2079-1372-2025-116-2-34-41

23. Bereziuk O.V. (2005) Vibratsiinyi hidropryvod plyty presuvannia tverdykh pobutovykh vidkhodiv u smittievozakh [Vibration hydraulic drive of the solid waste pressing plate in garbage trucks] Diss. Cand.of Eng.Sciences: 05.02.03 –Drive systems, Vinnytsia, 217.

Березюк О.В., Савуляк В.І., Харжевський В.О., Ivanov S.Cv., Алексеєв А.Є. Аналітичне дослідження удосконаленої математичної моделі гідроприводу механізму ущільнюючої плити сміттєвоза із урахуванням зносу його гідроциліндра.

Стаття присвячена аналітичному дослідженню вдосконаленої математичної моделі гідроприводу механізму ущільнювальної плити сміттєвоза, у якій додатково враховано вплив зношення гідроциліндра на його роботу. На основі проведених числових досліджень удосконаленої нелінійної математичної моделі гідроприводу механізму ущільнювальної плити сміттєвоза, що враховує зношування гідроциліндра, було сформовано її лінеаризовану модифікацію, подану у вигляді системи звичайних лінійних диференціальних рівнянь другого порядку. Для виконання проектних розрахунків нових модифікацій сміттєвозів отримано наближені аналітичні вирази, що описують зміну в часі тиску в напірній магістралі гідроциліндра, а також швидкість і переміщення ущільнювальної плити на основі запропонованої лінеаризованої математичної моделі гідроприводу механізму ущільнюючої плити сміттєвоза з урахуванням зношування гідроциліндра. Отримане рівняння регресії, що забезпечує можливість орієнтовного визначення тривалості процесу ущільнення твердих побутових відходів у сміттєвозі з урахуванням зносу гідроциліндра. Це рівняння може бути застосоване під час проектування нових конструкцій сміттєвозів, дозволяючи враховувати зміну технічного стану виконавчих механізмів без необхідності проведення аналізу повної нелінійної математичної моделі приводу робочих органів. Крім того, воно є придатним для використання в процедурах оптимізації основних параметрів гідроприводу. З’ясовано, що формування удосконаленої методики проектних розрахунків нових конструкцій сміттєвозів з урахуванням зношування виконавчих механізмів потребує проведення додаткових наукових досліджень та подальшого розвитку відповідного теоретичного апарату.

Ключові слова: лінеаризована математична модель, урахування зносу, перетворення за Лапласом, гідропривод, знос, гідроциліндр, механізм ущільнюючої плити, сміттєвоз, тверді побутові відходи

ISSN 2079-1372 Problems of Tribology, V. 30, No 4/118-2025, 72-78

Problems of Tribology
Website: http://tribology.khnu.km.ua/index.php/ProbTrib
E-mail: tribosenator@gmail.com

DOI: https://doi.org/10.31891/2079-1372-2025-118-4-72-78

Enhancing the reliability and wear resistance of high-speed cutting tools through the use of ionized air-oil lubrication media in machine part restoration

D.D. Marchenko* 0000-0002-0808-2923, **K.S. Matvyeyeva** 0000-0003-0974-3022, **O.O. Lymar** 0000-0002-0301-7313, **V.M. Kurepin** 0000-0003-4383-6177

**Mykolayiv National Agrarian University, Mykolayiv, Ukraine*
E-mail: marchenkodd@mnau.edu.ua

Received: 15 November 2025: Revised 30 November 2025: Accept:11 December 2025

Abstract

A comprehensive analysis of the wear processes of high-speed cutting tools and methods of improving their performance during machining has been carried out in this work. An analytical review of scientific sources on modern methods of supplying lubricating and cooling technological means (LCTM) was performed, including the activation of air and air–oil flows and their influence on friction and cutting processes. Special attention is given to the micro-dosed supply of industrial oil Mobil DTE 22 in the form of sprayed air–oil mixtures activated by the electric field of a corona discharge. A nozzle device for the metered supply of viscous fluids with subsequent activation of the air stream has been developed and investigated, ensuring reduced operating pressure and improved operational safety. A tribometric test stand was designed and used to study the lubricating ability of activated LCTM and to determine the friction coefficients of various materials. It was established that ionized air–oil media significantly reduce friction torque, stabilize contact interaction, and decrease surface roughness. Experimental studies of the cutting process demonstrated a substantial increase in the tool life of high-speed steel cutters when using ionized air–oil flow: up to three times compared with dry cutting and up to 2.5 times compared with free oil flooding. The application of the desirability function enabled a comprehensive evaluation of the effectiveness of different LCTM options, showing an increase in machining efficiency of up to 40%.

Keywords: ionized air–oil medium, lubricating and cooling technological means, corona discharge, tribological studies, tool life, micro-dosed oil supply, friction and wear, industrial oil Mobil DTE 22, cutting machining, activated media, surface roughness.

Introduction

Increasing the efficiency of mechanical engineering is inextricably linked to increasing the efficiency of metalworking and reducing the costs associated with the wear of metal-cutting tools. The wear resistance of cutting tools during turning operations largely depends on the used lubricating and cooling technological means (LCTM). In modern mechanical engineering, increased requirements are imposed not only on the functional, but also on the environmental properties of LCTM, since LCTM must not only increase the efficiency of the tool and the quality of the machined surface, but also must not have a technogenic impact on personnel and the environment [1]. In the manufacture of LCTM, they strive to reduce the amount of mineral oil and minimize, and sometimes even eliminate, some effective, but hazardous to health, inorganic and organic components of CTU. Currently, the method of supplying lubricating and cooling fluids (LCF) in the form of sprayed liquids, i.e. in the form of an air-liquid mixture, deserves special attention. However, sometimes the effectiveness of such LCFs is not sufficient. An additional method of increasing the efficiency of processing could be the activation of the environment by electric discharges. Currently, these methods of improving the processes of mechanical processing of materials are actively being developed for metalworking [2]. One of the ways to create environmentally friendly LCFs is to minimize the amount of required LCFs, in particular, this is achieved by introducing microdoses of the LCF air flow with its subsequent activation by electric discharges.

Literature review

Currently, there is no generally accepted theory that explains the numerous aspects of the mechanism of action of the LCF, no scientific principles have been developed for the synthesis and selection of the composition of effective LCFs. The LCF is selected mainly empirically based on the personal experience of specialists or based on the results of machine tests [3 – 5]. This method of selecting the optimal composition requires large time and material costs and guarantees the best results. The results of tests of different LCFs conducted with different tool and machined materials are difficult to compare. If when selecting tool materials it is enough to take into account two or three indicators, for example, such as heat resistance, hardness, then for LCFs these criteria have not been found. The study of complex and diverse processes occurring in the cutting zone is complicated by large temperature and pressure gradients in the surface layers of the tool and workpiece, high deformation rates. Increasing the technological efficiency of LCFs is a complex multi-criteria problem, and the chosen direction of research is relevant [6 – 9].

The choice of coolant for the development of workpiece processing technology is based on the specified technological, economic and operational parameters.

Technological parameters include:

• achieving the required machining accuracy, which is ensured by reducing cutting forces and friction in the contact zones of the workpiece and the tool, better placement of chips in the grooves of multi-toothed tools and better removal of chips and abrasive particles from the cutting zone, which helps reduce deformation of the workpiece and the tool;

• ensuring the specified quality of the machined surface: reducing its roughness, depth and intensity of hardening;

• reducing the intensity of dimensional wear of the tool.

The selection of LCF should be carried out taking into account the material being machined, the operation being performed, the requirements for the quality of the machined surface (roughness, microhardness, etc.), the material and geometry of the cutting tool, machining modes and the associated temperature in the cutting zone.

Research by famous scientists H.H. Zorev, A.I. Isaeva, A.Ya. Malkina, T.J. Burns, M.C. Shaw, K.J. Trigger, B. T. Chao, H. Kopp, Y. Kamata, S. Yamamoto, P. Marty etc. showed that the composition of the LCFs affects the process of surface layer formation and the amount of chip shrinkage [10 – 14]. Currently, a large number of works have been published on the study and implementation of mass-produced LCFs in certain machining operations. It is difficult to determine whether these compositions can be used in other metal cutting operations using other tool or workpiece materials. As a result of the analysis, it is concluded that the development and selection of LCFs for various metal cutting operations should be carried out on the basis of a fundamentally new approach that allows predicting the effectiveness of cutting fluids according to scientifically sound criteria. The use of LCTM in metalworking, as practice shows, has an effective effect on increasing the stability of tools. The physicochemical mechanism of action of LCTM is quite complex and is mainly due to a change in the conditions of interaction of the surfaces of the cutting wedge of the tool with the workpiece, which is expressed, first of all, in a change in the contact conditions. It is generally accepted that when cutting metals, chemically active surfaces of the tool and chips enter into a chemical reaction with the components of the LCTM, as a result of which protective films are formed that shield adhesion between the juvenile surfaces of the tool and the processed materials [15]. At the same time, the constantly increasing requirements for protecting the environment and service personnel from technogenic influences put the safety of LCTM and the ease of its disposal in the first place. Thus, the development of new LCTM compositions and methods of their supply to the cutting zone would improve the ecology of metalworking processes without worsening technological characteristics in comparison with traditionally used compositions of lubricating and cooling compositions [16 – 18]. The study of the mechanisms of influence of such LCTM on chip separation processes and tool stability is an urgent scientific problem. Analysis of the works of scientists M.I. Klushin, V.N. Latyshev, V.V. Podgorkova, R. Beckert, T. Moriwaki and others shows that currently the method of supplying LCF in the form of sprayed liquids, that is, in the form of an air-liquid mixture, deserves special attention [19 – 22].

The effectiveness of LCF is explained by the following features of this method:

- high speed of the jet of the air-liquid mixture provides a significant cooling effect;

- sharp increase in the surface activity of finely dispersed particles of the liquid, the possibility of air penetration into the contact zone of the rubbing surfaces of the tool, chips and the workpiece, some electrical phenomena associated with the electrification of liquid droplets in the jet of the air-liquid mixture, provide an increase in the lubricating effect of LCF;

- blowing the jet of the air-liquid mixture over the cutting zone helps to remove chips and wear products of the cutting tool from the cutting zone, in particular, from the chip grooves of the tool, providing a certain "washing" effect.

Purpose

The purpose of the research is to increase the efficiency of a high-speed cutting tool by using ionization of an air flow containing microdoses of industrial oil Mobil DTE 22, with a corona discharge of different polarity.

Research methodology

The air environment was activated by specially designed units using electrical discharges, with a modified nozzle that allowed for the measured delivery of viscous liquids to the cutting zone.

The unit operates as follows: air from the ionizer chamber enters an air-liquid channel, which passes through a reservoir containing liquid and exits through the diffuser section of the nozzle [23]. The air-liquid channel has an opening inside the reservoir through which the liquid enters, partially mixing with the air. This mixture then enters the diffuser section of the nozzle and is finally broken down by the main air flow, after which it is ionized. The flow rate of the supplied fluid is regulated by needle valves. In our case, this system was calibrated for the flow rate of industrial oil Mobil DTE 22, which ranged from 0.2 to 50 g/hour, in 0.2 g/hour increments [24].

Studies on the particle size of atomized industrial oil Mobil DTE 22 with an oil flow rate of 0.5 g/hour showed that in a non-ionized flow the particle sizes range from 15 to 25 μm, and when using ionization from 5 to 10 μm. To study the lubricating properties of LCTM and determine the friction coefficients of various metals in ionized air-oil environments, a tribometric rig was used [25]. This rig consists of a pendulum tribometer connected to a computer via an ADC. Friction is achieved using a disc-to-disc system. The operating principle of the setup is as follows: the sample is rotated by an electric motor through a gearbox, while the counterweight, attached to a free shaft with a pendulum, remains stationary. The resulting friction rotates the pendulum, and when the torques are equal, slippage begins. The friction torque is determined by the pendulum's angle of rotation. The measurement range is adjusted by varying the pendulum's mass and length. The load is generated by weights on a special platform. The tribometer allows the use of disks of different diameters and variable friction speed. To test the lubricity of ionized LCTM with microdoses of industrial oil Mobil DTE 22, disks with a diameter of 30 mm and a width of 5 mm were made of grade 45, 12Kh18N10T steel, AMg2 alloy, and VT1-0 titanium; the counterweight was made of grade 45 steel with 57 HRC. The contact patch was 2 mm², and the friction speed was 0.5 m/s. The LCTM was supplied through a nozzle at a flow rate of 0.2 – 1 g/h at different corona electrode voltages; comparisons were made with an oil bath. The surfaces were cleaned after each test.

Research results

Comparative studies of the tool life of cutting tools were conducted in positively and negatively ionized air environments with different potential values at the corona electrode, as well as with the introduction of nano- and microdoses of industrial oil Mobil DTE 22 (0.2, 0.5, and 1 g/hour) into the air flow, followed by ionization of the mixture. The effectiveness of various cutting fluid delivery methods and their impact on tool wear were determined by comparing the wear rate and tool life of cutters using pure industrial oil Mobil DTE 22 as the LCTM. During the experiments, wear on the rake and flank surfaces was recorded at regular intervals. The wear criterion was a chamfer width of 0.6 mm on the flank surface. As the results shown in Figures 1 – 2 show, an ionized air flow with microdoses of oil is significantly more effective than either a jet of oil or a non-ionized air-oil mixture at the same oil concentrations. It was also found that the results are significantly affected by the oil concentration, charge sign, and potential at the corona electrode.

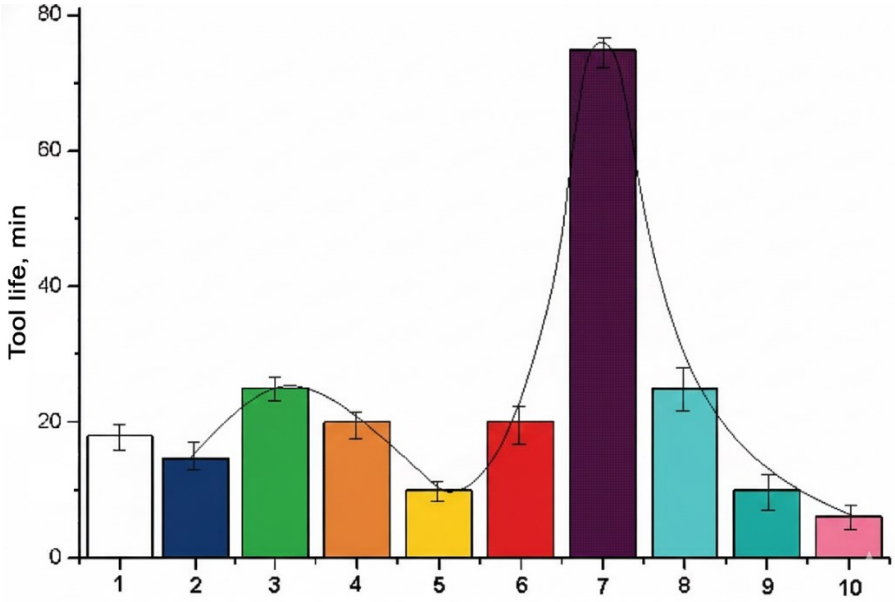

Fig. 1. The tool life of persistent cutters made of high-speed steel R6M5 when turning steel 45 with the introduction of industrial oil Mobil DTE 22 particles into the air flow at a rate of 0.2 g/h: 1 - free irrigation; 2 - blowing with industrial oil Mobil DTE 22 0.2 g/h; 3 - voltage on the electrode 5.5 kV; 4 - voltage 10 kV; 5 - voltage 14 kV; 6 - voltage -1.5 kV; 7 - voltage -3 kV; 8 - voltage -5 kV; 9 - voltage -8 kV; 10 - voltage -10 kV. V = 1.2 m/s, S = 0.1 mm/rev., t = 0.5 mm

For example, at low oil flow rates (approximately 0.2 g/hour), maximum tool wear resistance was observed with negative electrode polarity, while with positive polarity, wear resistance was comparable to that of a non-ionized air flow. Increasing the flow rate to 0.5 g/hour, tool wear resistance with positive and negative ionization became approximately the same, matching that of a non-ionized air-oil mixture [26]. A further increase in flow rate to 1 g/hour resulted in maximum tool performance being achieved with positive corona, while using negative ionization reduced wear resistance to the level of a non-ionized air flow.

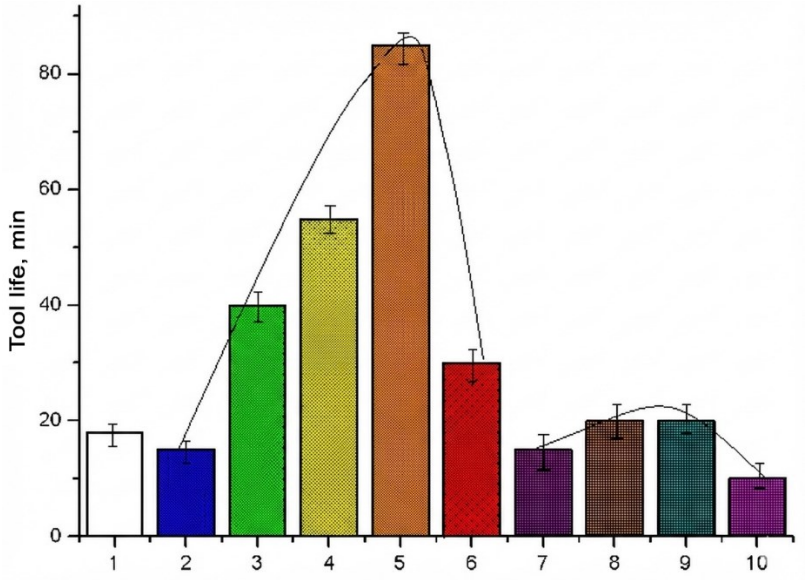

Fig. 2. The tool life of persistent cutters made of high-speed steel R6M5 when turning steel 45 with the introduction of industrial oil Mobil DTE 22 into the air flow at a flow rate of 1 g/h: 1 - free irrigation; 2 - oil blowing 1 g/h; 3 - voltage on the electrode 3 kV; 4 - voltage 5 kV; 5 - voltage 10 kV; 6 - voltage 14 kV; 7 - voltage -3 kV; 8 - voltage -5 kV; 9 - voltage -8 kV; 10 - voltage -10 kV. V = 1.2 m / s, S = 0.1 mm/rev., t = 0.5 mm

Experiments also revealed that, with the same potential sign, increasing the oil content in the air flow shifts the tool's maximum performance to higher potential values.

These data indicate the occurrence of complex, parallel physicochemical processes both in the plasma environment and in the tool-workpiece contact zone. We believe these processes are based on the transition of LCTM particles to an excited state, as well as the partial or complete decomposition of the mixture components in the corona discharge zone. The intensity and sequence of these processes depend significantly on the oil concentration in the air flow. At these potential values, the formation of new compounds is possible, the phase composition of which is determined by the content of the starting materials and the electric field strength around the corona electrode [27].

Studies examining the effect of corona discharge on the physicochemical properties of industrial oil Mobil DTE 22 showed that corona discharge, regardless of its polarity, leads to a decrease in the viscosity, surface tension, and contact angle of the oil. After the corona discharge ceases, the oil's physicomechanical properties are only partially restored [28].

Additionally, the parameters of secondary deformation zones, surface roughness, and chip shrinkage were studied. A summary of the best results is presented in Table 1.

Table 1

Tool life, surface roughness, and chip shrinkage under different treatment conditions

Processing mode	No.	Tool life, min	Surface roughness Ra, μm	Chip shrinkage coefficient, K
Dry machining	1	11	5.684	2.24
Ozone blowing	2	–	3.041	1.72
Air blowing with electrode voltage +10 kV	3	30	3.018	1.89
Air blowing with electrode voltage −9 kV	4	15	4.544	1.60
Oil mist 0.2 g/h, voltage +5.5 kV	5	26	3.770	1.57
Oil mist 0.2 g/h, voltage −3 kV	6	75	3.875	1.45
Oil mist 0.5 g/h, voltage +10 kV	7	30	2.926	1.34
Oil mist 0.5 g/h, voltage −8 kV	8	18	3.302	1.53
Oil mist 1 g/h, voltage +10 kV	9	63	2.821	1.62
Oil mist 1 g/h, voltage −5 kV	10	19	2.246	1.51
Oil flooding	11	18	3.523	1.49

As can be seen from the data in Table 1, the ionized air-oil flow not only positively impacts tool life but also reduces chip shrinkage and improves the roughness of the machined surface.

Conclusions

Using an ionized air stream with microdoses of industrial oil Mobil DTE 22 improves the performance of high-speed cutting tools during turning: up to three times compared to dry machining and up to 2.5 times compared to a free-falling oil jet.

Using an air-oil mixture as a LCTM reduces the average surface roughness Ra by 2.3 times compared to dry machining and by 1.6 times compared to using industrial oil jet.

The effectiveness of an ionized oil LCTM depends on the amount of oil in the stream and the voltage at the discharge electrode. It has been established that at a flow rate of 0.2 g/hour, the best effect is achieved with negative ionization, while at a flow rate of 1 g/hour, optimal results are achieved with positive ionization.

Feeding an ionized air-oil stream to the cutting zone increases the overall efficiency of machining by up to 40%, based on a comprehensive indicator.

The increased efficiency of the ionized air-oil environment is explained by its enhanced lubricating effect. Tribological studies have shown that it reduces the frictional moment of grade 45 steel by 0.75–1.5 times compared to friction in an oil bath and stabilizes contact processes.

References

1. Aulin, V. V. (2022). Parameters of the lubrication process during operational wear of crankshaft bearings. Problems of Tribology, 102, 33–41. https://doi.org/10.31891/2079-1372-2022-106-4-69-81

2. Gutsalenko, Y. H. (2021). Diamond spark grinding with solid lubricants: implications for tool life. Baltic Engineering Journal, 7(2), 112–120

3. Xu, W., Li, C., Zhang, Y., et al. (2022). Electrostatic atomization minimum quantity lubrication machining: from mechanism to application. International Journal of Extreme Manufacturing, 4(4), 042003. https://doi.org/10.1088/2631-7990/ac9652

4. Ma, H., & Yang, M. (2023). Mechanism and experimental study on electrostatic atomization using needle-shaped electrodes. Lubricants, 11(6), 235. https://doi.org/10.3390/lubricants11060235

5. Jia, D., Li, C., Liu, J., Zhang, Y., Yang, M., Gao, T., Said, Z., & Sharma, S. (2023). Prediction model of volume average diameter and analysis of atomization characteristics in electrostatic atomization minimum quantity lubrication. Friction, 11(11), 2107–2131. https://doi.org/10.1007/s40544-022-0734-2

6. He, Z., Jia, D., Zhang, Y., Qu, D., Lv, Z., & Zeng, E. (2024). Investigation into the heat transfer behavior of electrostatic atomization minimum quantity lubrication (EMQL) during grinding. Lubricants, 12(5), 158. https://doi.org/10.3390/lubricants12050158

7. Lv, T., Xu, X.-F., Yu, A.-B., & Hu, X.-D. (2021). Oil mist concentration and machining characteristics of SiO_2 water-based nano-lubricants in electrostatic minimum quantity lubrication (EMQL) milling. Journal of Materials Processing Technology, 290, 116964. https://doi.org/10.1016/j.jmatprotec.2020.116964

8. Iwasaki, M., Hirai, K., Fukumori, K., Higashi, H., Inomata, Y., & Seto, T. (2020). Characterization of submicron oil mist particles generated by metal machining processes. Aerosol and Air Quality Research, 20(6), 1469–1479. https://doi.org/10.4209/aaqr.2019.11.0607

9. Bermúdez, M.-D., Jiménez, A.-E., Sanes, J., & Carrión, F.-J. (2009). Ionic liquids as advanced lubricant fluids. Molecules, 14(8), 2888–2908. https://doi.org/10.3390/molecules14082888

10. Shokrani, A., Dhokia, V., & Newman, S. T. (2012). Environmentally conscious machining of difficult-to-machine materials with regard to cutting fluids. International Journal of Machine Tools & Manufacture, 57, 83–101. https://doi.org/10.1016/j.ijmachtools.2012.02.002

11. Huang, S., Tao, L., Wang, M., & Xu, X. (2018). Enhanced machining performance and lubrication mechanism of electrostatic minimum quantity lubrication — EMQL milling process. International Journal of Advanced Manufacturing Technology, 94, 655–666. https://doi.org/10.1007/s00170-017-0935-4

12. Lv, T., Huang, S.-Q., Hu, X.-D., Feng, B.-H., & Xu, X. (2019). Study on aerosol characteristics of electrostatic minimum quantity lubrication and its turning performance. Chinese Journal of Mechanical Engineering, 55, 129–138. https://doi.org/10.1186/s10033-019-0412-1

13. Lee, P.-H., Kim, J.-W., & Lee, S.-W. (2018). Experimental characterization on eco-friendly micro-grinding process of titanium alloy using airflow-assisted electrospray lubrication with nanofluid. Journal of Cleaner Production, 201, 452–462. https://doi.org/10.1016/j.jclepro.2018.08.264

14. Shah, P., Gadkari, A., Sharma, A., Shokrani, A., & Khanna, N. (2021). Comparison of machining performance under MQL and ultra-high voltage EMQL conditions based on tribological properties. Tribology International, 153, 106595. https://doi.org/10.1016/j.triboint.2020.106595

15. Gajrani, K. K., Sankar, M. R., & Kumar, K. (2018). Performance assessment of nano-lubricants in machining. Tribology International, 119, 400–412. https://doi.org/10.1016/j.triboint.2017.11.030

16. Zhang, Y., Yang, J., & Liu, W. (2020). Electrostatic atomization MQL: review and perspectives. Journal of Cleaner Production, 250, 119587. https://doi.org/10.1016/j.jclepro.2019.119587

17. Ezugwu, E. O., & Wang, Z. M. (2005). Key improvements in the machining of difficult-to-cut materials. International Journal of Machine Tools & Manufacture, 45(5), 483–504. https://doi.org/10.1016/j.ijmachtools.2004.10.022

18. Shah, P., Gadkari, A., Sharma, A., Shokrani, A., & Khanna, N. (2021). Comparison of machining performance under MQL and ultra-high voltage EMQL conditions based on tribological properties. Tribology International, 153, 106595. https://doi.org/10.1016/j.triboint.2020.106595

19. Huang, S., Tao, L., Wang, M., & Xu, X. (2018). Enhanced machining performance and lubrication mechanism of electrostatic minimum quantity lubrication — EMQL milling process. International Journal of Advanced Manufacturing Technology, 94, 655–666. https://doi.org/10.1007/s00170-017-0935-4

20. Lv, T., Xu, X.-F., Yu, A.-B., & Hu, X.-D. (2021). Oil mist concentration and machining characteristics of SiO_2 water-based nano-lubricants in electrostatic minimum quantity lubrication (EMQL) milling. Journal of Materials Processing Technology, 290, 116964. https://doi.org/10.1016/j.jmatprotec.2020.116964

21. Iwasaki, M., Hirai, K., Fukumori, K., Higashi, H., Inomata, Y., & Seto, T. (2020). Characterization of submicron oil mist particles generated by metal machining processes. Aerosol and Air Quality Research, 20(6), 1469–1479. https://doi.org/10.4209/aaqr.2019.11.0607

22. Cui, Z., Xie, Y., & Zhang, Y. (2024). Lubricant activity enhanced technologies for sustainable machining: Mechanisms and processability. Chinese Journal of Aeronautics, 38(6), 103203. https://doi.org/10.1016/j.cja.2024.08.034

23. Ghasemi, A., & Bariani, P. F. (2020). Corona-assisted surface treatments and tribological effects. Wear, 452–453, 203270. https://doi.org/10.1016/j.wear.2020.203270

24. Xu, W., Li, C., Zhang, Y., et al. (2022). Electrostatic atomization minimum quantity lubrication machining: from mechanism to application. International Journal of Extreme Manufacturing, 4(4), 042003. https://doi.org/10.1088/2631-7990/ac9652

25. Lymar, O., & Marchenko, D. (2022). Prospects for the application of restoring electric arc coatings in the repair of machines and mechanisms. In Proceedings of the 2022 IEEE 4th International Conference on Modern Electrical and Energy System (MEES 2022). https://doi.org/10.1109/MEES58014.2022.10005709

26. Marchenko, D., Matvyeyeva, K. (2023). Research of Increase of the Wear Resistance of Machine Parts and Tools by Surface Alloying. Problems of Tribology, 28(3/109), 32–40. https://doi.org/10.31891/2079-1372-2023-109-3-32-40

27. Marchenko, D., Matvyeyeva, K., Kurepin, V. (2024). Increasing the wear resistance of plunger pairs of high-pressure fuel pumps using extreme pressure additives. Problems of Tribology, 29(4/114), 24–31. https://doi.org/10.31891/2079-1372-2024-114-4-24-31

28. Marchenko, D., Matvyeyeva, K. (2024). Study of Wear Resistance of Cylindrical Parts by Electromechanical Surface Hardening. Problems of Tribology, 29(1/111), 25–31. https://doi.org/10.31891/2079-1372-2024-111-1-25-31

Марченко Д.Д., Матвєєва К.С., Лимар О.О., Курепін В.М. Підвищення надійності і стійкості швидкорізального інструменту шляхом використання іонізованих повітряно-оливних змащувальних середовищ при відновленні деталей машин

У роботі виконано комплексний аналіз процесів зношування швидкорізального інструменту та шляхів підвищення його працездатності під час механічної обробки. Проведено аналітичний огляд наукових джерел щодо сучасних методів подачі змащувально-охолоджувальних технологічних середовищ (ЗОТС), включаючи активацію повітряних та повітряно-оливних потоків і їхній вплив на процеси тертя та різання. Особливу увагу приділено мікродозованій подачі індустріальної оливи Mobil DTE 22 у вигляді розпилених повітряно-оливних сумішей, активованих електричним полем коронного розряду. Розроблено та досліджено сопловий пристрій для дозованої подачі в'язких рідин з подальшою активацією повітряного потоку, що забезпечує зниження робочого тиску та підвищення безпечності експлуатації. Створено та використано трибометричний стенд для вивчення змащувальної здатності активованих ЗОТС і визначення коефіцієнтів тертя різних матеріалів. Встановлено, що іонізоване повітряно-оливне середовище істотно знижує момент тертя, стабілізує контактну взаємодію та зменшує шорсткість поверхні. Експериментальні дослідження процесу різання показали значне підвищення стійкості різців із швидкорізальної сталі при використанні іонізованого повітряно-оливного потоку: до трьох разів порівняно з різанням «насухо» та до 2,5 раза – порівняно з вільним поливом оливи. Застосування функції бажаності дало змогу виконати комплексну оцінку ефективності різних варіантів ЗОТС, що показало підвищення ефективності обробки до 40%.

Ключові слова: іонізоване повітряно-оливне середовище, змащувально-охолоджувальне технологічне середовище, коронний розряд, трибологічні дослідження, стійкість інструменту, мікродозована подача оливи, тертя та зношування, індустріальна олива Mobil DTE 22, обробка різанням, активовані середовища, шорсткість поверхні.